

# **Structure-Function Studies of Nicotinic Acetylcholine Receptors Using Unnatural Amino Acids**

Thesis by

**Nyssa Leigh Puskar**

In Partial Fulfillment of the  
Requirements for the Degree of  
Doctor of Philosophy



California Institute of Technology

Pasadena, CA

2012

(Defended January 20, 2012)

© 2012

Nyssa Leigh Puskar

All Rights Reserved

*To my loving mother and father:*

*Cynthia Jean Puskar and James Michael Puskar*

## ACKNOWLEDGMENTS

It feels like only yesterday when my mom and grandpa drove me across the United States with everything I owned in the back of my grandpa's pick-up truck. During these past five-and-a-half years I have grown immensely not only as a scientist, but also as a person. And for that, I would like to personally thank the special people who helped me along the way.

First, I would like to thank my advisor, Professor Dennis Dougherty. I was determined to join Dennis' lab from the start and as such, I sat in his lab as if I was already a member for several months (a tactic encouraged by Katie McMenimen and Ariele Hanek). I remember feeling so victorious when Dennis eventually caved in and let me join his lab. Dennis is an awesome advisor and has played a huge role in making my time in graduate school a rewarding and positive experience. I really appreciate his mentoring style, which fosters scientific and personal growth through giving his students the flexibility to pursue multiple projects while keeping us focused on the end goal.

I have a great deal of respect and appreciation for Professor Henry Lester, a longtime collaborator of the Dougherty lab. Henry has really been a coadvisor for several of my projects. Henry has the ability to offer unique perspectives for our research projects and I will always remember our many "hallway" chats about science. I also owe many thanks to my thesis committee, Professor Peter Dervan, Professor Jacqueline Barton, and Professor Harry Gray. Their words of encouragement and advice on life after graduate school have greatly contributed to my positive experience at Caltech.

After moving cross-country and not knowing a single person, the Dougherty group took me in and made me feel at home. The Dougherty group is a unique and

amazing group of people, and I have truly been fortunate to cross paths with each and every one of them. I am greatly indebted to many of the older students who were essential in getting me up to speed in the ways of the Dougherty lab. I especially express gratitude to Joanne (Xinan) Xiu who was my early mentor in the lab and collaborator on the  $\alpha 4\beta 2$  project. In addition to having an incredible work ethic, she is a sweet and patient lady with the cutest babies.

I was initially drawn to the middle bay where I shared many laughs and interesting conversations with Michael Torrice, Ariele Hanek, Katie McMenimen, Kiowa Bower, and Jai Shanata. As my TAs in physical organic chemistry, Ariele and Katie were my first friends in the lab. Ariele is one of the kindest people I have ever met, and I cherish all of our talks (and swims) that we shared over the years. Katie is hilarious and I will never forget her spot-on impressions of “classic” C&E News pictures. I also had the privilege of being a part of the interesting and thought-provoking discussions regarding zombies initiated by Mike, Kiowa, or Jai. These guys always made me laugh. Mike has the best sense of humor, and his ability to deliver the punch line got me every single time. I have so many fun memories with Kiowa in L.A., and he is one of the most interesting people ever. I appreciate his sensitive heart and positive outlook on life.

I also spent a lot of time with Amy Eastwood and I truly miss her sweet personality. She taught me how to screen print T-shirts and has the most adorable hypoallergenic kitties. Erik Rodriguez is extremely focused and a very hardworker. I know he will make a great professor. I became close to Kristin Gleitsman during the last year she was at Caltech. She is truly an inspirational person, and I know she can achieve anything she puts her mind to.

Given that I was the only one in my class to join the Dougherty group, I always felt a close kinship to the group above me – Angela Blum, Kay Limapichat, Sean Kedrowski, and Jai Shanata. Angela and I quickly became friends in my first year and I do not know what I would have done without her. We grew a special bond that is difficult to explain. Though I do not have any siblings, I imagine it would be similar to my relationship with Angela. Kay is a very unique individual and quite brilliant. I am often inspired by her dedication to science and her love for salsa dancing. Sean is a very talented and driven synthetic chemist, and I know he will do great things in life. Jai and I became friends early on. He is a caring and enigmatic character who always challenges you to think more.

Noah Duffy and Darren Nakamura joined the lab a year after me. Noah is a great person and I am glad that we got to know each other. We share the joy for the simpler things in life, like cowboy boots and open spaces. I have a soft spot for Darren as I mentored him when he joined the lab. Darren is hilarious, ridiculous, and very smart. We had lots of funny talks and sang together while the radio was on in lab (or at my karaoke party).

The representatives of the following year are Kristina McCleary, Ethan Van Arnam, Ximena Da Silva, and Maggie Thompson. I spent a lot of time with Kristina during this last year as we collaborated on the mammalian project. She is very bright and a joy to work with. Additionally, we both had gotten engaged around the same time so we always had so much to talk about. Ethan is one smart cookie and an interesting character who always keeps things lively with his impromptu voice impressions. Ximena is a kind-hearted person whom I am lucky to call a friend. She is charismatic, honest, and

very intelligent. I could always count on her to go shopping with or meet me in the pool for a swim. I have a lot of respect for Maggie as she is a very strong and brave individual. She will certainly make a fantastic physician.

I would also like to thank the newer members of the lab – Erin Lamb, Clint Regan, Tim Miles, Fan Liu, Chris Marrota, and Oliver Shafaat – for continuing the pursuits of the Dougherty lab and contributing to the general enjoyment of the lab.

While at Caltech, I have formed some deep friendships, and I am truly grateful for Pam Sontz, Beverly Lu, and Heather Williamson. Pam is my rapping buddy; she always makes me laugh and has an infectious personality. Beverly is my shopping buddy; she has impeccable taste and has been a great friend to me over the years. Heather is my line-dancing buddy and has been my roommate for the last five-and-a-half years. Heather is just the sweetest thing, and I am so blessed to have her in my life.

Katrina McKay has been my best friend since we met at the University of Florida. She has been a constant source of comfort and support through the years and I love her dearly. From Florida to Vegas to California, we have shared many adventures together, and I know we have so much more to come.

Last, but certainly not least, I want to thank my family – my mother, my father, my Aunt Niki and Uncle Steve, and my loving husband. My mom is the best person in the world. She and I are very close and always will be. I thank my mom for always believing in me and teaching me that I can achieve anything. Her support and love has provided a firm sense of stability that has allowed me to stand on my own two feet and accomplish my goals. I love you, mom. My dad is my biggest fan from timing my swim meets in high school to walking me down the aisle. He has always provided me with

unconditional support and has taught me the importance of being an individual. Hugs and kisses, dad. I cherish my relationship with my Aunt Niki and Uncle Steve. I thank them for always praying for me and checking up on me. I will always remember singing Prince in the car and feeding the baby ducks together. And last, I am completely indebted to my loving husband, Cory Clark. He has been an amazing source of comfort and peace during this last stretch of graduate school and I could not have done it without him. Cory, you are the love of my life.

## ABSTRACT

This dissertation primarily describes structure-function studies of the nicotinic acetylcholine receptors (nAChRs). These studies use a combination of unnatural amino acid mutagenesis and electrophysiology to determine the specific molecular interactions required for neurotransmitter binding to nAChRs.

Chapter 2 examines the mode of agonist activation for the  $\alpha 4\beta 2$  nAChR, the receptor responsible for nicotine addiction. This study investigates the molecular interactions that differentiate the  $\alpha 4\beta 2$  receptor from other receptor subtypes and endow it with the ability to mediate nicotine addiction. We report that the high affinity for nicotine at the  $\alpha 4\beta 2$  receptor is a result of a strong cation- $\pi$  interaction and a strengthened backbone hydrogen bond to a conserved tryptophan (TrpB) of this receptor. We also establish that a point mutation just four residues away from TrpB appears to influence the shape of the agonist binding site, such that it can differentiate the agonist binding mode of the  $\alpha 4\beta 2$  and muscle-type receptors.

Chapter 3 extends studies of the point mutation near TrpB, termed the “loop B glycine.” We examine the muscle-type,  $\alpha 4\beta 2$ , and  $\alpha 7$  subtypes and show that the identity of this residue strongly correlates with agonist potency. Low-potency receptor subtypes have a glycine at the loop B site, while high-potency receptors have a lysine at this site. We establish that mutation of this residue can to convert a low-potency receptor to a high-potency receptor and vice versa.

Chapter 4 investigates the agonist binding mechanism of the  $\alpha 4\beta 4$  receptor. We show both ACh and nicotine make a strong cation- $\pi$  interaction to TrpB, and nicotine makes a strong hydrogen bond to the backbone carbonyl of TrpB. Additionally, chimeric

$\beta$  subunits are used to examine the influence of the complementary binding component on receptor pharmacology for the  $\alpha 4\beta 2$  and  $\alpha 4\beta 4$  receptors.

Last, chapter 5 is a methodology-based project focused on optimizing the incorporation of unnatural amino acids into mammalian cells. Using HEK293T cells, we successfully suppressed an amber stop codon using HSAS, an *in vivo* aminoacylated tRNA. Additional studies will pursue the viability of *in vitro* aminoacylated tRNAs for nonsense suppression in mammalian cells.

## TABLE OF CONTENTS

<b>LIST OF FIGURES.....</b>	<b>xv</b>
<b>LIST OF TABLES.....</b>	<b>xviii</b>
<b>CHAPTER 1: Using Chemical Biology to Study the Brain.....</b>	<b>1</b>
1.1 Chemical Signaling in the Brain	1
1.2 Nicotinic Acetylcholine Receptors: The Longest Known and Best-Studied Neuroreceptor	3
1.3 The Nonsense Suppression Methodology: An Invaluable Tool	8
1.4 Electrophysiology: A Sensitive Assay of Receptor Function	12
1.5 Summary of Dissertation Work	14
1.6 References	16
<b>CHAPTER 2: Nicotine Binding to Brain Receptors Requires a Strong Cation-<math>\pi</math> Interaction.....</b>	<b>20</b>
2.1 Abstract	20
2.2 Introduction	21
2.3 Results and Discussion	24
2.3.1 Challenges in Studying Neuronal nAChRs	24
2.3.2 TrpB Makes a Cation- $\pi$ Interaction in the $\alpha 4\beta 2$ Receptor	29
2.3.3 TyrA is a Hydrogen Bond Donor in the $\alpha 4\beta 2$ Receptor	31
2.3.4 The Functions of TyrC1 and TyrC2 are Conserved in the $\alpha 4\beta 2$ and Muscle-type Receptors	33
2.3.5 A Strong Hydrogen Bond in the $\alpha 4\beta 2$ Receptor	34

2.3.6	Studies with the Smoking Cessation Drug Varenicline at the $\alpha 4\beta 2$ Receptor	35
2.3.7	A Residue Outside of the Aromatic Box Differentiates the $\alpha 4\beta 2$ and Muscle-type Receptors	38
2.3.8	Summary	41
2.4	Methods	41
2.5	Acknowledgements	44
2.6	References	45
<b>CHAPTER 3: Probing the Effects of Residues Located Outside the Agonist Binding Site on Drug-Receptor Selectivity in the Nicotinic Receptor.....</b>		<b>48</b>
3.1	Abstract	48
3.2	Introduction	49
3.3	Results and Discussion	52
3.3.1	Probing the G153 Site in the Low-Potency ( $\alpha 1$ ) <sub>2</sub> $\beta 1\gamma\delta$ (Muscle-type) Receptor	52
3.3.2	Probing the G152 Site in the Low-Potency ( $\alpha 7$ ) <sub>5</sub> Receptor	56
3.3.3	Probing the K158 Site in the High-Potency ( $\alpha 4$ ) <sub>2</sub> ( $\beta 2$ ) <sub>3</sub> Receptor	59
3.3.4	Probing the Proposed Loop B-Loop C Hydrogen Bond	62
3.3.5	Implications for nAChR Function and Subtype Selectivity	64
3.4	Methods	67
3.5	Acknowledgements	71
3.6	References	72

<b>CHAPTER 4: Contrasting Drug-Receptor Interactions at Neuronal vs. Muscle-Type Nicotinic Acetylcholine Receptors: The Neuronal <math>\alpha 4\beta 4</math> Receptor.....</b>	<b>74</b>
4.1 Abstract	74
4.2 Introduction	75
4.3 Results	78
4.3.1 Part 1: Using Unnatural Amino Acid Mutagenesis to Probe the Principal Binding Site of the Neuronal $\alpha 4\beta 4$ Receptor	78
4.3.2 Part 2: Using Chimeric $\beta$ Subunits to Examine the Contribution of the Complementary Binding Site to Subtype-Specific Receptor Pharmacology	87
4.4 Discussion	93
4.5 Methods	97
4.6 Acknowledgements	100
4.7 References	101
<b>CHAPTER 5: Optimizing Techniques to Implement Nonsense Suppression in Mammalian Cells.....</b>	<b>104</b>
5.1 Abstract	104
5.2 Introduction	105
5.3 Methods	107
5.3.1 Molecular Biology	107
5.3.2 Mammalian Cell Culture	107
5.3.3 The FlexStation 3	109
5.3.4 Fluorescent Dye Experiments	113

5.4	Results and Discussion	113
5.4.1	Determining the Optimal PMT Setting to Detect Small Fluorescence Signals	113
5.4.2	Transfection of Mammalian Cells	114
5.4.3	Possible Challenges for Nonsense Suppression in Mammalian Cells	133
5.5	Conclusions and Future Directions	138
5.6	Acknowledgments	140
5.7	References	141

## LIST OF FIGURES

<b>Figure 1.1</b>	Synaptic transmission	2
<b>Figure 1.2</b>	nAChR agonists studied in this dissertation	4
<b>Figure 1.3</b>	nAChR structure	5
<b>Figure 1.4</b>	nAChR subtypes studied in this dissertation	6
<b>Figure 1.5</b>	A model of the nAChR agonist binding site from AChBP	7
<b>Figure 1.6</b>	Mutation of tyrosine: Comparison of conventional mutagenesis and unnatural amino acid mutagenesis	9
<b>Figure 1.7</b>	Hijacking protein translation: Using nonsense suppression to incorporate unnatural amino acids	11
<b>Figure 1.8</b>	Illustration of the <i>in vivo</i> nonsense suppression technique, a method for incorporating unnatural amino acids into ion channels expressed in <i>Xenopus</i> oocytes	12
<b>Figure 1.9</b>	Electrophysiology as an assay of ion channel function	14
<b>Figure 2.1</b>	The binding site of AChBP, thought to resemble that of nAChRs	23
<b>Figure 2.2</b>	Sequence alignment for loops A, B, C, and D in the vicinity of the aromatic binding box	23
<b>Figure 2.3</b>	Agonists and unnatural amino acids considered here	25
<b>Figure 2.4</b>	Rectification behaviors of A2B3 and A3B2 $\alpha$ 4L9' A $\beta$ 2 nAChRs	28
<b>Figure 2.5</b>	Nonsense suppression in the $\alpha$ 4 $\beta$ 2 receptor	29
<b>Figure 2.6</b>	Fluorination plots for ACh and nicotine at $\alpha$ 4 $\beta$ 2 and muscle-type receptors	30
<b>Figure 2.7</b>	Fluorination plot for varenicline at $\alpha$ 4 $\beta$ 2 (A2B3)	36
<b>Figure 2.8</b>	Electrostatic potential surfaces of indole and F <sub>4</sub> -indole, corresponding to the aromatic portions of the side chains of Trp and F <sub>4</sub> -Trp, respectively	37
<b>Figure 2.9</b>	Fluorination plot testing nicotine at the muscle-type receptor containing the G153K point mutation in the $\alpha$ 1 subunit	40
<b>Figure 3.1</b>	Sequence alignment of the nAChR agonist binding site	49

<b>Figure 3.2</b>	nAChR agonist binding site, based on the structure of AChBP	51
<b>Figure 3.3</b>	Agonists and unnatural amino acids used in the present study	53
<b>Figure 3.4</b>	Fluorination plots probing the effect of the $\alpha 1$ G153K mutation on the muscle-type nAChR	54
<b>Figure 3.5</b>	Fluorination plots probing the effect of the $\alpha 7$ G152K mutation on the $(\alpha 7)_5$ nAChR	58
<b>Figure 3.6</b>	Fluorination plots probing the effect of the $\alpha 4$ K158G mutation on the $(\alpha 4)_2(\beta 2)_3$ nAChR	61
<b>Figure 3.7</b>	Comparing the effect on agonist potency of mutating select residues located outside of the $(\alpha 4)_2(\beta 2)_3$ agonist binding site	62
<b>Figure 4.1</b>	nAChR structure	76
<b>Figure 4.2</b>	Wild type recovery experiments for the $\alpha 4\beta 4$ nAChR	81
<b>Figure 4.3</b>	Key structures employed in this study	82
<b>Figure 4.4</b>	Cation- $\pi$ binding plots for $\alpha 4\beta 4$ nAChR at position TrpB with ACh and nicotine	84
<b>Figure 4.5</b>	The backbone ester strategy for modulating a hydrogen bond; $\alpha$ -hydroxy acid incorporation	87
<b>Figure 4.6.</b>	Design of chimeric $\beta$ subunits	88
<b>Figure 4.7</b>	Bar graph comparing F <sub>3</sub> -Trp/Trp fold shifts for chimeric receptors	91
<b>Figure 4.8</b>	Cation- $\pi$ binding (fluorination) plots monitor the relative strength of a cation- $\pi$ interaction at TrpB	92
<b>Figure 4.9</b>	Summary of ligand-receptor interactions present for the muscle-type, $\alpha 4\beta 2$ , $\alpha 4\beta 4$ , and $\alpha 7$ nAChRs	94
<b>Figure 5.1</b>	Schematic of the FlexStation 3 microplate reader	110
<b>Figure 5.2</b>	Membrane potential assay	111
<b>Figure 5.3</b>	SOFTmax PRO data analysis of a 96-well plate	112
<b>Figure 5.4</b>	Confocal images of HEK293T cells expressing mouse $\alpha 4\beta 4$ or $\alpha 4\beta 2$ receptors containing GFP in the $\alpha 4$ subunit	115

<b>Figure 5.5</b>	Dose-reponse curves of human 5HT <sub>3A</sub> receptors expressed in HEK293T cells	117
<b>Figure 5.6</b>	Dose-response curves of 5HT <sub>3A</sub> W183A or W183Y mutant receptors expressed in HEK293T cells	118
<b>Figure 5.7</b>	Confocal images of HEK293T cells expressing eGFP	125
<b>Figure 5.8</b>	THG73-W in response to Neon transfection	134
<b>Figure 5.9</b>	THG73-W after <i>TransIT</i> transfection	136
<b>Figure 5.10</b>	Deprotection of THG73-W-NVOC	137

## LIST OF TABLES

<b>Table 2.1</b>	Injection ratio of $\alpha 4(\text{L9}'\text{A})\text{:}\beta 2$ mRNA controls receptor stoichiometry	26
<b>Table 2.2</b>	Functional characterization of TrpB in $\alpha 4\beta 2$ (A2B3)	30
<b>Table 2.3</b>	Functional characterization of TyrA in $\alpha 4\beta 2$ (A2B3)	32
<b>Table 2.4</b>	Functional characterization of TyrC1 in $\alpha 4\beta 2$ (A2B3)	33
<b>Table 2.5</b>	Functional characterization of TyrC2 in $\alpha 4\beta 2$ (A2B3)	34
<b>Table 2.6</b>	Functional characterization of Thr (TrpB + 1) in $\alpha 4\beta 2$ (A2B3)	35
<b>Table 2.7</b>	Functional characterization of varenicline at TrpB in $\alpha 4\beta 2$ (A2B3)	36
<b>Table 2.8</b>	Evaluation of binding interactions in the $\alpha 4\beta 2$ (A2B3) receptor	37
<b>Table 2.9</b>	Functional characterization of varenicline at Thr (TrpB + 1) in $\alpha 4\beta 2$ (A2B3)	38
<b>Table 2.10</b>	Functional characterization of the muscle-type receptor containing the G153K point mutation in the $\alpha 1$ subunit	40
<b>Table 3.1</b>	Mutation of the loop B Gly/Lys site	52
<b>Table 3.2</b>	$\text{EC}_{50}$ values ( $\mu\text{M}$ ) and Hill coefficients for mutant $(\alpha 1)_2\beta 1\gamma\delta$ nAChRs	53
<b>Table 3.3</b>	Amide-to-ester experiments for the backbone carbonyl of TrpB residue for $(\alpha 1)_2\beta 1\gamma\delta$ , $(\alpha 7)_5$ , and $(\alpha 4)_2(\beta 2)_3$	55
<b>Table 3.4</b>	$\text{EC}_{50}$ values ( $\mu\text{M}$ ) and Hill coefficients for mutant $(\alpha 7)_5$ nAChRs	57
<b>Table 3.5</b>	$\text{EC}_{50}$ values ( $\mu\text{M}$ ) and Hill coefficients for mutant $(\alpha 4)_2(\beta 2)_3$ nAChRs	60
<b>Table 3.6</b>	$\text{EC}_{50}$ values ( $\mu\text{M}$ ) and Hill coefficients for mutant $(\alpha 4)_2(\beta 2)_3$ nAChRs probing the Loop B-Loop C hydrogen bond	63
<b>Table 3.7</b>	Injection ratios of $\alpha 4$ K158G: $\beta 2$ mRNA used to control $\alpha 4\beta 2$ receptor stoichiometry in <i>Xenopus</i> oocytes	69

<b>Table 4.1</b>	Stoichiometries of $\alpha 4\beta 4$ nAChRs expressed in <i>Xenopus</i> oocytes injected with different ratios of human $\alpha 4:\beta 4$ subunit mRNA	80
<b>Table 4.2</b>	Data for mutant $\alpha 4\beta 4$ (A2B3) nAChRs	83
<b>Table 4.3</b>	EC <sub>50</sub> values ( $\mu$ M) and Hill coefficients for $\alpha 4\beta 2/\beta 4$ chimeras	90
<b>Table 4.4</b>	EC <sub>50</sub> values ( $\mu$ M) and Hill coefficients for chimera F	92
<b>Table 4.5</b>	Ratios of mutant EC <sub>50</sub> to wild type EC <sub>50</sub> , such that ratios > 1 represent loss-of-function	93
<b>Table 5.1</b>	Optimization of HEK293T cell seeding for 100 mm dishes	108
<b>Table 5.2</b>	Optimization of HEK293T cell seeding for 35 mm dishes	108
<b>Table 5.3</b>	Comparison of RFU signal detected by the FlexStation 3 for each PMT settings for a serial dilution of rhodamine B	114
<b>Table 5.4</b>	Human $\alpha 4\beta 4$ receptors expressed in HEK293T cells for given ratios of $\alpha 4:\beta 4$ DNA	116
<b>Table 5.5</b>	Conventional 5HT <sub>3A</sub> mutant receptors expressed in HEK293T cells	118
<b>Table 5.6</b>	Using ExpressFect to perform wild type recovery of tryptophan at position W183 in the 5HT <sub>3A</sub> receptor	120
<b>Table 5.7</b>	Using PEI to perform wild type recovery of tryptophan at position W183 in the 5HT <sub>3A</sub> receptor	120
<b>Table 5.8</b>	Optimizing wild type 5HT <sub>3A</sub> DNA transfection using the Neon Transfection System	121
<b>Table 5.9</b>	Optimization of Neon electroporation protocol	121
<b>Table 5.10</b>	Using Neon electroporation for wild type recovery incorporating tryptophan at position W183 in the 5HT <sub>3A</sub> receptor	122
<b>Table 5.11</b>	Using Neon electroporation for wild type recovery of a frameshift codon at position W183 in the 5HT <sub>3A</sub> receptor	123
<b>Table 5.12</b>	Comparison of Neon electroporation and PEI transfection using HSAS to incorporate serine at position W183 in the 5HT <sub>3A</sub> receptor	126

<b>Table 5.13</b>	Comparison of Neon electroporation, PEI, and ExpressFect: Wild type recovery using HSAS to incorporate serine at position S61 in the 5HT <sub>3A</sub> receptor	126
<b>Table 5.14</b>	Monitoring RFU using the 1:2 dye dilution: Wild type recovery using HSAS to incorporate serine at site S61 in the 5HT <sub>3A</sub> receptor	127
<b>Table 5.15</b>	Optimization of Neon electroporation for double transfection of HSAS to incorporate serine at position S61 in the 5HT <sub>3A</sub> receptor	128
<b>Table 5.16</b>	Double Neon Transfection: Wild type recovery incorporating tryptophan at position W183 in the 5HT <sub>3A</sub> receptor	128
<b>Table 5.17</b>	Optimization of <i>TransIT</i> Transfection	129
<b>Table 5.18</b>	Optimization of <i>TransIT</i> Transfection: Wild type recovery using HSAS to incorporate serine at position S61 in the 5HT <sub>3A</sub> receptor	130
<b>Table 5.19</b>	Double <i>TransIT</i> Transfection: Wild type recovery using HSAS to incorporate serine at position S61 in the 5HT <sub>3A</sub> receptor	131
<b>Table 5.20</b>	Double <i>TransIT</i> Transfection: Wild type recovery of tryptophan at position W183 in the 5HT <sub>3A</sub> receptor	131
<b>Table 5.21</b>	Optimization of TransMessenger transfection conditions	132
<b>Table 5.22</b>	Optimization of TransMessenger transfection conditions: Wild type recovery incorporating serine at position S61 in the 5HT <sub>3A</sub> receptor	132
<b>Table 5.23</b>	Optimization of Lipofectamine RNAiMAX transfection conditions	133
<b>Table 5.24</b>	Optimization of Lipofectamine RNAiMAX transfection conditions: Wild type recovery incorporating serine at position S61 in the 5HT <sub>3A</sub> receptor	133
<b>Table 5.25</b>	Comparison of Neon electroporation and <i>TransIT</i> transfection to incorporate tryptophan $\alpha$ -hydroxy at position W183 in the 5HT <sub>3A</sub> receptor	138

# *Chapter 1*

## **Using Chemical Biology to Study the Brain**

### **1.1 Chemical Signaling in the Brain**

As scientists, we continually strive to understand complex biological and chemical systems with the ultimate goal of comprehending the human condition and improving human health. From Hippocrates and Aristotle to the modern scientist, we have been fixated on studying the most complex organ in the human body – the brain. The adult human brain contains approximately  $10^{11}$  neurons, and each neuron forms thousands of connections to other neurons through junctions called synapses. As such, the resulting  $10^{14}$  to  $10^{15}$  synapses form the complex neural network responsible for the intricacies of cognition and behavioral function. Efficient communication between neurons is facilitated by neuroreceptors located at these synapses. Modern neurobiology aims to understand the relationship between the properties of these fundamental brain components and cognitive function/dysfunction.

Neurons communicate via synaptic transmission; a process in which a presynaptic neuron produces a signal and a postsynaptic neuron receives this signal (**Figure 1.1A**). This process begins when the presynaptic nerve cell receives information from other neurons via its dendrites. This information is processed and the presynaptic neuron fires an electrical signal, called an action potential, which travels down the axon of the presynaptic neuron. Upon reaching the axon terminal, the action potential triggers the release of vesicles containing small-molecule neurotransmitters into the synaptic cleft, the space between neurons. Neurotransmitters diffuse across the synaptic cleft and bind to receptors embedded within the postsynaptic membrane, the so-called neurotransmitter-

gated ion channels. Upon neurotransmitter binding, the receptor undergoes a conformational change from a closed (non-conducting) state to an open (ion-conducting) state allowing the flow of ions across the postsynaptic membrane (**Figure 1.1B**). Thus, an electrical signal (the action potential) is converted into a chemical signal (the neurotransmitter) and subsequently back into an electrical signal (ion flow across the membrane), thereby completing the transmission of information from one cell to another.

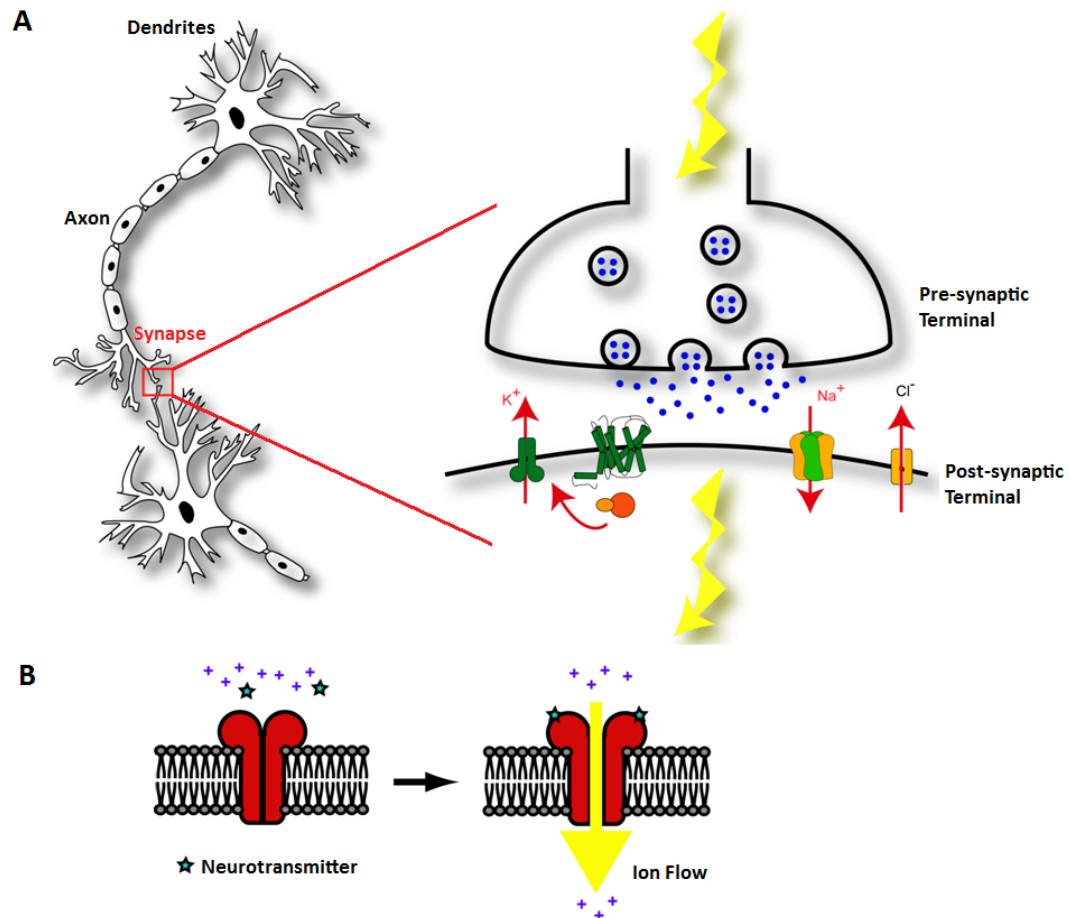


**Figure 1.1.** Synaptic transmission. A. The communication between two neurons occurs at the synapse, boxed in red. The presynaptic neuron receives a message from other neurons and transmits this information to the postsynaptic neuron. Enlargement of the synapse shows that various receptors are embedded within the postsynaptic membrane. These neuroreceptors recognize and bind neurotransmitters (blue circles). B. Upon agonist activation, the ion channel undergoes a conformational change from a closed (non-conducting) state to an open (ion-conducting) state, thereby propagating the signal.

These neuroreceptors are among the molecules of sensory perception, learning, and memory, and can function at either the presynaptic or the postsynaptic neuron. If located at the presynaptic terminal, the ligand-gated ion channel usually has a regulatory function, such as facilitating neurotransmitter release, whereas postsynaptic receptors propagate rapid electrical signal transmission between neurons.<sup>1-3</sup> Regardless of synaptic location of the ligand-gated ion channel, neurotransmitter binding and receptor activation are chemical-scale events essential to proper receptor function. As chemists, we are interested in developing chemical strategies to understand specific chemical interactions that mediate the structure/function relationship of these complex proteins. We employ chemical neurobiology to understand the process by which small-molecule neurotransmitters activate these much larger neuroreceptors proteins.

## **1.2 Nicotinic Acetylcholine Receptors: The Longest Known and Best-Studied Neuroreceptor**

The nicotinic acetylcholine receptor (nAChR) represents a class of neurotransmitter-gated ion channels belonging to the Cys-loop superfamily of neuroreceptors, which also includes the  $\gamma$ -aminobutyric acid type A and type C (GABA<sub>A</sub> and GABA<sub>C</sub>), glycine (Gly), and serotonin type 3 (5-HT<sub>3</sub>) receptors.<sup>4</sup> As a family of complex transmembrane proteins, nAChRs are activated by the endogenous neurotransmitter acetylcholine. Coincidentally, nAChRs are also activated by the addictive lipophilic alkaloid, nicotine and other structurally related molecules (**Figure 1.2**). This class of neuroreceptors is essential to rapid synaptic transmission in the mammalian central nervous system (CNS) and peripheral nervous system (PNS).<sup>4-6</sup>

Given the abundant source of nAChRs available from the *Torpedo* electroplax, the nAChR has become the best-studied and prototypical Cys-loop receptor.<sup>4-8</sup>

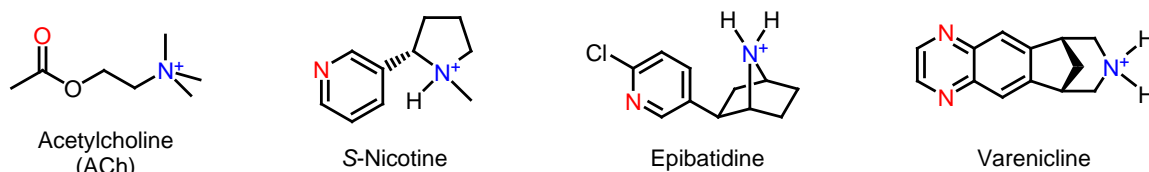


**Figure 1.2.** nAChR agonists studied in this dissertation. Structures are shown for acetylcholine (ACh), S-nicotine, epibatidine, and varenicline (Chantix<sup>®</sup>).

Over the past 20 years, several studies have greatly increased our understanding of nAChR structure. To begin with, a cryo-electron microscopic structure of the *Torpedo californica* nAChR (4 Å) obtained by Unwin *et al.* revealed the gross topology of a full-length nAChR.<sup>9, 10</sup> As shown in **Figure 1.3**, nAChRs are composed of five homologous subunits arranged pseudosymmetrically around a central ion-conducting pore. Each subunit contains a large, principally  $\beta$ -sheet extracellular N-terminal domain, four transmembrane  $\alpha$ -helices (M1-M4), and a small extracellular C-terminal domain. The agonist binding site resides within the N-terminal extracellular domain, whereas the channel gate is located 60 Å away in the transmembrane domain. The M2 helix from each subunit lines the ion-conducting pore and the L9' residue has been identified as the channel gate.<sup>9</sup> (In Cys-loop receptors, these highly homologous M2 sequences are numbered from the cytoplasmic end, termed position 1'.)

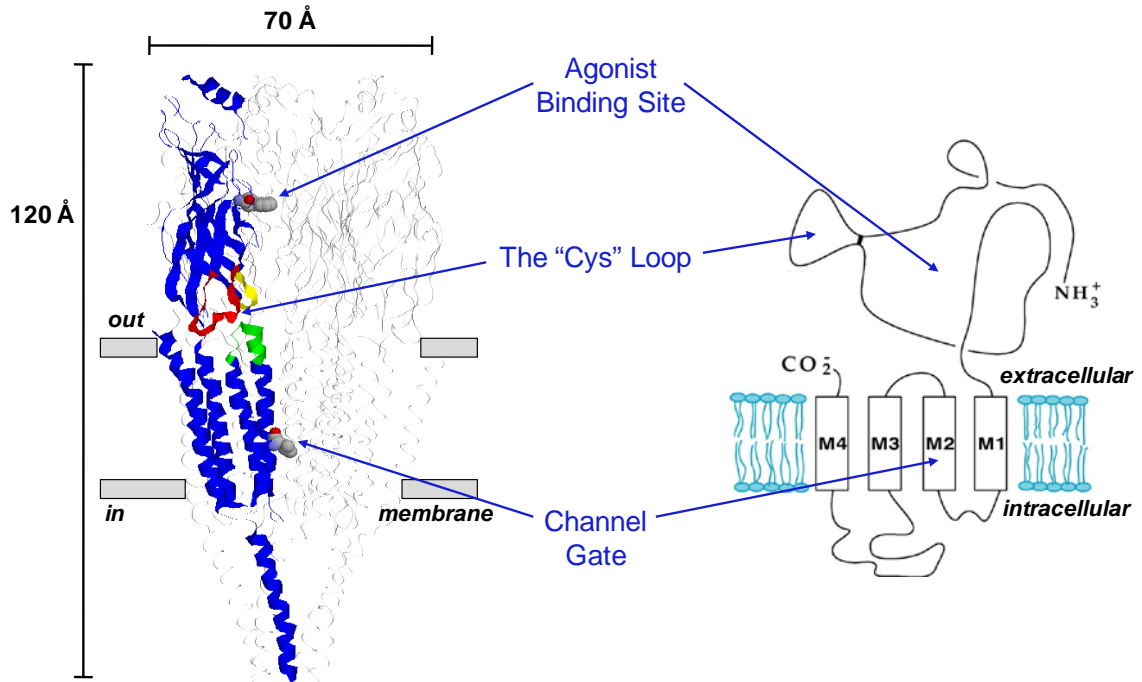


**Figure 1.3.** nAChR structure. Detailed view of nAChR with one subunit highlighted in blue. Structure is based in Unwin's model of the *Torpedo* receptor (left, pdb file 2BG9).<sup>9</sup> The highlighted subunit is compared to a cartoon (on right) describing the topology of a Cys-loop receptor subunit.

A significant advance in the field of nAChR research was the discovery of the water-soluble, snail acetylcholine binding proteins (AChBPs).<sup>11-16</sup> The pentameric AChBPs are structural surrogates for the extracellular ligand-binding domain of the nAChR, sharing 20%–25% sequence identity with the extracellular domain of the significantly larger ion channel proteins.<sup>11</sup> As such, crystal structures of AChBPs bound to various ligands have guided our structure-function studies of the nAChR binding site presented herein. The major caveat, however, is that AChBPs are not a neurotransmitter-gated ion channel, like the nAChR. Instead, AChBPs are merely proteins that contain an acetylcholine binding site, and therefore offer little guidance regarding the nAChR gating mechanism.

There are 16 mammalian genes that encode nAChR subunits, termed  $\alpha 1$ – $\alpha 7$ ,  $\alpha 9$ ,  $\alpha 10$ ,  $\beta 1$ – $\beta 4$ ,  $\delta$ ,  $\gamma$ , and  $\epsilon$ . nAChRs are modular in nature, so these subunits arrange into pentamers to form as many as 25 different nAChR subtypes in humans.<sup>7, 8</sup> The muscle-type receptor is the prototypical nAChR with its precise stoichiometry of  $(\alpha 1)_2\beta 1\gamma\delta$ , fetal form (the adult form is  $(\alpha 1)_2\beta 1\epsilon\delta$ ) (**Figure 1.4**).<sup>4-6</sup> This nAChR subtype is localized at the neuromuscular junction and mediates electrical transmission responsible for skeletal muscle tone. The neuronal nAChRs comprise the remaining nAChR subtypes, which are formed by combinations of  $\alpha 2$ – $\alpha 7$ ,  $\alpha 9$ ,  $\alpha 10$  and  $\beta 2$ – $\beta 4$  subunits (**Figure 1.4**).<sup>7</sup> The diverse array of neuronal subtypes is involved in maintaining multiple cognitive processes such as learning, memory, reward, and motor control.<sup>7, 8</sup>

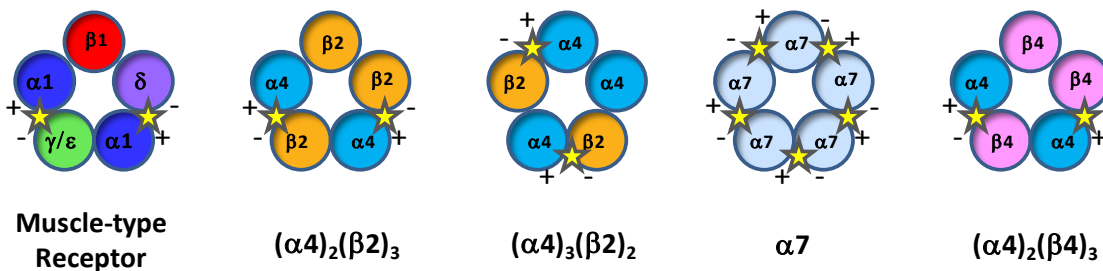


**Figure 1.4.** nAChR subtypes studied in this dissertation.

In the CNS, the two major neuronal subtypes are the  $\alpha 4\beta 2$  and  $\alpha 7$  receptors.<sup>8, 17</sup> The  $\alpha 4\beta 2$  receptor accounts for over 90% of the high affinity nicotine binding sites in the brain,<sup>7, 18-20</sup> and as such, Pfizer’s smoking cessation drug varenicline was designed to target this receptor.<sup>21-23</sup> The  $\alpha 4\beta 2$  receptor exists in two stoichiometries,  $(\alpha 4)_2(\beta 2)_3$  and  $(\alpha 4)_3(\beta 2)_2$ , and chronic exposure to nicotine leads to upregulation of  $(\alpha 4)_2(\beta 2)_3$ , the form most relevant to nicotine addiction.<sup>24, 25</sup> The homopentameric  $\alpha 7$  receptor has been implicated in schizophrenia and is considered a treatment target for Alzheimer’s disease

and other cognitive disorders.<sup>7</sup> The last nAChR subtype discussed in this thesis is the  $\alpha 4\beta 4$  subtype, which like  $\alpha 4\beta 2$ , can arrange in variable stoichiometries and is associated with nicotine addiction.<sup>7, 26, 27</sup>

Agonists bind at select subunit interfaces<sup>4-6</sup> originally identified by photoaffinity labeling and mutagenesis experiments.<sup>11, 28-32</sup> The agonist binding site is formed from several loops contributed by the principal and complementary binding interfaces. The principal binding site (an  $\alpha$  subunit) contributes loops A, B, and C, while the complementary binding site (a non- $\alpha$  subunit, *e.g.*,  $\gamma$ ,  $\delta$ ,  $\beta 2$ ,  $\beta 4$ ) contributes loops D, E, and F. The cationic moiety of agonist molecules interacts with a cluster of five aromatic amino acids, termed TyrA, TrpB, TyrC1, TyrC2, and TrpD (**Figure 1.5**). These residues are conserved for all nAChR subtypes and named according to the loop on which they reside. A major focus of this thesis focus is TrpB, a residue shown to bind agonists via a cation- $\pi$  interaction in several nAChR subtypes.<sup>33-35</sup>

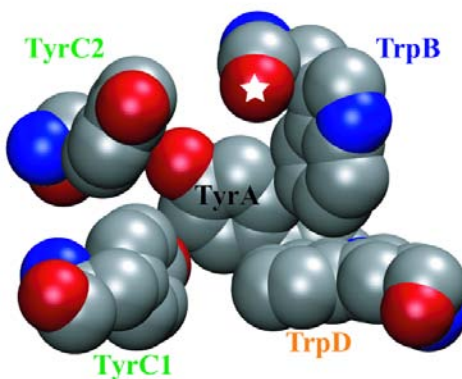


**Figure 1.5.** A model of the nAChR agonist binding site from AChBP (pdb file 1I9B).<sup>11</sup> Residues are labeled according to the loop on which they reside. Residues TyrA, TrpB, TyrC1, and TyrC2 are from the  $\alpha$  subunit, but residue TrpD is from a non- $\alpha$  subunit.

### 1.3 The Nonsense Suppression Methodology: An Invaluable Tool

Nonsense suppression is a broadly applicable technique that can dissect the structure-function relationship of various complex proteins,<sup>33-36</sup> and is especially useful for understanding proteins in the absence of a crystal structure. The major advantage of this approach is the ability to introduce minimal structural modifications to amino acid side chains, thereby allowing for more accurate interpretations of the effects of a specific perturbation. This strategy is complementary to conventional site-directed mutagenesis which can more globally alter or completely abolish side chain functionality within the confines of the naturally occurring amino acids.

Conventional mutagenesis can severely limit the ability to probe the functionality of a multifunctional residue. Consider a tyrosine residue, which may serve as a hydrogen bond donor, a hydrogen bond acceptor, a site for a cation- $\pi$  interaction, or a source of steric bulk (**Figure 1.6**). When Tyr is mutated to an Ala, all possible side-chain functionality is abolished, and this mutation can only determine if Tyr is essential for protein function. Alternatively, mutating the Tyr to either Phe or Ser can probe for a hydrogen bonding interaction. Both mutations can only establish if the hydroxyl group is necessary for proper function, which can act as either a hydrogen bond donor or acceptor. The Tyr to Phe mutation is more conservative as it leaves the  $\pi$  system of the phenyl ring intact. The Tyr to Ser mutation, however, is more complicated due to the significant size discrepancy between Ser and Tyr. This mutant may result in decreased protein function, which could be attributed to the smaller size of the Ser residue unable to provide an OH group at the same point in space as that provided by Tyr.

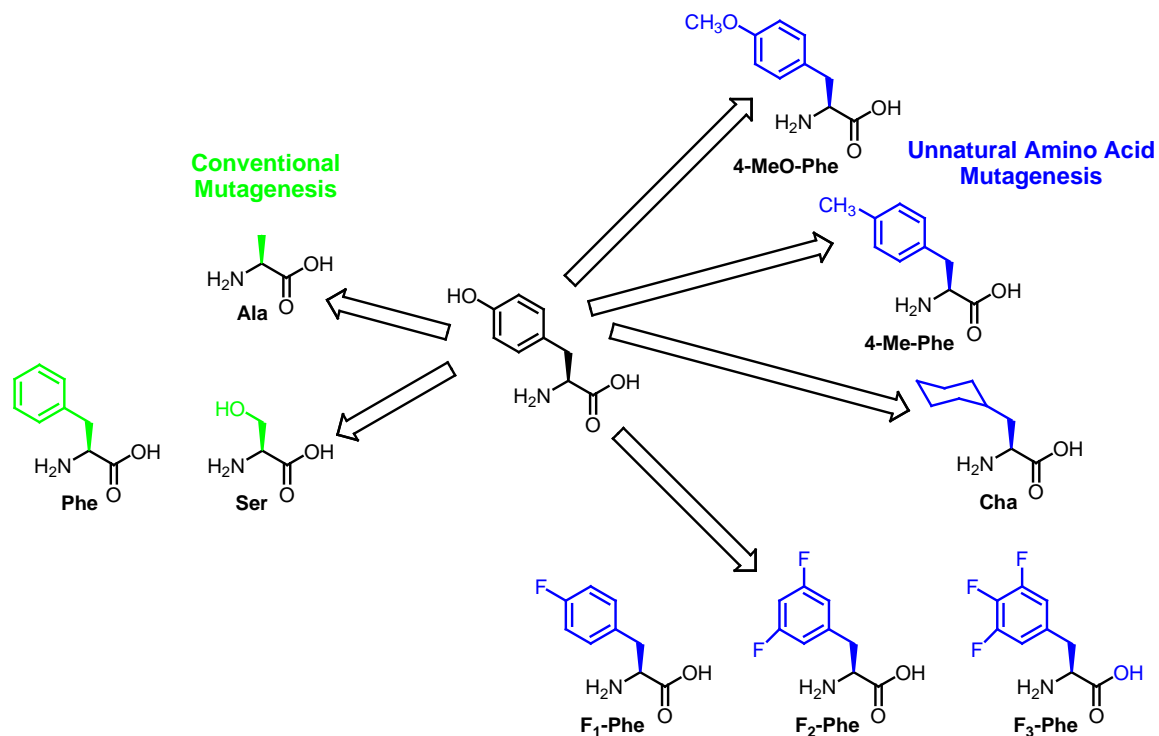


**Figure 1.6.** Mutation of tyrosine: Comparison of conventional mutagenesis and unnatural amino acid mutagenesis.

Unnatural amino acid mutagenesis, however, can address all of these issues by expanding the repertoire of amino acids offered by nature (**Figure 1.6**). For instance, incorporation of 4-methoxy phenylalanine (4-MeOPhe) allows one to determine whether the residue of interest acts as a hydrogen bond acceptor. The issue of steric bulk can be examined by incorporation of 4-methyl phenylalanine (4-MePhe), a residue that would occupy the same relative space as Tyr. Incorporation of cyclohexylalanine (Cha) can establish if the aromatic nature of Tyr is important to proper function. Additionally, incorporation of fluorinated Phe derivatives can investigate the presence of a cation- $\pi$  interaction, a non-covalent interaction between the face of an electron-rich  $\pi$  system and a cation.<sup>37-40</sup>

We use the nonsense suppression methodology, developed by Schultz in 1989,<sup>41</sup> to site-specifically incorporate unnatural amino acids into proteins heterologously

expressed in *Xenopus laevis* oocytes.<sup>42, 43</sup> Using this method, our lab has successfully determined the ligand binding mechanism and channel gating properties of numerous ion channels and neuroreceptors.<sup>33-35, 44-52</sup>

In normal protein synthesis, the ribosome is a multisubunit complex of RNAs and proteins that functions to decode a template mRNA strand and generate a specific protein target. The mRNA sequence contains a series of codons that directs the succession of “charged” tRNA molecules (*i.e.*, tRNA with an amino acid appended to the 3’ end) containing the appropriate anticodons. Amino acids are linked together via peptide bonds to form the growing polypeptide chain. Termination of protein synthesis occurs when the ribosome encounters a STOP or nonsense codon (*e.g.*, UAA, UAG, or UGA), after which, the polypeptide chain is released.

Nonsense suppression, however, “hijacks” the endogenous translational machinery of the *Xenopus* oocyte (**Figure 1.7**). In this process, either a nonsense codon<sup>35, 41</sup> or four-base codon<sup>50-52</sup> (*e.g.*, TAG or GGGT) is placed at the amino acid position of interest in DNA containing the subunit gene. Naturally occurring tRNAs do not recognize these codons, and as such these codons would normally elicit termination of protein synthesis or a frameshift mutation, respectively. Instead, we employ a special suppressor tRNA that contains the correct anticodon and is charged with the unnatural amino acid of choice linked through a highly reactive ester bond.<sup>51-53</sup> The fidelity of this method relies on the orthogonality of the suppressor tRNA, meaning that the tRNA is not recognized by the endogenous aminoacyl-tRNA synthetases of the cell and thereby avoids recharging with natural amino acids.

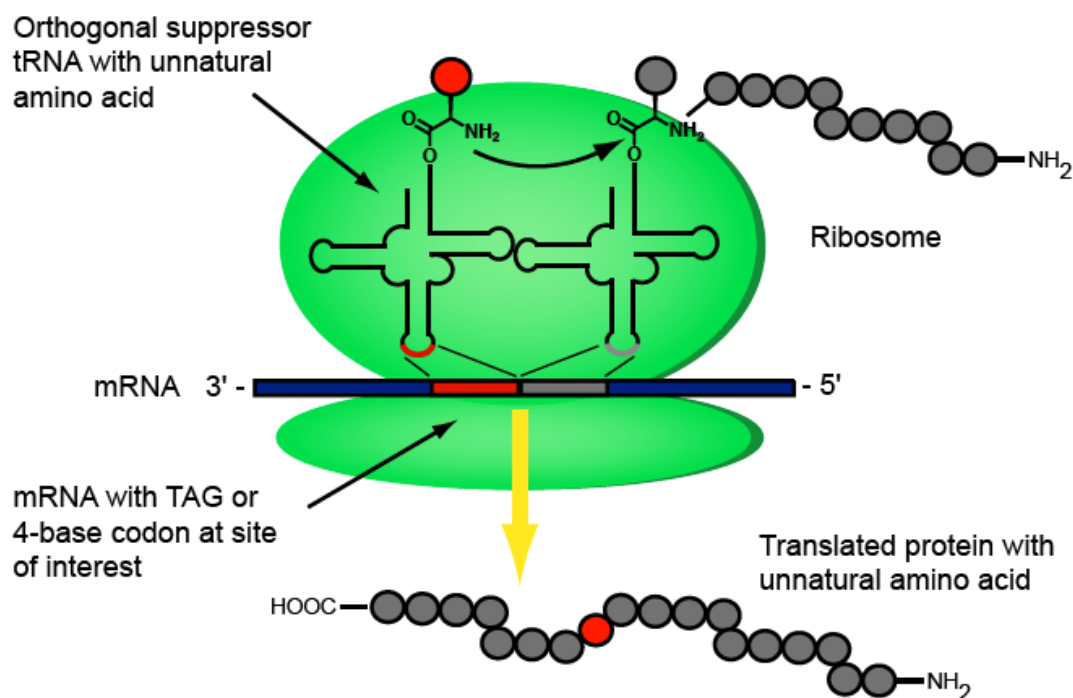


**Figure 1.7.** Hijacking protein translation: Using nonsense suppression to incorporate unnatural amino acids.

A full-length, 76 nucleotide suppressor tRNA is made through a non-trivial process using a combination of synthetic and molecular biology techniques.<sup>42, 43, 53, 54</sup> First, the suppressor tRNA is *in vitro* transcribed as a 74-nucleotide fragment, which is missing the last two nucleotides of the acceptor stem (cytosine; C and adenine; A). The deoxy-C and A (dCA) dinucleotide is synthesized and chemically acylated with the unnatural amino acid (UAA) of choice. Chemical ligation of the dCA- UAA to the 74mer tRNA produces a complete tRNA-UAA molecule.

In the last step of nonsense suppression, *in vitro* transcribed mRNA containing the nonsense codon and the tRNA-UAA are coinjected into a *Xenopus laevis* oocyte, an unfertilized frog egg (**Figure 1.8**). The endogenous translational machinery of the oocyte completes this process by synthesizing, processing, and exporting the desired protein to the surface of the cell membrane. We then examine the functional properties of the novel

protein, which can be attributed to the subtle structural perturbation induced by the unnatural amino acid.

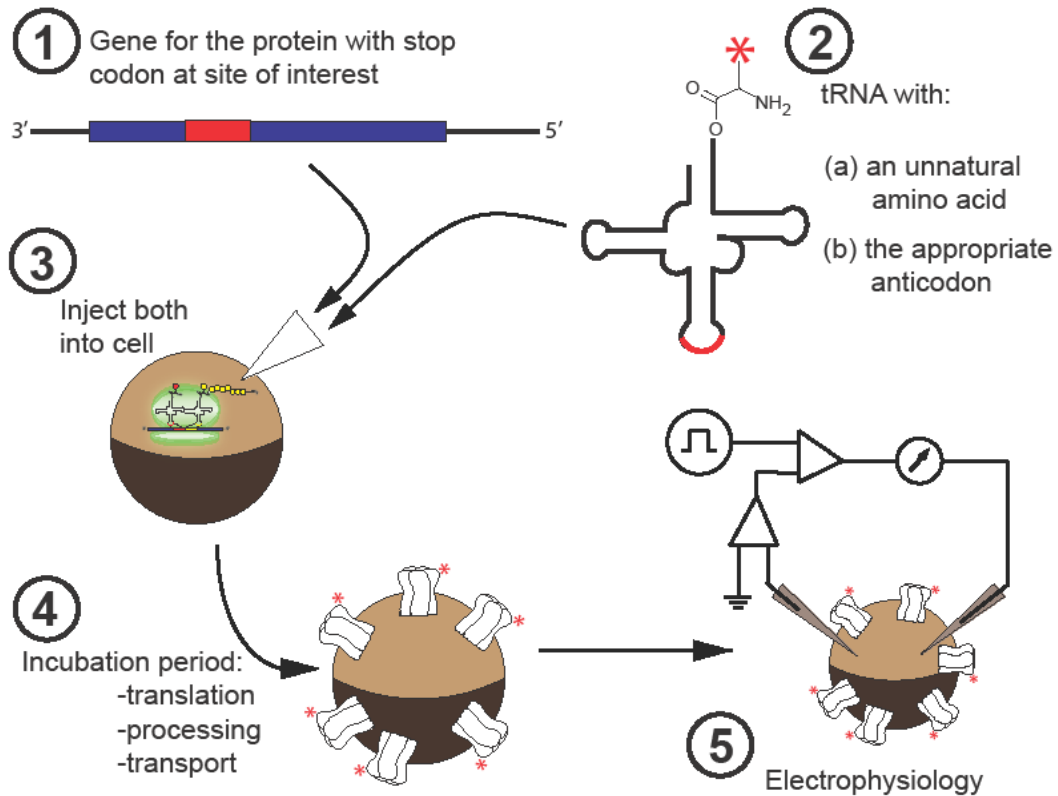


**Figure 1.8.** Illustration of the *in vivo* nonsense suppression technique, a method for incorporating unnatural amino acids into ion channels expressed in *Xenopus* oocytes.

#### 1.4 Electrophysiology: A Sensitive Assay of Receptor Function

The nAChR proteins are ion channels, and as such they mediate the flow of ions (*e.g.*, an electrical current) across a cell membrane. Conveniently, this electrical signal can be readily measured and reports the functionality of the protein under study. Recall, however, that the orthogonal suppressor tRNAs are a stoichiometric reagent – once they deliver their unnatural amino acid to the protein, they are not recharged with additional unnatural amino acid. Additionally, the efficiency of nonsense suppression is inherently variable due to mRNA surveillance mechanisms of the cell (*e.g.*, nonsense-mediated

decay).<sup>55, 56</sup> These processes complicate suppression of a nonsense codon and therefore limit the production of the desired protein. We overcome these potential challenges by using a very sensitive assay of ion channel function, termed two-electrode voltage clamp electrophysiology.

Using this assay, receptors expressed on the cell membrane are exposed to increasing concentrations of agonists. This results in electrical currents proportional to the amount of receptor activation (**Figure 1.9A**). These data are then fit to the Hill equation to generate a dose-response relationship, a curve that plots the agonist concentration against the normalized current responses (**Figure 1.9B**). From this curve, we measure the  $EC_{50}$  value, the concentration required to achieve half-maximal activation.  $EC_{50}$  is a functional measure of the induced structural perturbation and is used to compare ion channel function. As such, a rightward shift in  $EC_{50}$  is a “loss-of-function” mutation, which would require more agonist to activate the channel, whereas a leftward shift in  $EC_{50}$  would indicate a “gain-of-function” mutation. We note that  $EC_{50}$  is a composite measurement of both agonist binding and receptor gating. As such, the studies presented herein focus mainly on mutation of the agonist binding site. Given that the agonist binding site is separated by a distance of  $\sim 60$  Å, we assume that such mutations primarily affect the binding parameter of  $EC_{50}$ . Additionally, single channel analysis has confirmed that the gating parameter is unaffected by mutations of the agonist binding site.<sup>34</sup>

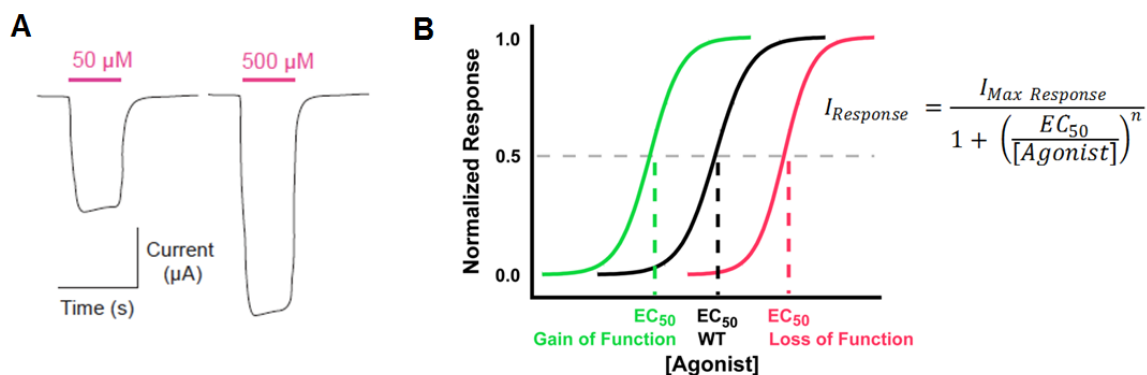


**Figure 1.9.** Electrophysiology as an assay of ion channel function. A. Illustration of agonist-induced current traces for two agonist concentrations (50 μM and 500 μM). B. Dose-response relationships. The dose-response curve for a wild type protein (in black), a gain-of-function mutation (in green), and a loss-of-function mutation (in pink).

## 1.5 Summary of Dissertation Work

The following work describes structure-function studies of the nAChR. These studies use unnatural amino acid mutagenesis and electrophysiology to elucidate the molecular determinants for agonist binding in several nAChR subtypes.

In chapter 2, we study the nAChR subtype responsible for nicotine addiction, the α4β2 nAChR. We determine the molecular interactions that differentiate this receptor from other nAChR subtypes and endow it with the ability to mediate nicotine addiction. We report that the high affinity for nicotine at α4β2 is a result of a strong cation-π interaction and a strengthened backbone hydrogen bond to TrpB of this receptor.<sup>34</sup> This result contrasts what was observed in the muscle-type nAChR, where a cation-π interaction was found with ACh, but not with nicotine.<sup>35, 44</sup> We also show that a point mutation near TrpB appears to influence the shape of the agonist binding site, such that it can differentiate the α4β2 and muscle-type receptors' binding mechanisms.<sup>34</sup>

In chapter 3, we further investigate the point mutation near TrpB, termed the “loop B glycine.” In three nAChR subtypes (*i.e.*, muscle-type, α4β2, and α7), we show

that the correlation between agonist potency and this loop B site is strong. Low-potency receptor subtypes have a glycine at the loop B site, while high-potency receptors have a lysine at this site. We establish that mutation of this residue can to convert a low-potency receptor to a high-potency receptor and vice versa.

Chapter 4 describes our efforts to understand the agonist binding mechanism of a fourth nAChR subtype, the  $\alpha 4\beta 4$  receptor. We confirm that the  $\alpha 4\beta 4$  receptor, like  $\alpha 4\beta 2$ , utilizes a strong cation- $\pi$  interaction to TrpB for both ACh and nicotine, and nicotine makes a strong hydrogen bond to the backbone carbonyl of TrpB.<sup>33</sup> Additionally, we use chimeric  $\beta$  subunits in an attempt to understand how the complementary binding component can influence agonist binding and receptor pharmacology in the  $\alpha 4\beta 2$  and  $\alpha 4\beta 4$  receptors. Together, chapters 2-4 identify structural features of the nAChR that contribute to differential receptor pharmacology and hold significant implications for drug discovery efforts seeking to selectively target nAChRs.

Last, chapter 5 takes a shift from the previous chapters and describes a methodology-based project. This chapter focuses on the optimization of unnatural amino acid incorporation into mammalian cells and its application to large-scale imaging techniques, such as the FlexStation 3. We have successfully suppressed an amber stop codon using HSAS, an *in vivo* aminoacylated tRNA, in HEK293T cells. Studies are ongoing to achieve nonsense suppression using *in vitro* aminoacylated tRNAs.

## 1.6 REFERENCES

1. Boehm, S.; Kubista, H., Fine tuning of sympathetic transmitter release via ionotropic and metabotropic presynaptic receptors. *Pharmacol Rev* **2002**, 54, (1), 43-99.
2. Ghijsen, W. E.; Leenders, A. G., Differential signaling in presynaptic neurotransmitter release. *Cell Mol Life Sci* **2005**, 62, (9), 937-54.
3. Wonnacott, S.; Barik, J.; Dickinson, J.; Jones, I. W., Nicotinic receptors modulate transmitter cross talk in the CNS: nicotinic modulation of transmitters. *J Mol Neurosci* **2006**, 30, (1-2), 137-40.
4. Corringer, P. J.; Le Novere, N.; Changeux, J. P., Nicotinic receptors at the amino acid level. *Annu Rev Pharmacol Toxicol* **2000**, 40, 431-58.
5. Grutter, T.; Changeux, J. P., Nicotinic receptors in wonderland. *Trends Biochem Sci* **2001**, 26, (8), 459-63.
6. Karlin, A., Emerging structure of the nicotinic acetylcholine receptors. *Nat Rev Neurosci* **2002**, 3, (2), 102-14.
7. Jensen, A. A.; Frolund, B.; Liljefors, T.; Krosggaard-Larsen, P., Neuronal nicotinic acetylcholine receptors: structural revelations, target identifications, and therapeutic inspirations. *J Med Chem* **2005**, 48, (15), 4705-45.
8. Romanelli, M. N.; Gratteri, P.; Guandalini, L.; Martini, E.; Bonaccini, C.; Gualtieri, F., Central Nicotinic Receptors: Structure, function, ligands, and therapeutic potential. *ChemMedChem* **2007**, 2, (6), 746-767.
9. Unwin, N., Refined structure of the nicotinic acetylcholine receptor at 4Å resolution. *J Mol Biol* **2005**, 346, (4), 967-89.
10. Miyazawa, A.; Fujiyoshi, Y.; Unwin, N., Structure and gating mechanism of the acetylcholine receptor pore. *Nature* **2003**, 423, (6943), 949-55.
11. Brejc, K.; van Dijk, W. J.; Klaassen, R. V.; Schuurmans, M.; van Der Oost, J.; Smit, A. B.; Sixma, T. K., Crystal structure of an ACh-binding protein reveals the ligand-binding domain of nicotinic receptors. *Nature* **2001**, 411, (6835), 269-76.
12. Celie, P. H.; van Rossum-Fikkert, S. E.; van Dijk, W. J.; Brejc, K.; Smit, A. B.; Sixma, T. K., Nicotine and carbamylcholine binding to nicotinic acetylcholine receptors as studied in AChBP crystal structures. *Neuron* **2004**, 41, (6), 907-14.
13. Hansen, S. B.; Sulzenbacher, G.; Huxford, T.; Marchot, P.; Bourne, Y.; Taylor, P., Structural characterization of agonist and antagonist-bound acetylcholine-binding protein from *Aplysia californica*. *J Mol Neurosci* **2006**, 30, (1-2), 101-2.
14. Hansen, S. B.; Sulzenbacher, G.; Huxford, T.; Marchot, P.; Taylor, P.; Bourne, Y., Structures of *Aplysia* AChBP complexes with nicotinic agonists and antagonists reveal distinctive binding interfaces and conformations. *EMBO J* **2005**, 24, (20), 3635-46.
15. Rucktooa, P.; Smit, A. B.; Sixma, T. K., Insight in nAChR subtype selectivity from AChBP crystal structures. *Biochem Pharmacol* **2009**, 78, (7), 777-87.
16. Taylor, P.; Talley, T. T.; Radic, Z.; Hansen, S. B.; Hibbs, R. E.; Shi, J., Structure-guided drug design: conferring selectivity among neuronal nicotinic receptor and acetylcholine-binding protein subtypes. *Biochem Pharmacol* **2007**, 74, (8), 1164-71.

17. Gotti, C.; Zoli, M.; Clementi, F., Brain nicotinic acetylcholine receptors: native subtypes and their relevance. *Trends Pharmacol Sci* **2006**, *27*, (9), 482-91.
18. Laviolette, S. R.; van der Kooy, D., The neurobiology of nicotine addiction: bridging the gap from molecules to behaviour. *Nat Rev Neurosci* **2004**, *5*, (1), 55-65.
19. Mansvelder, H. D.; Keath, J. R.; McGehee, D. S., Synaptic mechanisms underlie nicotine-induced excitability of brain reward areas. *Neuron* **2002**, *33*, (6), 905-19.
20. Mansvelder, H. D.; McGehee, D. S., Cellular and synaptic mechanisms of nicotine addiction. *J Neurobiol* **2002**, *53*, (4), 606-17.
21. Coe, J. W.; Brooks, P. R.; Vetelino, M. G.; Wirtz, M. C.; Arnold, E. P.; Huang, J.; Sands, S. B.; Davis, T. I.; Lebel, L. A.; Fox, C. B.; Shrikhande, A.; Heym, J. H.; Schaeffer, E.; Rollema, H.; Lu, Y.; Mansbach, R. S.; Chambers, L. K.; Rovetti, C. C.; Schulz, D. W.; Tingley, F. D., 3rd; O'Neill, B. T., Varenicline: an alpha4beta2 nicotinic receptor partial agonist for smoking cessation. *J Med Chem* **2005**, *48*, (10), 3474-7.
22. Gonzales, D.; Rennard, S. I.; Nides, M.; Oncken, C.; Azoulay, S.; Billing, C. B.; Watsky, E. J.; Gong, J.; Williams, K. E.; Reeves, K. R., Varenicline, an alpha4beta2 nicotinic acetylcholine receptor partial agonist, vs sustained-release bupropion and placebo for smoking cessation: a randomized controlled trial. *JAMA* **2006**, *296*, (1), 47-55.
23. Mihalak, K. B.; Carroll, F. I.; Luetje, C. W., Varenicline is a partial agonist at alpha4beta2 and a full agonist at alpha7 neuronal nicotinic receptors. *Mol Pharmacol* **2006**, *70*, (3), 801-5.
24. Moroni, M.; Bermudez, I., Stoichiometry and pharmacology of two human alpha4beta2 nicotinic receptor types. *J Mol Neurosci* **2006**, *30*, (1-2), 95-6.
25. Moroni, M.; Zwart, R.; Sher, E.; Cassels, B. K.; Bermudez, I., alpha4beta2 nicotinic receptors with high and low acetylcholine sensitivity: pharmacology, stoichiometry, and sensitivity to long-term exposure to nicotine. *Mol Pharmacol* **2006**, *70*, (2), 755-68.
26. Improgo, M. R.; Scofield, M. D.; Tapper, A. R.; Gardner, P. D., The nicotinic acetylcholine receptor CHRNA5/A3/B4 gene cluster: dual role in nicotine addiction and lung cancer. *Prog Neurobiol* **92**, (2), 212-26.
27. Wu, J.; Liu, Q.; Yu, K.; Hu, J.; Kuo, Y. P.; Segerberg, M.; St John, P. A.; Lukas, R. J., Roles of nicotinic acetylcholine receptor beta subunits in function of human alpha4-containing nicotinic receptors. *J Physiol* **2006**, *576*, (Pt 1), 103-18.
28. Chabala, L. D.; Lester, H. A., Activation of acetylcholine receptor channels by covalently bound agonists in cultured rat myoballs. *J Physiol* **1986**, *379*, 83-108.
29. Czajkowski, C.; Kaufmann, C.; Karlin, A., Negatively charged amino acid residues in the nicotinic receptor delta subunit that contribute to the binding of acetylcholine. *Proc Natl Acad Sci USA* **1993**, *90*, (13), 6285-9.
30. Dennis, M.; Giraudat, J.; Kotzyba-Hibert, F.; Goeldner, M.; Hirth, C.; Chang, J. Y.; Lazure, C.; Chretien, M.; Changeux, J. P., Amino acids of the Torpedo marmorata acetylcholine receptor alpha subunit labeled by a photoaffinity ligand for the acetylcholine binding site. *Biochemistry* **1988**, *27*, (7), 2346-57.
31. Karlin, A., Chemical modification of the active site of the acetylcholine receptor. *J Gen Physiol* **1969**, *54*, (1), 245-64.

32. Silman, I.; Karlin, A., Acetylcholine receptor: covalent attachment of depolarizing groups at the active site. *Science* **1969**, 164, (3886), 1420-1.
33. Puskar, N. L.; Xiu, X.; Lester, H. A.; Dougherty, D. A., Two neuronal nicotinic acetylcholine receptors, alpha4beta4 and alpha7, show differential agonist binding modes. *J Biol Chem* 286, (16), 14618-27.
34. Xiu, X.; Puskar, N. L.; Shanata, J. A.; Lester, H. A.; Dougherty, D. A., Nicotine binding to brain receptors requires a strong cation-pi interaction. *Nature* **2009**, 458, (7237), 534-7.
35. Zhong, W.; Gallivan, J. P.; Zhang, Y.; Li, L.; Lester, H. A.; Dougherty, D. A., From ab initio quantum mechanics to molecular neurobiology: a cation-pi binding site in the nicotinic receptor. *Proc Natl Acad Sci U S A* **1998**, 95, (21), 12088-93.
36. Dougherty, D. A., Unnatural amino acids as probes of protein structure and function. *Curr Opin Chem Biol* **2000**, 4, (6), 645-52.
37. Dougherty, D. A., Cation-pi interactions in chemistry and biology: a new view of benzene, Phe, Tyr, and Trp. *Science* **1996**, 271, (5246), 163-8.
38. Gallivan, J. P.; Dougherty, D. A., Cation-pi interactions in structural biology. *Proc Natl Acad Sci U S A* **1999**, 96, (17), 9459-64.
39. Ma, J. C.; Dougherty, D. A., The Cation-pi Interaction. *Chem Rev* **1997**, 97, (5), 1303-1324.
40. Zacharias, N.; Dougherty, D. A., Cation-pi interactions in ligand recognition and catalysis. *Trends Pharmacol Sci* **2002**, 23, (6), 281-7.
41. Noren, C. J.; Anthony-Cahill, S. J.; Griffith, M. C.; Schultz, P. G., A general method for site-specific incorporation of unnatural amino acids into proteins. *Science* **1989**, 244, (4901), 182-8.
42. Nowak, M. W.; Gallivan, J. P.; Silverman, S. K.; Labarca, C. G.; Dougherty, D. A.; Lester, H. A., In vivo incorporation of unnatural amino acids into ion channels in *Xenopus* oocyte expression system. *Methods Enzymol* **1998**, 293, 504-29.
43. Nowak, M. W.; Kearney, P. C.; Sampson, J. R.; Saks, M. E.; Labarca, C. G.; Silverman, S. K.; Zhong, W.; Thorson, J.; Abelson, J. N.; Davidson, N.; et al., Nicotinic receptor binding site probed with unnatural amino acid incorporation in intact cells. *Science* **1995**, 268, (5209), 439-42.
44. Beene, D. L.; Brandt, G. S.; Zhong, W.; Zacharias, N. M.; Lester, H. A.; Dougherty, D. A., Cation-pi interactions in ligand recognition by serotonergic (5-HT<sub>3A</sub>) and nicotinic acetylcholine receptors: the anomalous binding properties of nicotine. *Biochemistry* **2002**, 41, (32), 10262-9.
45. Cashin, A. L.; Petersson, E. J.; Lester, H. A.; Dougherty, D. A., Using physical chemistry to differentiate nicotinic from cholinergic agonists at the nicotinic acetylcholine receptor. *J Am Chem Soc* **2005**, 127, (1), 350-6.
46. Gallivan, J. P.; Lester, H. A.; Dougherty, D. A., Site-specific incorporation of biotinylated amino acids to identify surface-exposed residues in integral membrane proteins. *Chem Biol* **1997**, 4, (10), 739-49.
47. Lummis, S. C.; Beene, D. L.; Lee, L. W.; Lester, H. A.; Broadhurst, R. W.; Dougherty, D. A., Cis-trans isomerization at a proline opens the pore of a neurotransmitter-gated ion channel. *Nature* **2005**, 438, (7065), 248-52.

48. Lummis, S. C.; D, L. B.; Harrison, N. J.; Lester, H. A.; Dougherty, D. A., A cation-pi binding interaction with a tyrosine in the binding site of the GABAC receptor. *Chem Biol* **2005**, 12, (9), 993-7.
49. Mu, T. W.; Lester, H. A.; Dougherty, D. A., Different binding orientations for the same agonist at homologous receptors: a lock and key or a simple wedge? *J Am Chem Soc* **2003**, 125, (23), 6850-1.
50. Rodriguez, E. A.; Lester, H. A.; Dougherty, D. A., In vivo incorporation of multiple unnatural amino acids through nonsense and frameshift suppression. *Proc Natl Acad Sci U S A* **2006**, 103, (23), 8650-5.
51. Rodriguez, E. A.; Lester, H. A.; Dougherty, D. A., Improved amber and opal suppressor tRNAs for incorporation of unnatural amino acids in vivo. Part 1: minimizing misacylation. *RNA* **2007**, 13, (10), 1703-14.
52. Rodriguez, E. A.; Lester, H. A.; Dougherty, D. A., Improved amber and opal suppressor tRNAs for incorporation of unnatural amino acids in vivo. Part 2: evaluating suppression efficiency. *RNA* **2007**, 13, (10), 1715-22.
53. Saks, M. E.; Sampson, J. R.; Nowak, M. W.; Kearney, P. C.; Du, F.; Abelson, J. N.; Lester, H. A.; Dougherty, D. A., An engineered Tetrahymena tRNA<sup>Gln</sup> for in vivo incorporation of unnatural amino acids into proteins by nonsense suppression. *J Biol Chem* **1996**, 271, (38), 23169-75.
54. Dougherty, D. A., Physical organic chemistry on the brain. *J Org Chem* **2008**, 73, (10), 3667-73.
55. Nicholson, P.; Yepiskoposyan, H.; Metze, S.; Zamudio Orozco, R.; Kleinschmidt, N.; Muhlemann, O., Nonsense-mediated mRNA decay in human cells: mechanistic insights, functions beyond quality control and the double-life of NMD factors. *Cell Mol Life Sci* 67, (5), 677-700.
56. Whitfield, T. T.; Sharpe, C. R.; Wylie, C. C., Nonsense-mediated mRNA decay in *Xenopus* oocytes and embryos. *Dev Biol* **1994**, 165, (2), 731-4.

## Chapter 2

### Nicotine Binding to Brain Receptors Requires a Strong Cation- $\pi$ Interaction\*

*\*This chapter is adapted in part from: Xiu, X.<sup>†</sup>; Puskar, N. L.<sup>†</sup>; Shanata, J. A. P.; Lester, H. A.; Dougherty, D. A. Nicotine binding to brain receptors requires a strong cation- $\pi$  interaction. *Nature*. **2009**; 458: 534-538. © Nature Publishing Group, a division of Macmillan Publishers Limited. *The work described in this chapter concerning varenicline was done in collaboration with Ximena Da Silva Tavares Bongoll, Dr. Angela P. Blum, Darren T. Nakamura, and Dr. Jai A. P. Shanata.**

<sup>†</sup>Denotes equal contribution.

#### 2.1 ABSTRACT

Nicotine addiction begins with high-affinity binding of nicotine to acetylcholine (ACh) receptors in the brain. The end result is over 4,000,000 smoking-related deaths annually worldwide and the largest source of preventable mortality in developed countries. Stress reduction, pleasure, improved cognition and other central nervous system effects are strongly associated with smoking. However, if nicotine activated ACh receptors found in muscle as potently as it does brain ACh receptors, smoking would cause intolerable and perhaps fatal muscle contractions. Despite extensive pharmacological, functional, and structural studies of ACh receptors, the basis for the differential action of nicotine on brain compared with muscle ACh receptors has not been determined. Here we show that at the  $\alpha 4\beta 2$  brain receptors thought to underlie nicotine addiction, the high affinity for nicotine binding is the result of a strong cation- $\pi$  interaction to a specific aromatic amino acid of the receptor, TrpB. In contrast, the low affinity for nicotine at the muscle-type ACh receptor is largely due to the fact that this key interaction is absent, even though the immediate binding site residues, including the

key amino acid TrpB, are identical in the brain and muscle receptors. At the same time a hydrogen bond from nicotine to the backbone carbonyl of TrpB is enhanced in the neuronal receptor relative to the muscle-type. The cation- $\pi$  interaction and hydrogen bond are also present between TrpB and the smoking cessation compound varenicline (Chantix<sup>®</sup>) in the  $\alpha 4\beta 2$  receptor. Additionally, a point mutation near TrpB that differentiates  $\alpha 4\beta 2$  and muscle-type receptors seems to influence the shape of the binding site, allowing nicotine to interact more strongly with TrpB in the neuronal receptor. ACh receptors are established therapeutic targets for Alzheimer's disease, schizophrenia, Parkinson's disease, smoking cessation, pain, attention-deficit hyperactivity disorder, epilepsy, autism, and depression.<sup>1</sup> Along with solving a chemical mystery in nicotine addiction, our results provide guidance for efforts to develop drugs that target specific types of nicotinic receptors.

## 2.2 INTRODUCTION

Nicotinic acetylcholine receptors (nAChRs) comprise a family of  $\geq 20$  homologous subtypes that mediate fast synaptic transmission throughout the central and peripheral nervous systems.<sup>2</sup> The neuronal nAChRs are found in the central nervous system (CNS) and autonomic ganglia. Of these, the subtype most strongly associated with nicotine addiction and the target of recently developed smoking cessation drugs is termed  $\alpha 4\beta 2$ .<sup>3-7</sup> The high nicotine affinity of  $\alpha 4\beta 2$  receptors, when combined with the ability of nicotine to cross the blood-brain barrier and its favourable pharmacokinetics, allows nicotine at the submicromolar concentrations in tobacco smoke to activate acutely these receptors, providing reward, cognitive sensitization, and perhaps other effects. In addition, the high-affinity interaction allows smoked nicotine to act as an intracellular

pharmacological chaperone of  $\alpha 4\beta 2$  receptors, leading to the upregulation of receptors thought to underlie effects of chronic exposure.<sup>6-8</sup>

In previous studies of the nAChR of the neuromuscular junction (muscle-type), we showed that an important contributor to ACh binding is a cation- $\pi$  interaction to a specific tryptophan (called TrpB, residue 149, **Figure 2.1**).<sup>9</sup> These results were subsequently supported by the important series of crystal structures of ACh binding proteins (AChBP).<sup>10, 11</sup> These structures revealed the “aromatic box” structural motif of **Figure 2.1**, and the aligning residues are predominantly aromatic throughout the Cys-loop family of neurotransmitter-gated ion channels. In other Cys-loop receptors, a cation- $\pi$  interaction between the natural agonist and one of the aromatics is always seen, although its precise location varies.<sup>12</sup> Interestingly, when nicotine activates the muscle-type nAChR, there is no cation- $\pi$  interaction,<sup>13</sup> consistent with its relatively low affinity for this receptor. This suggested that a cation- $\pi$  interaction could discriminate between high-affinity neuronal receptors and low-affinity muscle-type receptors. However, subtle effects must be involved, as the nAChRs of the CNS and neuromuscular junction are homologous throughout most regions of sequence and are essentially identical in the immediate vicinity of the agonist binding site (**Figure 2.2**).

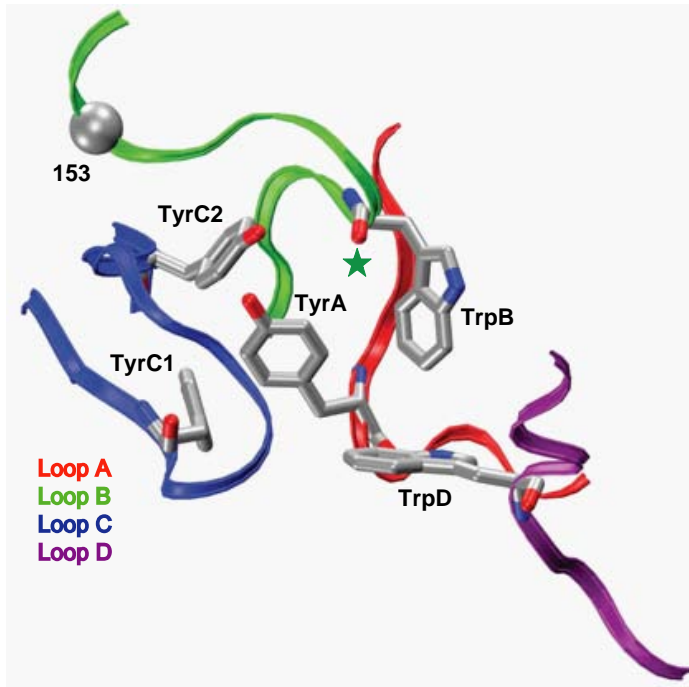


**Figure 2.1.** The binding site of AChBP, thought to resemble that of nAChRs. Shown are the four principal “loops” that define the binding site.<sup>2</sup> Also highlighted are TrpB (149); its backbone carbonyl (green star); the remaining aromatic residues (TyrA, TyrC1, TyrC, and TrpD); and the  $\alpha$  carbon on position 153, which has also been mutated here. The image is of Protein Data Bank file 1I9B.<sup>10</sup>

	Loop A					Loop B					Loop C																
$\alpha$ 1 mouse	W	R	P	D	V	V	L	Y	W	T	Y	D	G	S	V	V	Y	S	C	C	P	T	T	P	Y	L	D
$\alpha$ 1 human	W	R	P	D	L	V	L	Y	W	T	Y	D	G	S	V	V	Y	S	C	C	P	D	T	P	Y	L	D
$\alpha$ 2 human	W	I	P	D	I	V	L	Y	W	T	Y	D	K	A	K	I	Y	D	C	C	A	E	-	I	Y	P	D
$\alpha$ 4 human	W	R	P	D	I	V	L	Y	W	T	Y	D	K	A	K	I	Y	E	C	C	A	E	-	I	Y	P	D
$\alpha$ 4 rat	W	R	P	D	I	V	L	Y	W	T	Y	D	K	A	K	I	Y	E	C	C	A	E	-	I	Y	P	D
$\alpha$ 3 human	W	K	P	D	I	V	L	Y	W	S	Y	D	K	A	K	I	Y	N	C	C	E	E	-	I	Y	P	D
$\alpha$ 6 human	W	K	P	D	I	V	L	Y	W	T	Y	D	K	A	E	I	Y	N	C	C	E	E	-	I	Y	T	D
$\alpha$ 7 human	W	K	P	D	I	L	L	Y	W	S	Y	G	G	W	S	L	Y	E	C	C	K	E	-	P	Y	P	D
$\alpha$ 9 human	W	R	P	D	I	V	L	Y	W	T	Y	N	G	N	Q	V	Y	G	C	C	S	E	-	P	Y	P	D

	Loop D					
$\gamma$ mouse	W	I	E	M	Q	W
$\gamma$ human	W	I	E	M	Q	W
$\delta$ mouse	W	I	D	H	A	W
$\delta$ human	W	I	E	H	G	W
$\beta$ 2 human	W	L	T	Q	E	W
$\beta$ 2 rat	W	L	T	Q	E	W
$\beta$ 3 human	W	L	K	Q	E	W
$\beta$ 4 human	W	L	K	Q	E	W
$\alpha$ 7 human	W	L	Q	M	S	W
$\alpha$ 9 human	W	I	R	Q	I	W

**Figure 2.2.** Sequence alignment for loops A, B, C, and D in the vicinity of the aromatic binding box. The five residues of the aromatic box: TyrA, TrpB, TyrC1, TyrC2, and TrpD are highlighted in green. They are universally conserved in these subunits. G153 ( $\alpha$ 1) is the fourth residue after TrpB, highlighted in blue.

Here we describe studies of the neuronal  $\alpha 4\beta 2$  receptor. We find a remarkable distinction in binding behaviour: both the endogenous neurotransmitter ACh *and* the addictive nicotine molecule make a strong cation- $\pi$  interaction to TrpB. In addition, a hydrogen bond from nicotine to the backbone carbonyl of TrpB that is weak in the muscle-type is much stronger in the  $\alpha 4\beta 2$  receptor. The smoking cessation drug varenicline (marketed as Chantix<sup>®</sup> in the U.S.) was designed to target  $\alpha 4\beta 2$  receptors,<sup>3, 14, 15</sup> and in fact makes the cation- $\pi$  interaction and hydrogen bond. Taken together, these two noncovalent interactions fully rationalize the differential affinity of nicotine in the brain *vs.* the neuromuscular junction.

## 2.3 RESULTS AND DISCUSSION

### 2.3.1 Challenges in Studying Neuronal nAChRs

A cation- $\pi$  interaction between a drug and a receptor can be revealed by incorporation of a series of fluorinated amino acid analogues (**Figure 2.3**); a consistent trend in receptor response indicates a binding interaction.<sup>9</sup> Such an experiment is enabled by the nonsense suppression methodology for incorporation of unnatural amino acids into receptors and channels expressed in *Xenopus* oocytes. Although we have found the nonsense suppression methodology to be broadly applicable,<sup>16, 17</sup> implementing the methodology for study of the  $\alpha 4\beta 2$  neuronal nAChRs proved to be especially challenging, requiring new strategies. The  $\alpha 4\beta 2$  receptors are expressed in *Xenopus* oocytes at inadequately low levels for nonsense suppression experiments. However, recent studies showed that the Leu9'Ala (L9'A) mutation in the M2 transmembrane helix of the  $\alpha 4$  subunit greatly improves expression without altering the pharmacological

selectivity of the receptor.<sup>18</sup> (In Cys-loop receptors, the highly homologous M2 sequences are often compared by numbering from the cytoplasmic end, termed position 1'.) Therefore, all studies of  $\alpha 4\beta 2$  described here included this mutation. As with other mutations of L9', the L9'A mutation lowers the agonist concentration for half-maximum response ( $EC_{50}$ ) by influencing receptor gating in ways that are fairly well understood and that do not distort the present analysis of the binding site (some 60 Å from the 9' position).<sup>19, 20</sup> In addition, previous studies of the muscle-type receptor used a comparable mutation at L9', and control experiments established that it did not alter binding trends.<sup>9,</sup>

21

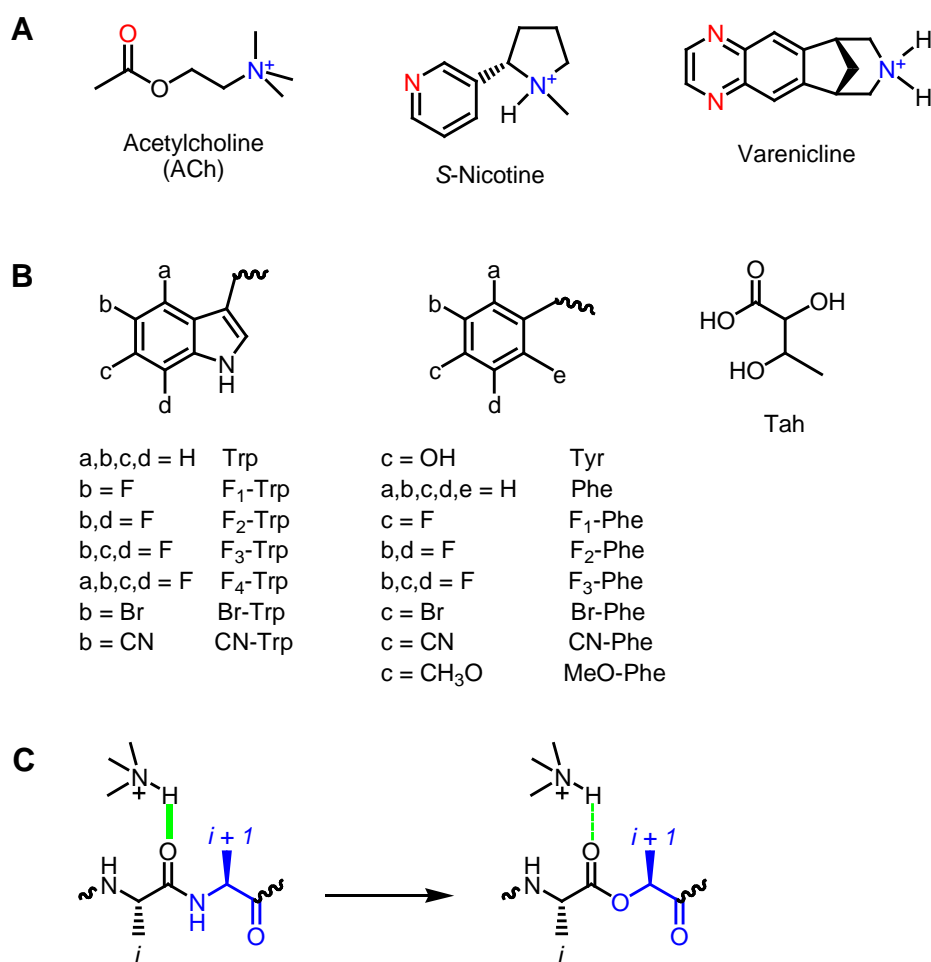


**Figure 2.3.** Agonists and unnatural amino acids considered here. A. Structures of ACh, nicotine, and varenicline. B. Unnatural amino acids considered here. If not indicated, an a, b, c, or d group is H. Br, bromo group; CN, cyano group; MeO, methoxy group. C. The backbone ester strategy for modulating a hydrogen bond.

The nAChRs are pentameric. The muscle-type receptor has a precise stoichiometry of  $(\alpha 1)_2\beta 1\gamma\delta$ , fetal form  $((\alpha 1)_2\beta 1\epsilon\delta)$ ; adult form).<sup>2, 22, 23</sup> However, the  $\alpha 4\beta 2$  receptor can have variable stoichiometry. In particular, there are two forms of  $\alpha 4\beta 2$ ,  $(\alpha 4)_2(\beta 2)_3$  and  $(\alpha 4)_3(\beta 2)_2$ , which we refer to hereafter as A2B3 and A3B2, respectively.<sup>8, 24, 25</sup> Agonist binding sites are at the appropriate  $\alpha$ - $\beta$  interfaces. The A2B3 form has higher sensitivity for nicotine and is upregulated during chronic exposure to nicotine; our studies have focused on it. Controlling the ratios of messenger RNAs injected into the oocyte can reliably control subunit stoichiometry in the wild type receptor. Injection of an mRNA subunit ratio  $\alpha 4(L9'A):\beta 2$  of 10:1 or higher produces pure populations of A3B2 receptors, while a ratio of 3:1 or lower guarantees a pure population of A2B3 (**Table 2.1**).

**Table 2.1.** Injection ratio of  $\alpha 4(L9'A):\beta 2$  mRNA controls receptor stoichiometry.  $EC_{50}$  values ( $\mu M$ ) and Hill coefficients ( $n_H$ ) are shown.

$\alpha 4L9'A:\beta 2$ ratio	ACh	$n_H$	Stoichiometry
100:1	$0.023 \pm 0.002$	$1.5 \pm 0.2$	A3B2
10:1	$0.023 \pm 0.001$	$1.4 \pm 0.1$	A3B2
6:1	$0.15 \pm 0.02$	$0.67 \pm 0.04$	Mixture
3:1	$0.44 \pm 0.03$	$1.2 \pm 0.1$	A2B3
1:1	$0.40 \pm 0.01$	$1.2 \pm 0.1$	A2B3
1:10	$0.43 \pm 0.02$	$1.2 \pm 0.1$	A2B3

Note that the  $\alpha 4(L9'A)$  mutation lowers  $EC_{50}$  in a multiplicative fashion, depending on how many  $\alpha 4$  subunits are present. As such, our A3B2 receptor (with three L9'A mutations) actually has a lower  $EC_{50}$  than our A2B3 receptor (with two L9'A mutations), even though the binding site from the A2B3 stoichiometry is clearly that of the high sensitivity receptor.

In a nonsense suppression experiment, however, the subunit that contains the stop codon where the unnatural amino acid has been incorporated can show low and variable expression levels. Therefore we sought a second, independent indicator of the stoichiometry of the  $\alpha 4\beta 2$  receptor. We now report that the A2B3 and A3B2 forms of the  $\alpha 4(L9'A)\beta 2$  receptor show markedly different rectification behaviours. As indicated by either voltage ramp or voltage jump experiments, A2B3 is substantially more inward rectifying than A3B2 (**Figure 2.4**). Thus, in all our experiments with unnatural amino acids, the stoichiometries of mutant receptors are monitored by measuring current–voltage relations with voltage jumps. For each mutant receptor studied, we determined the fraction (outward current at +70 mV/inward current at –110 mV), and a value  $\leq 0.1$  establishes the desired A2B3 stoichiometry (**Tables 2.2-2.7**). With these methodological developments in hand, incorporation of unnatural amino acids into the  $\alpha 4\beta 2$  receptor becomes feasible (**Figure 2.5**).

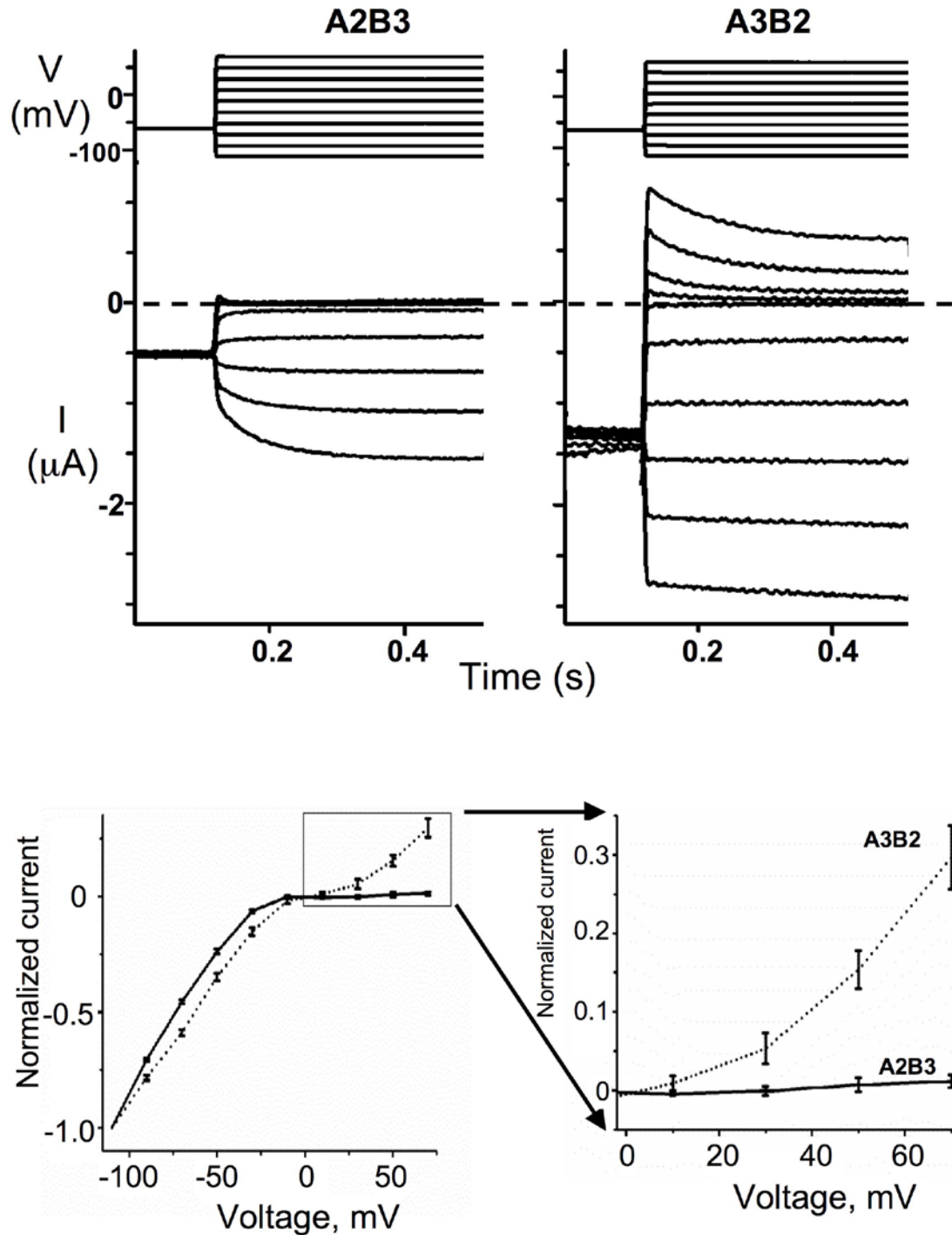


**Figure 2.4.** Rectification behaviors of A2B3 and A3B2  $\alpha 4\text{L9}'\text{A}\beta 2$  nAChRs. Upper: Representative voltage traces and current responses for voltage jump experiments. Lower: I-V curves for A2B3 (solid line) and A3B2 (dotted line). The inset shows positive voltages, where A2B3 and A3B2 exhibit markedly different behavior.

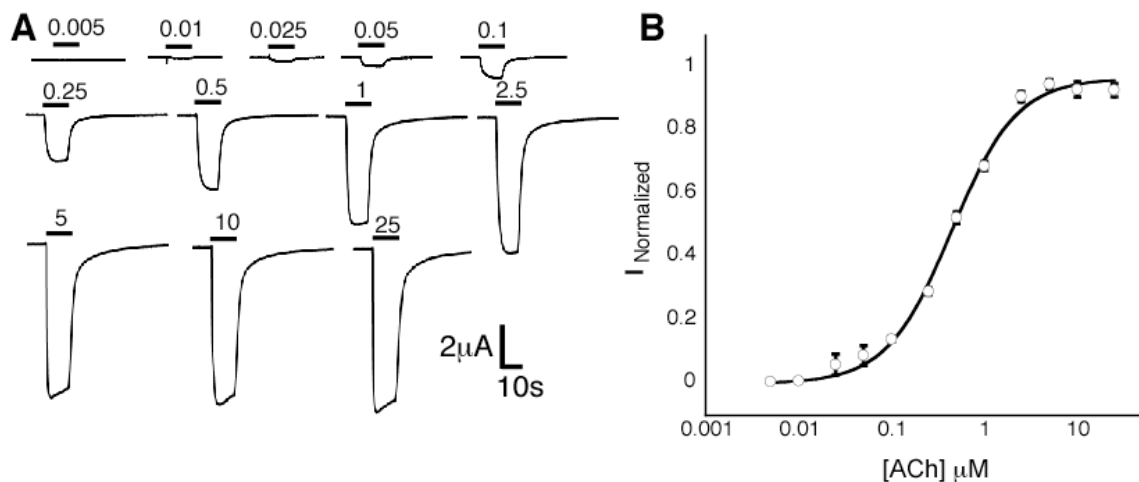


**Figure 2.5.** Nonsense suppression in the  $\alpha 4\beta 2$  receptor. Shown is a wild type recovery experiment, in which Trp is incorporated at the TrpB position. A. Representative traces of voltage-clamp currents. Bars represent application of ACh at concentrations noted ( $\mu\text{M}$ ). B. Fit of data in A to the Hill equation. Error bars indicate s.e.m.;  $n = 6-8$ .

### 2.3.2 TrpB Makes a Cation- $\pi$ Interaction in the $\alpha 4\beta 2$ Receptor

Given the results with the muscle-type nAChR,<sup>9</sup> a logical starting point to search for a cation- $\pi$  interaction in the  $\alpha 4\beta 2$  receptor is at TrpB ( $\alpha 4\text{Trp}149$ ). It is well established that fluorine is deactivating in a cation- $\pi$  interaction, and that multiple fluorines have an additive effect. If a cation- $\pi$  interaction is present, successively replacing the wild type aromatic amino acid with monofluoro, difluoro, trifluoro, and tetrafluoro analogues should lead to a systematic increase in  $\text{EC}_{50}$ . As shown in **Table 2.2** and **Figure 2.6**, a compelling “fluorination” trend is seen for both ACh and nicotine at TrpB of the  $\alpha 4\beta 2$  receptor. This is in contrast to the results at the muscle-type receptor, in which no such trend is seen for nicotine activation.<sup>9</sup> Further support for an important cation- $\pi$  interaction for both agonists is provided by the large perturbation induced by a cyano (CN) group—which is strongly deactivating in a cation- $\pi$  interaction—compared

to a bromo (Br) group, which is roughly isosteric to a cyano group but much less deactivating.

**Table 2.2.** Functional characterization of TrpB in  $\alpha 4\beta 2$  (A2B3).  $EC_{50}$  values ( $\mu M$ ), Hill coefficients ( $n_H$ ) and current size at +70 mV (normalized to current size at -110 mV).

Mutation	ACh	$n_H$	Nicotine	$n_H$	Norm. I (+70mV)
<b>Wild type</b>					
A2B3	$0.42 \pm 0.01$	$1.2 \pm 0.1$	$0.08 \pm 0.01$	$1.2 \pm 0.1$	$0.041 \pm 0.005$
A3B2	$0.023 \pm 0.001$	$1.3 \pm 0.1$	$0.01 \pm 0.001$	$1.7 \pm 0.2$	$0.297 \pm 0.041$
<b>TrpB A2B3</b>					
Trp	$0.44 \pm 0.03$	$1.3 \pm 0.1$	$0.09 \pm 0.01$	$1.5 \pm 0.1$	$0.006 \pm 0.014$
F <sub>1</sub> -Trp	$1.9 \pm 0.1$	$1.2 \pm 0.1$	$0.26 \pm 0.02$	$1.3 \pm 0.1$	$-0.065 \pm 0.047$
F <sub>2</sub> -Trp	$2.0 \pm 0.1$	$1.3 \pm 0.1$	$0.32 \pm 0.04$	$1.3 \pm 0.1$	$0.032 \pm 0.025$
F <sub>3</sub> -Trp	$13 \pm 1$	$1.3 \pm 0.1$	$1.2 \pm 0.1$	$1.4 \pm 0.2$	$-0.073 \pm 0.029$
F <sub>4</sub> -Trp	$29 \pm 2$	$1.1 \pm 0.1$	$4.2 \pm 0.4$	$1.3 \pm 0.2$	$-0.027 \pm 0.023$
CN-Trp	$12 \pm 1$	$1.2 \pm 0.1$	$0.90 \pm 0.07$	$1.4 \pm 0.1$	$0.009 \pm 0.017$
Br-Trp	$1.1 \pm 0.1$	$1.3 \pm 0.1$	$0.20 \pm 0.02$	$1.3 \pm 0.2$	$0.020 \pm 0.005$

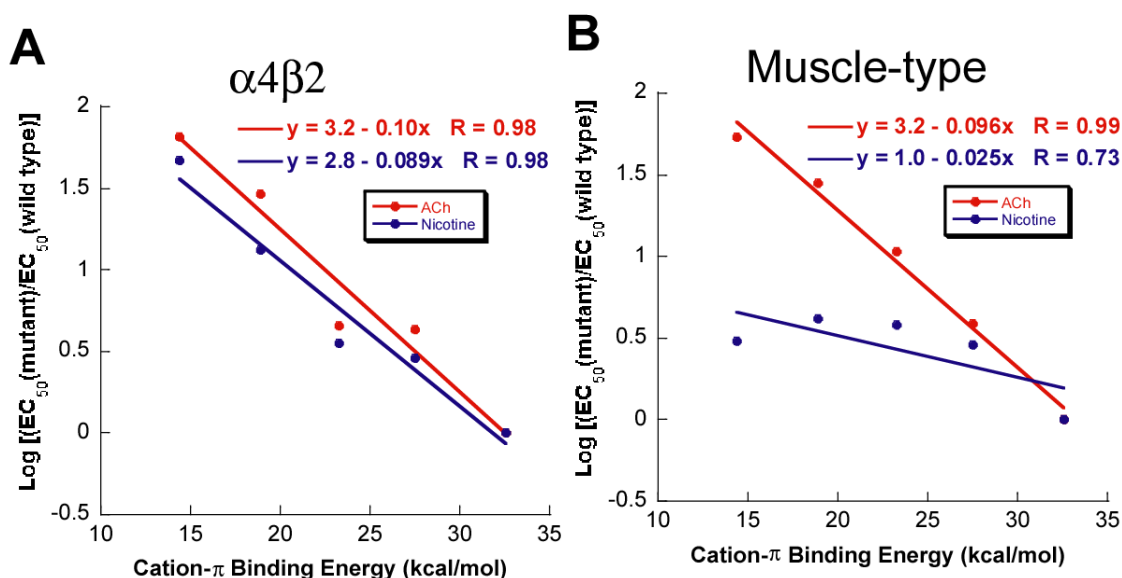


**Figure 2.6.** Fluorination plots for ACh and nicotine at  $\alpha 4\beta 2$  and muscle-type receptors. Note that in both plots, all data sets share the point  $x = 32.6$  kcal/mol (cation- $\pi$  binding energy for Trp). Moving to the left then corresponds to monofluoro-, difluoro-, trifluoro-, and tetrafluoro-TrpB. ACh (red), nicotine (blue). Cation- $\pi$  binding energies ( $x$ -axes) are from Zhong 1998.<sup>9</sup> A.  $\alpha 4\beta 2$  receptor. B. Muscle-type receptor, previously reported in Zhong 1998 and Beene 2002.<sup>9, 13</sup>

The EC<sub>50</sub> values reported here represent a measure of receptor function; shifts in EC<sub>50</sub> can result from changes in ligand binding and/or receptor gating properties. By ascribing the results to attenuation of a cation- $\pi$  interaction, we are effectively concluding that it is agonist binding that is being modulated by fluorination, but that conclusion is not incontrovertible. However, single-channel experiments of  $\alpha 4\beta 2$  established that shifts in EC<sub>50</sub> caused by subtle mutation of TrpB are a consequence of changes in agonist binding, not receptor gating.<sup>26</sup> As such, fluorination of TrpB of the  $\alpha 4\beta 2$  (A2B3) receptor primarily has an impact on the sensitivity to nicotine by decreasing nicotine's cation- $\pi$  interaction with this residue.

### 2.3.3 TyrA is a Hydrogen Bond Donor in the $\alpha 4\beta 2$ Receptor

The remaining residues (TyrA, TyrC1, and TyrC2) of the aromatic box were also probed with unnatural amino acid mutagenesis. We have found fluorination of tyrosine more challenging than tryptophan because progressive fluorination of tyrosine will lower the pK<sub>a</sub> of the side chain hydroxyl group.<sup>27</sup> In fact, the pK<sub>a</sub> for tetrafluorotyrosine is ~5.3 (lowered from ~10 for tyrosine) and can induce ionization of the OH in unnatural tyrosine analogues and complicate analysis. To address this issue, we first tested the phenylalanine mutant, and then successively fluorinated phenylalanine derivatives (**Figure 2.3B**), as Phe can be fluorinated without pK<sub>a</sub> complications.

TyrA has been extensively studied in many Cys-loop receptors; it was identified as a hydrogen bond donor in the muscle-type receptor and a cation- $\pi$  binding site in the GABA<sub>A</sub> receptor.<sup>27, 28</sup> Here, in the  $\alpha 4\beta 2$  receptor, we find that TyrA is sensitive to substituents in the para position for both ACh and nicotine (**Table 2.3**). This indicates that the hydroxyl group is important to channel function, since deletion or substitution

with a cyano, bromo, or fluoro group resulted in a deleterious effect on channel function for both ACh and nicotine. Incorporation of MeO-Phe at TyrA resulted in a 6-fold and 4-fold increase in  $EC_{50}$  for ACh and nicotine, respectively, indicating that TyrA is likely a hydrogen bond donor. Furthermore, TyrA is not sensitive to fluorination and therefore neither nicotine nor ACh interact with TyrA via a cation- $\pi$  interaction.

**Table 2.3.** Functional characterization of TyrA in  $\alpha 4\beta 2$  (A2B3).  $EC_{50}$  values ( $\mu\text{M}$ ), Hill coefficients ( $n_H$ ) and current size at +70 mV (normalized to current size at -110 mV).

Mutation	ACh	$n_H$	Nicotine	$n_H$	Norm. I (+70mV)
<b>Wild type</b>					
<b>A2B3</b>	$0.42 \pm 0.01$	$1.2 \pm 0.1$	$0.08 \pm 0.01$	$1.2 \pm 0.1$	$0.041 \pm 0.005$
<b>A3B2</b>	$0.023 \pm 0.001$	$1.3 \pm 0.1$	$0.01 \pm 0.001$	$1.7 \pm 0.2$	$0.297 \pm 0.041$
<b>TyrA A2B3</b>					
<b>Tyr</b>	$0.42 \pm 0.03$	$1.2 \pm 0.1$	$0.08 \pm 0.01$	$1.7 \pm 0.3$	$0.023 \pm 0.009$
<b>Phe</b>	$12 \pm 1$	$1.3 \pm 0.1$	$0.77 \pm 0.05$	$2.1 \pm 0.3$	$0.064 \pm 0.011$
<b>MeO-Phe</b>	$2.3 \pm 0.2$	$1.2 \pm 0.1$	$0.40 \pm 0.02$	$1.7 \pm 0.2$	$0.054 \pm 0.032$
<b>F<sub>1</sub>-Phe</b>	$15 \pm 1$	$1.2 \pm 0.1$	$0.32 \pm 0.03$	$1.4 \pm 0.2$	$-0.076 \pm 0.046$
<b>F<sub>2</sub>-Phe</b>	$16 \pm 2$	$1.8 \pm 0.3$	$0.39 \pm 0.05$	$1.8 \pm 0.4$	$0.028 \pm 0.005$
<b>F<sub>3</sub>-Phe</b>	$14 \pm 1$	$1.2 \pm 0.1$	$0.53 \pm 0.04$	$1.4 \pm 0.1$	$0.044 \pm 0.010$
<b>Br-Phe</b>	$3.3 \pm 0.2$	$1.2 \pm 0.1$	$0.54 \pm 0.04$	$1.5 \pm 0.1$	$-0.003 \pm 0.031$
<b>CN-Phe</b>	$73 \pm 4$	$1.7 \pm 0.1$	$8.8 \pm 0.9$	$1.5 \pm 0.2$	$0.075 \pm 0.008$

TyrA behaves consistently in both the  $\alpha 4\beta 2$  and the muscle-type receptors; however, the importance of this interaction appears to differ for these two receptors. In  $\alpha 4\beta 2$ , TyrA is much more sensitive to mutations at the para position. With ACh as the agonist, a Tyr to Phe mutation in  $\alpha 4\beta 2$  causes a 29-fold increase in  $EC_{50}$ , but only a 9-fold increase in the muscle-type receptor. As such, it is likely that the hydrogen bond made by TyrA in  $\alpha 4\beta 2$  is more crucial for receptor function than in the muscle-type receptor.

### 2.3.4 The Functions of TyrC1 and TyrC2 are Conserved in the $\alpha 4\beta 2$ and Muscle-type Receptors

TyrC1 is highly sensitive to any mutation that obliterates hydrogen bond donating ability. This is shown by a rightward shift in  $EC_{50}$  of over 100-fold for ACh and over 25-fold for nicotine in response to the Phe, MeO-Phe, and CN-Phe mutations (**Table 2.4**). If TyrC1 function was compromised by a lack of steric bulk, then incorporation of CN-Phe should have returned normal receptor function. Additionally, if this position served as a hydrogen bond acceptor, then incorporation of MeO-Phe should have rescued wild type behavior. However, MeO-Phe incorporation gave a dramatic increase in  $EC_{50}$  for both ACh and nicotine, and we therefore conclude that TyrC1 is an important hydrogen bond donor.

**Table 2.4.** Functional characterization of TyrC1 in  $\alpha 4\beta 2$  (A2B3).  $EC_{50}$  values ( $\mu M$ ), Hill coefficients ( $n_H$ ) and current size at +70 mV (normalized to current size at -110 mV).

Mutation	ACh	$n_H$	Nicotine	$n_H$	Norm. I (+70mV)
<b>Wild type</b>					
<b>A2B3</b>	$0.42 \pm 0.01$	$1.2 \pm 0.1$	$0.08 \pm 0.01$	$1.2 \pm 0.1$	$0.041 \pm 0.005$
<b>A3B2</b>	$0.023 \pm 0.001$	$1.3 \pm 0.1$	$0.01 \pm 0.001$	$1.7 \pm 0.2$	$0.297 \pm 0.041$
<b>TyrC1 A2B3</b>					
<b>Tyr</b>	$0.42 \pm 0.03$	$1.5 \pm 0.1$	$0.07 \pm 0.01$	$1.3 \pm 0.1$	$0.042 \pm 0.014$
<b>Phe</b>	$53 \pm 4$	$1.3 \pm 0.1$	$3.3 \pm 0.2$	$1.2 \pm 0.1$	$0.059 \pm 0.014$
<b>MeO-Phe</b>	$48 \pm 5$	$1.4 \pm 0.2$	$2.8 \pm 0.4$	$1.2 \pm 0.2$	$0.064 \pm 0.028$
<b>CN-Phe</b>	$210 \pm 10$	$1.6 \pm 0.1$	$19 \pm 2$	$1.6 \pm 0.2$	$0.057 \pm 0.011$

In contrast, substitution of TyrC2 displays a strikingly different pattern compared to TyrC1. TyrC2 is extremely permissive to the same mutations tested at TyrC1. All TyrC2  $EC_{50}$  values were essentially unaltered ( $\sim 1.5$ -fold shifts in  $EC_{50}$ ) for both ACh and nicotine (**Table 2.5**). This indicates that TyrC2 primarily serves a structural role in shaping the binding box rather than ligand recognition.

**Table 2.5.** Functional characterization of TyrC2 in  $\alpha 4\beta 2$  (A2B3).  $EC_{50}$  values ( $\mu M$ ), Hill coefficients ( $n_H$ ) and current size at +70 mV (normalized to current size at -110 mV).

Mutation	ACh	$n_H$	Nicotine	$n_H$	Norm. I (+70mV)
<b>Wild type</b>					
<b>A2B3</b>	$0.42 \pm 0.01$	$1.2 \pm 0.1$	$0.08 \pm 0.01$	$1.2 \pm 0.1$	$0.041 \pm 0.005$
<b>A3B2</b>	$0.023 \pm 0.001$	$1.3 \pm 0.1$	$0.01 \pm 0.001$	$1.7 \pm 0.2$	$0.297 \pm 0.041$
<b>TyrC2 A2B3</b>					
<b>Tyr</b>	$0.34 \pm 0.01$	$1.2 \pm 0.1$	$0.08 \pm 0.01$	$1.3 \pm 0.1$	$0.052 \pm 0.012$
<b>Phe</b>	$0.87 \pm 0.03$	$1.3 \pm 0.1$	$0.15 \pm 0.01$	$1.4 \pm 0.1$	$0.039 \pm 0.007$
<b>MeO-Phe</b>	$0.49 \pm 0.02$	$1.3 \pm 0.1$	$0.12 \pm 0.01$	$1.3 \pm 0.1$	$0.033 \pm 0.013$
<b>CN-Phe</b>	$0.64 \pm 0.02$	$1.1 \pm 0.1$	$0.41 \pm 0.03$	$1.1 \pm 0.1$	$0.035 \pm 0.009$

The results for  $\alpha 4\beta 2$  very much parallel our previous findings for the muscle-type receptor. This indicates that it is specifically the interaction with TrpB that discriminates the two receptor subtypes.

### 2.3.5 A Strong Hydrogen Bond in the $\alpha 4\beta 2$ Receptor

Our results suggest that nicotine is positioned more closely to TrpB in the  $\alpha 4\beta 2$  agonist binding site than in the muscle-type. This suggested that another nicotine-binding interaction could also be altered. An important chemical distinction between ACh and nicotine is that only the latter can act as a hydrogen bond donor, through the pyrrolidine  $N^+H$  (**Figure 2.3A**). Examination of the AChBP crystal structures (**Figure 2.1**)<sup>29</sup> suggested that the backbone carbonyl associated with TrpB could act as the hydrogen bond acceptor, and several groups have shown the importance of this interaction.<sup>29-31</sup> Previously, we probed this potential hydrogen bond in the muscle-type receptor by replacing the ( $i + 1$ ) residue with its  $\alpha$ -hydroxy analogue (**Figure 2.3C**).<sup>32</sup> This converts the backbone amide to a backbone ester, which is well established to be a substantially poorer hydrogen bond acceptor. In the muscle-type receptor, this change raised the nicotine  $EC_{50}$  by a modest factor of 1.6.<sup>32</sup> We now find that for precisely the same change in the  $\alpha 4\beta 2$  receptor, the nicotine  $EC_{50}$  increases 19-fold, a relatively large effect for such

a subtle mutation.<sup>33-35</sup> Recall that the backbone ester substitution does not destroy the hydrogen bond, it simply attenuates it. Notably, ACh, which cannot make a conventional hydrogen bond to the carbonyl, shows no shift in EC<sub>50</sub> in response to this mutation (**Table 2.6**). This establishes that the ester mutation does not globally alter the binding/gating characteristics of the receptor.

**Table 2.6.** Functional characterization of Thr (TrpB + 1) in  $\alpha 4\beta 2$  (A2B3). EC<sub>50</sub> values ( $\mu\text{M}$ ), Hill coefficients ( $n_{\text{H}}$ ) and current size at +70 mV (normalized to current size at -110 mV).

Mutation	ACh	$n_{\text{H}}$	Nicotine	$n_{\text{H}}$	Norm. I (+70mV)
<b>Wild type</b>					
<b>A2B3</b>	0.42 $\pm$ 0.01	1.2 $\pm$ 0.1	0.08 $\pm$ 0.01	1.2 $\pm$ 0.1	0.041 $\pm$ 0.005
<b>A3B2</b>	0.023 $\pm$ 0.001	1.3 $\pm$ 0.1	0.01 $\pm$ 0.001	1.7 $\pm$ 0.2	0.297 $\pm$ 0.041
<b>Thr (TrpB+1) A2B3</b>					
<b>Thr</b>	0.41 $\pm$ 0.02	1.4 $\pm$ 0.1	0.09 $\pm$ 0.01	1.6 $\pm$ 0.1	0.044 $\pm$ 0.007
<b>Tah</b>	0.37 $\pm$ 0.02	1.3 $\pm$ 0.1	1.71 $\pm$ 0.14	1.2 $\pm$ 0.1	0.018 $\pm$ 0.013

### 2.3.6 Studies with the Smoking Cessation Drug Varenicline at the $\alpha 4\beta 2$ Receptor

We also evaluated the agonist binding mode of varenicline, a smoking cessation drug. Varenicline (marketed by Pfizer as Chantix<sup>®</sup> in the U.S.) was designed to target  $\alpha 4\beta 2$  receptors, and was approved for use in smoking cessation in 2006.<sup>3</sup> Using the fluorination approach and the CN/Br effect, we show that varenicline, like nicotine, binds to TrpB of the  $\alpha 4\beta 2$  receptor via a cation- $\pi$  interaction (**Table 2.7, Figure 2.7**).

**Table 2.7.** Functional characterization of varenicline at TrpB in  $\alpha 4\beta 2$  (A2B3).  $EC_{50}$  values ( $\mu M$ ), Hill coefficients ( $n_H$ ) and current size at +70 mV (normalized to current size at -110 mV).

Mutation	Varenicline	$n_H$	Norm. I (+70mV)
<b>Wild type</b>			
A2B3	$2.9 \pm 0.1$	$1.4 \pm 0.1$	$0.037 \pm 0.007$
A3B2	$0.75 \pm 0.06$	$1.4 \pm 0.1$	$0.166 \pm 0.014$
<b>TrpB A2B3</b>			
Trp	$2.4 \pm 0.2$	$1.2 \pm 0.1$	$0.043 \pm 0.005$
F <sub>1</sub> -Trp	$5.7 \pm 0.2$	$1.2 \pm 0.1$	$0.040 \pm 0.007$
F <sub>2</sub> -Trp	$9.0 \pm 0.4$	$1.2 \pm 0.1$	$0.050 \pm 0.011$
F <sub>3</sub> -Trp	$27 \pm 1$	$1.3 \pm 0.1$	$0.044 \pm 0.009$
F <sub>4</sub> -Trp	$56 \pm 5$	$1.1 \pm 0.1$	$0.033 \pm 0.008$
Br-Trp	$7.1 \pm 0.5$	$1.1 \pm 0.1$	$0.039 \pm 0.007$
CN-Trp	$31 \pm 2$	$1.1 \pm 0.1$	$0.040 \pm 0.009$

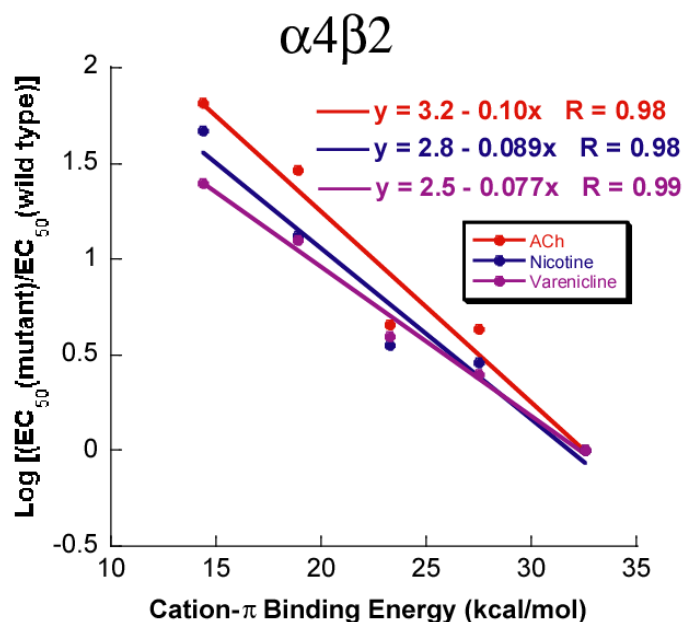


**Figure 2.7.** Fluorination plot for varenicline at  $\alpha 4\beta 2$  (A2B3). All data sets share the point  $x = 32.6$  kcal/mol (cation- $\pi$  binding energy for Trp). Moving to the left then corresponds to monofluoro-, difluoro-, trifluoro-, and tetrafluoro-TrpB. ACh (red), nicotine (blue), varenicline (purple). Cation- $\pi$  binding energies ( $x$ -axes) are from Zhong 1998.<sup>9</sup>

We have previously argued that the magnitude of the perturbation to  $EC_{50}$  induced by fluorination can be taken as an indicator of the relative strength of a cation- $\pi$

interaction. In **Table 2.8** we characterize the strength of a cation- $\pi$  interaction by the ratio of  $EC_{50}$  values for the F<sub>4</sub>-Trp mutant vs. the wild type. The F<sub>4</sub>-Trp residue represents a side chain in which the electrostatic component of the cation- $\pi$  interaction has been completely removed, but other features of the residue are essentially intact (**Figure 2.8**). All drug-receptor pairings reported here show a significant “cation- $\pi$  ratio,” thus establishing a common anchor point for the binding of the drugs considered here to the  $\alpha 4\beta 2$  receptor.

**Table 2.8.** Evaluation of binding interactions in the  $\alpha 4\beta 2$  (A2B3) receptor. a. Values are corrected for the effects of  $\alpha 4L9'A$  mutation according to the procedure of Moroni *et al.*<sup>24</sup> As such, these are  $EC_{50}$  for true wild type receptors. b. Ratio of  $EC_{50}$  values for F<sub>4</sub>-Trp/Trp at position TrpB in  $\alpha 4$ . c. Ratio of  $EC_{50}$  values for Tah/Thr at position Thr (TrpB + 1) in  $\alpha 4$ .

	Measured $EC_{50}$ ( $\mu M$ )	Wild type $EC_{50}$ ( $\mu M$ ) <sup>a</sup>	Cation- $\pi$ interaction <sup>b</sup>	$N^+-H\cdots O=C$ (Backbone H-bond) <sup>c</sup>
<b>ACh</b>	0.42	4.0	69	1.1
<b>Nicotine</b>	0.08	0.76	53	19
<b>Varenicline</b>	0.00285	0.027	20	14

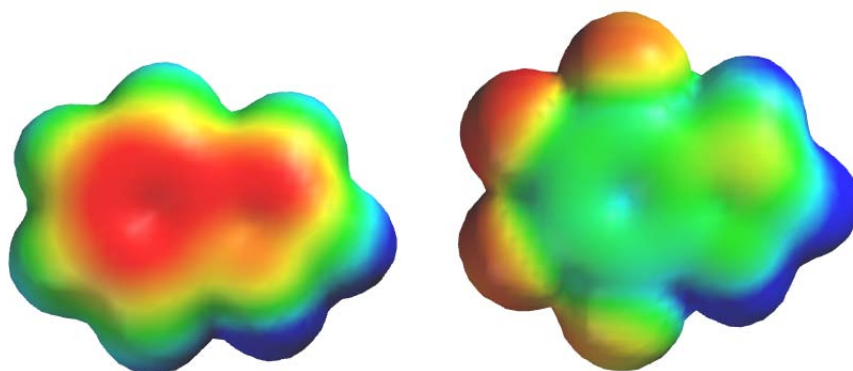


**Figure 2.8.** Electrostatic potential surfaces of indole (left) and F<sub>4</sub>-indole, corresponding to the aromatic portions of the side chains of Trp and F<sub>4</sub>-Trp, respectively. Results are from HF-6-31G\*\* calculations. Electrostatic potential ranges from -25 kcal/mol (red) to +25 kcal/mol (blue), so that green represents ~0 electrostatic potential.

Using the backbone amide-to-ester strategy for perturbing a hydrogen bond, we examined whether the N<sup>+</sup>H moiety of varenicline functions as a hydrogen bond donor to  $\alpha 4\beta 2$ . Replacing the (TrpB + 1) residue, which is threonine with threonine- $\alpha$ -hydroxy (Tah) significantly impacts EC<sub>50</sub>, suggesting the hydrogen bond donor interaction to the backbone carbonyl of TrpB is significant. To facilitate comparison, we have expressed variations as a ratio of EC<sub>50</sub> values, comparing the receptor with Tah at residue the (TrpB + 1) residue to the wild type Thr (**Table 2.9**). Varenicline, like nicotine, shows an EC<sub>50</sub> ratio significantly greater than 1, with only modest variations in magnitude (**Table 2.8**).

**Table 2.9.** Functional characterization of varenicline at Thr (TrpB + 1) in  $\alpha 4\beta 2$  (A2B3). EC<sub>50</sub> values ( $\mu$ M), Hill coefficients ( $n_H$ ) and current size at +70 mV (normalized to current size at -110 mV).

<b>Mutation</b>	<b>Varenicline</b>	<b><math>n_H</math></b>	<b>Norm. I (+70mV)</b>
<b>Wild type</b>			
<b>A2B3</b>	2.9 $\pm$ 0.1	1.4 $\pm$ 0.1	0.037 $\pm$ 0.007
<b>A3B2</b>	0.75 $\pm$ 0.06	1.4 $\pm$ 0.1	0.166 $\pm$ 0.014
<b>Thr (TrpB + 1) A2B3</b>			
<b>Thr</b>	2.2 $\pm$ 0.1	1.3 $\pm$ 0.1	0.020 $\pm$ 0.002
<b>Tah</b>	30 $\pm$ 2	1.2 $\pm$ 0.1	0.029 $\pm$ 0.006

### 2.3.7 A Residue Outside of the Aromatic Box Differentiates the $\alpha 4\beta 2$ and Muscle-type Receptors

The differential affinity of nicotine for  $\alpha 4\beta 2$  versus muscle-type receptors results from stronger interactions in the former with TrpB—both cation- $\pi$  and hydrogen bonding. Because the two receptors are identical with regard to the five residues that make up the aromatic box, a factor “outside the box” must be influencing its precise geometry, such that nicotine can approach TrpB more closely in  $\alpha 4\beta 2$  than in muscle-type nAChR. Pioneering work has identified residues responsible for the fact that  $\alpha 4\beta 2$  receptors show consistently higher affinity than the homopentameric  $\alpha 7$  neuronal

receptors.<sup>36</sup> At a particular residue in loop B—position 153, just four residues from TrpB—mutations strongly influence affinity. In high-affinity  $\alpha 4\beta 2$  receptors this residue is a Lys, and this residue is proposed to help shape the aromatic box by forming a backbone hydrogen bond between loops B and C (**Figure 2.1**). In the lower affinity  $\alpha 7$  neuronal receptor, residue 153 is a Gly, and molecular dynamics simulations of  $\alpha 7$  suggest that a Gly at 153 discourages the formation of the hydrogen bond between loops B and C.<sup>36</sup> Interestingly, the aligning residue in the muscle-type receptor is also Gly, and a naturally occurring G153S mutation is gain-of-function and associated with a congenital myasthenic syndrome.<sup>37</sup> We now report that the muscle-type  $\alpha 1$  G153K mutant shows much higher affinity for nicotine, and that, when this mutation is present, the cation– $\pi$  interaction to TrpB is strong. The data are summarized in **Table 2.10** and **Figure 2.9**. As expected, the ACh cation– $\pi$  interaction is maintained in the muscle-type receptor with the G153K mutation. These data indicate that the loop B–loop C hydrogen bond that is naturally present in  $\alpha 4\beta 2$  shapes the aromatic box so that nicotine can make a closer contact to TrpB, and that this structural feature is absent or weaker in the muscle-type receptor.

**Table 2.10.** Functional characterization of the muscle-type receptor containing the G153K point mutation in the  $\alpha 1$  subunit.  $EC_{50}$  values ( $\mu M$ ), Hill coefficients ( $n_H$ ). All studies of the muscle-type receptor contain a L9'S mutation in the  $\beta$  subunit.

Mutation	ACh	$n_H$	Nicotine	$n_H$
<b>Conventional Mutagenesis</b>				
$\alpha 1G153K$	$0.021 \pm 0.001$	$1.3 \pm 0.1$	$0.76 \pm 0.05$	$1.7 \pm 0.2$
<b>TrpB Muscle-type (<math>\alpha 1G153K</math>)</b>				
Trp	$0.019 \pm 0.001$	$1.5 \pm 0.1$	$0.59 \pm 0.04$	$1.8 \pm 0.2$
F <sub>1</sub> -Trp	$0.094 \pm 0.004$	$1.6 \pm 0.1$	$2.8 \pm 0.1$	$1.3 \pm 0.1$
F <sub>2</sub> -Trp	$0.079 \pm 0.004$	$1.3 \pm 0.1$	$2.3 \pm 0.1$	$1.3 \pm 0.1$
F <sub>3</sub> -Trp	$1.05 \pm 0.03$	$1.3 \pm 0.1$	$11 \pm 1$	$1.5 \pm 0.1$
F <sub>4</sub> -Trp	$7.5 \pm 0.5$	$1.2 \pm 0.1$	$32 \pm 4$	$1.5 \pm 0.2$
CN-Trp	$2.4 \pm 0.1$	$1.5 \pm 0.1$	$36 \pm 3$	$1.7 \pm 0.2$
Br-Trp	$0.047 \pm 0.001$	$1.4 \pm 0.1$	$4.5 \pm 0.4$	$1.2 \pm 0.1$

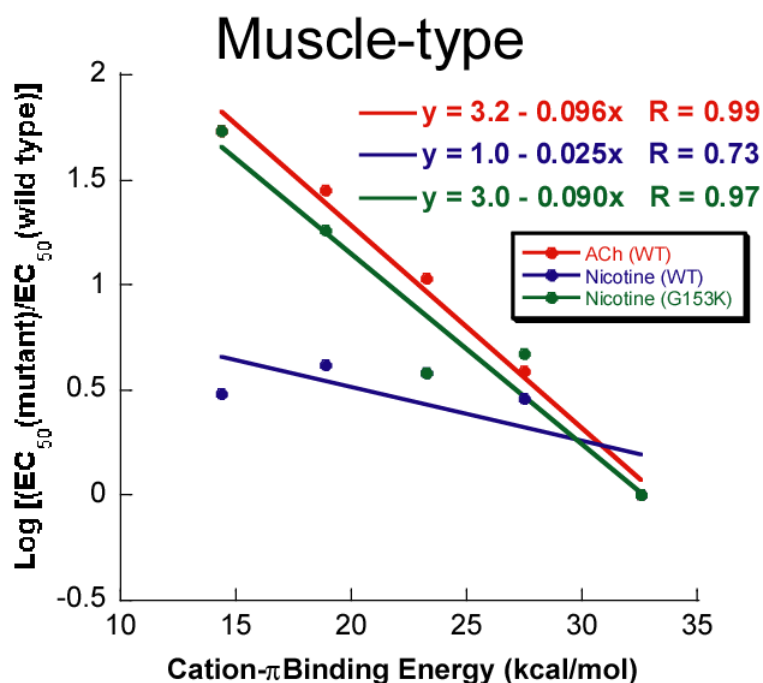


**Figure 2.9.** Fluorination plot testing nicotine at the muscle-type receptor containing the G153K point mutation in the  $\alpha 1$  subunit. All data sets share the point  $x = 32.6$  kcal/mol (cation- $\pi$  binding energy for Trp). Moving to the left then corresponds to monofluoro-, difluoro-, trifluoro-, and tetrafluoro-TrpB. ACh at the WT receptor (red), nicotine at the WT receptor (blue), previously reported in Zhong 1998 and Beene 2002.<sup>9, 13</sup> WT indicates glycine at position 153. Nicotine at the  $\alpha 1G153K$  receptor (green). Cation- $\pi$  binding energies ( $x$ -axes) are from Zhong 1998.<sup>9</sup>

### 2.3.8 Summary

Taken together, the present results indicate that the higher affinity of nicotine in the brain relative to the neuromuscular junction is a consequence of enhanced interactions with TrpB. A cation- $\pi$  interaction that is absent in the muscle-type receptor is quite strong in  $\alpha 4\beta 2$ . In addition, a hydrogen bond to a backbone carbonyl that is weak in the muscle-type is enhanced in  $\alpha 4\beta 2$ . Varenicline, the smoking cessation drug designed to target  $\alpha 4\beta 2$  receptors and block nicotine binding, also employ the same cation- $\pi$  and hydrogen bonding interactions. Both effects are quite substantial, and in combination they are more than adequate to account fully for the differential sensitivity to nicotine of the two receptors. The side chain of residue 153 in loop B distinguishes the two receptor types and apparently influences the shape of the binding site aromatic box, allowing a stronger interaction between nicotine and TrpB in high-affinity receptors.

## 2.4 METHODS

### *mRNA Synthesis and Mutagenesis*

All nAChR subunit genes were in the pAMV vector (rat  $\alpha 4$  and  $\beta 2$ ; mouse  $\alpha 1$ ,  $\beta 1$ ,  $\gamma$  and  $\delta$ ). nAChR subunit mRNA was obtained from NotI linearizations of the expression vector pAMV, followed by *in vitro* transcription using the mMessage mMachine T7 kit (Ambion, Austin, TX). The mutations for each subunit were introduced according to the QuikChange mutagenesis protocol (Stratagene, La Jolla, CA).

### *Ion Channel Expression*

To express the ion channels with a wild type ligand binding box,  $\alpha 4L9'A$  mRNA was coinjected with  $\beta 2$  mRNA at various ratios, see **Table 2.1** (total mRNA 10-

25 ng/cell). For muscle-type nAChR experiments,  $\alpha 1:\beta 1:\gamma:\delta$  mRNA was injected at a ratio of 2:1:1:1 by mass for wild type protein. Note that for all experiments reported, we use a previously reported L9'S mutation in the  $\beta 1$  subunit to increase receptor sensitivity.<sup>9</sup> For nonsense suppression experiments of the muscle-type receptor, an mRNA ratio of 10:1:1:1 was employed. For wild type and nonsense suppression experiments, the total mRNA injected was 30-65 ng/oocyte. Stage V-VI oocytes *Xenopus laevis* were injected and incubated in ND96 solution (96 mM NaCl, 2 mM KCl, 1 mM MgCl<sub>2</sub>, 1.8 mM CaCl<sub>2</sub>, and 5 mM HEPES, pH 7.5) with 0.005% (w/v) gentamycin and 2% (v/v) horse serum at 18 °C for 24-48 hours.

#### ***Unnatural Amino Acid / $\alpha$ -hydroxy Acid Incorporation***

Nitroveratryloxycarbonyl (NVOC) protected cyanomethyl ester form of unnatural amino acids and  $\alpha$ -hydroxythreonine cyanomethyl ester were synthesized, coupled to the dinucleotide dCA, and enzymatically ligated to 74-mer THG73 tRNA<sub>CUA</sub>.<sup>17, 38</sup> The unnatural amino acid-conjugated tRNA was deprotected by photolysis immediately prior to coinjection with mRNA containing the UAG mutation at the site of interest. Approximately 10-25 ng mRNA and 25 ng tRNA-amino acid or tRNA-hydroxy acid were injected into stage V-VI oocytes in a total volume of 70 nL.

The fidelity of unnatural amino acid incorporation was confirmed at each site with a "wild type recovery" experiment and a "read-through/reaminoacylation" test. In the "wild type recovery" experiment, UAG mutant mRNA was coinjected with tRNA charged with the amino acid that is present at this residue in the wild type protein. Generation of receptors that were indistinguishable from the wild type protein indicated that the residue carried by the suppressor tRNA was successfully and exclusively

integrated into the protein. In the “read-through/reaminoacylation” test, the UAG mutant mRNA was introduced with (1) no tRNA, (2) tRNA THG73 that was not charged with any amino acid or (3) tRNA THG73 enzymatically ligated with dinucleotide dCA. Lack of currents in these experiments validated the reliability of the nonsense suppression experiments.

### ***Whole-Cell Electrophysiological Characterization of Ion Channels***

Agonist-induced currents were recorded in two-electrode voltage clamp mode using the OpusXpress 6000A (Molecular Devices Axon Instruments) at a holding potential of -60 mV. Agonists were prepared in Ca<sup>2+</sup>-free ND96 solution and applied for 12 seconds followed by a 2 minute wash with Ca<sup>2+</sup>-free ND96 solution between each concentration. Acetylcholine chloride and (-)-nicotine tartrate were purchased from Sigma/Aldrich/RBI (St. Louis, MO). Varenicline tartrate was obtained from Targacept. Dose-response data were obtained for at least 6 concentrations of agonists and for a minimum of 5 oocytes. Mutants with I<sub>max</sub> of at least 100 nA of current were defined as functional. EC<sub>50</sub> and Hill coefficient were calculated by fitting the dose-response relation to the Hill equation. All data are reported as mean ± SE.

Voltage jump experiments were performed in the absence of ACh and at EC<sub>50</sub> concentration of ACh. The membrane potential was held at -60 mV, and stepped to 10 test potentials at 20 mV increments between +70 mV and -110 mV for 400 ms each. 600 ms at the -60 mV holding potential was allowed between each test potential. Background traces (no ACh) were subtracted from data traces, which were used to measure the steady-state amplitudes of the ACh-induced currents approaching the end of the test pulses. Normalized I-V curves were generated using current amplitudes

normalized to that at -110 mV. For each  $\alpha 4L9'A\beta 2$  mutant, normalized  $I_{-70\text{mV}} \pm \text{SE}$  from at least 5 cells was reported.

## **2.5 ACKNOWLEDGEMENTS**

We thank B. N. Cohen for advice on single-channel recording and analysis. This work was supported by the NIH (NS 34407; NS 11756) and the California Tobacco-Related Disease Research Program of the University of California, grant number 16RT-0160. J.A.P.S. was partially supported by an NRSA training grant. Varenicline tartrate was a generous gift from Targacept.

## 2.6 REFERENCES

1. Romanelli, M. N.; Gratteri, P.; Guandalini, L.; Martini, E.; Bonaccini, C.; Gualtieri, F., Central Nicotinic Receptors: Structure, Function, Ligands, and Therapeutic Potential. *ChemMedChem* **2007**, 2, (6), 746-767.
2. Corringer, P. J.; Le Novere, N.; Changeux, J. P., Nicotinic receptors at the amino acid level. *Annu Rev Pharmacol Toxicol* **2000**, 40, 431-58.
3. Coe, J. W.; Brooks, P. R.; Vetelino, M. G.; Wirtz, M. C.; Arnold, E. P.; Huang, J.; Sands, S. B.; Davis, T. I.; Lebel, L. A.; Fox, C. B.; Shrikhande, A.; Heym, J. H.; Schaeffer, E.; Rollema, H.; Lu, Y.; Mansbach, R. S.; Chambers, L. K.; Rovetti, C. C.; Schulz, D. W.; Tingley, F. D., 3rd; O'Neill, B. T., Varenicline: an alpha4beta2 nicotinic receptor partial agonist for smoking cessation. *J Med Chem* **2005**, 48, (10), 3474-7.
4. Gotti, C.; Zoli, M.; Clementi, F., Brain nicotinic acetylcholine receptors: native subtypes and their relevance. *Trends Pharmacol Sci* **2006**, 27, (9), 482-91.
5. Mansvelder, H. D.; Keath, J. R.; McGehee, D. S., Synaptic mechanisms underlie nicotine-induced excitability of brain reward areas. *Neuron* **2002**, 33, (6), 905-19.
6. Tapper, A. R.; McKinney, S. L.; Nashmi, R.; Schwarz, J.; Deshpande, P.; Labarca, C.; Whiteaker, P.; Marks, M. J.; Collins, A. C.; Lester, H. A., Nicotine activation of alpha4\* receptors: sufficient for reward, tolerance, and sensitization. *Science* **2004**, 306, (5698), 1029-32.
7. Nashmi, R.; Xiao, C.; Deshpande, P.; McKinney, S.; Grady, S. R.; Whiteaker, P.; Huang, Q.; McClure-Begley, T.; Lindstrom, J. M.; Labarca, C.; Collins, A. C.; Marks, M. J.; Lester, H. A., Chronic nicotine cell specifically upregulates functional alpha 4\* nicotinic receptors: basis for both tolerance in midbrain and enhanced long-term potentiation in perforant path. *J Neurosci* **2007**, 27, (31), 8202-18.
8. Kuryatov, A.; Luo, J.; Cooper, J.; Lindstrom, J., Nicotine acts as a pharmacological chaperone to up-regulate human alpha4beta2 acetylcholine receptors. *Mol Pharmacol* **2005**, 68, (6), 1839-51.
9. Zhong, W.; Gallivan, J. P.; Zhang, Y.; Li, L.; Lester, H. A.; Dougherty, D. A., From ab initio quantum mechanics to molecular neurobiology: a cation-pi binding site in the nicotinic receptor. *Proc Natl Acad Sci U S A* **1998**, 95, (21), 12088-93.
10. Brejc, K.; van Dijk, W. J.; Klaassen, R. V.; Schuurmans, M.; van Der Oost, J.; Smit, A. B.; Sixma, T. K., Crystal structure of an ACh-binding protein reveals the ligand-binding domain of nicotinic receptors. *Nature* **2001**, 411, (6835), 269-76.
11. Sixma, T. K.; Smit, A. B., Acetylcholine binding protein (AChBP): a secreted glial protein that provides a high-resolution model for the extracellular domain of pentameric ligand-gated ion channels. *Annu Rev Biophys Biomol Struct* **2003**, 32, 311-34.
12. Dougherty, D. A., Cys-loop neuroreceptors: structure to the rescue? *Chem Rev* **2008**, 108, (5), 1642-53.
13. Beene, D. L.; Brandt, G. S.; Zhong, W.; Zacharias, N. M.; Lester, H. A.; Dougherty, D. A., Cation-pi interactions in ligand recognition by serotonergic (5-HT3A) and nicotinic acetylcholine receptors: the anomalous binding properties of nicotine. *Biochemistry* **2002**, 41, (32), 10262-9.

14. Gonzales, D.; Rennard, S. I.; Nides, M.; Oncken, C.; Azoulay, S.; Billing, C. B.; Watsky, E. J.; Gong, J.; Williams, K. E.; Reeves, K. R., Varenicline, an  $\alpha 4\beta 2$  nicotinic acetylcholine receptor partial agonist, vs sustained-release bupropion and placebo for smoking cessation: a randomized controlled trial. *JAMA* **2006**, 296, (1), 47-55.
15. Mihalak, K. B.; Carroll, F. I.; Luetje, C. W., Varenicline is a partial agonist at  $\alpha 4\beta 2$  and a full agonist at  $\alpha 7$  neuronal nicotinic receptors. *Mol Pharmacol* **2006**, 70, (3), 801-5.
16. Dougherty, D. A., Physical organic chemistry on the brain. *J Org Chem* **2008**, 73, (10), 3667-73.
17. Nowak, M. W.; Gallivan, J. P.; Silverman, S. K.; Labarca, C. G.; Dougherty, D. A.; Lester, H. A., In vivo incorporation of unnatural amino acids into ion channels in *Xenopus* oocyte expression system. *Methods Enzymol* **1998**, 293, 504-29.
18. Fonck, C.; Cohen, B. N.; Nashmi, R.; Whiteaker, P.; Wagenaar, D. A.; Rodrigues-Pinguet, N.; Deshpande, P.; McKinney, S.; Kwoh, S.; Munoz, J.; Labarca, C.; Collins, A. C.; Marks, M. J.; Lester, H. A., Novel seizure phenotype and sleep disruptions in knock-in mice with hypersensitive  $\alpha 4^*$  nicotinic receptors. *J Neurosci* **2005**, 25, (49), 11396-411.
19. Filatov, G. N.; White, M. M., The role of conserved leucines in the M2 domain of the acetylcholine receptor in channel gating. *Mol Pharmacol* **1995**, 48, (3), 379-84.
20. Labarca, C.; Nowak, M. W.; Zhang, H.; Tang, L.; Deshpande, P.; Lester, H. A., Channel gating governed symmetrically by conserved leucine residues in the M2 domain of nicotinic receptors. *Nature* **1995**, 376, (6540), 514-6.
21. Kearney, P. C.; Nowak, M. W.; Zhong, W.; Silverman, S. K.; Lester, H. A.; Dougherty, D. A., Dose-response relations for unnatural amino acids at the agonist binding site of the nicotinic acetylcholine receptor: tests with novel side chains and with several agonists. *Mol Pharmacol* **1996**, 50, (5), 1401-12.
22. Grutter, T.; Changeux, J. P., Nicotinic receptors in wonderland. *Trends Biochem Sci* **2001**, 26, (8), 459-63.
23. Karlin, A., Emerging structure of the nicotinic acetylcholine receptors. *Nat Rev Neurosci* **2002**, 3, (2), 102-14.
24. Moroni, M.; Zwart, R.; Sher, E.; Cassels, B. K.; Bermudez, I.,  $\alpha 4\beta 2$  nicotinic receptors with high and low acetylcholine sensitivity: pharmacology, stoichiometry, and sensitivity to long-term exposure to nicotine. *Mol Pharmacol* **2006**, 70, (2), 755-68.
25. Nelson, M. E.; Kuryatov, A.; Choi, C. H.; Zhou, Y.; Lindstrom, J., Alternate stoichiometries of  $\alpha 4\beta 2$  nicotinic acetylcholine receptors. *Mol Pharmacol* **2003**, 63, (2), 332-41.
26. Xiu, X.; Puskar, N. L.; Shanata, J. A.; Lester, H. A.; Dougherty, D. A., Nicotine binding to brain receptors requires a strong cation- $\pi$  interaction. *Nature* **2009**, 458, (7237), 534-7.
27. Nowak, M. W.; Kearney, P. C.; Sampson, J. R.; Saks, M. E.; Labarca, C. G.; Silverman, S. K.; Zhong, W.; Thorson, J.; Abelson, J. N.; Davidson, N.; et al., Nicotinic receptor binding site probed with unnatural amino acid incorporation in intact cells. *Science* **1995**, 268, (5209), 439-42.

28. Padgett, C. L.; Hanek, A. P.; Lester, H. A.; Dougherty, D. A.; Lummis, S. C., Unnatural amino acid mutagenesis of the GABA(A) receptor binding site residues reveals a novel cation- $\pi$  interaction between GABA and beta 2Tyr97. *J Neurosci* **2007**, 27, (4), 886-92.
29. Celie, P. H.; van Rossum-Fikkert, S. E.; van Dijk, W. J.; Brejc, K.; Smit, A. B.; Sixma, T. K., Nicotine and carbamylcholine binding to nicotinic acetylcholine receptors as studied in AChBP crystal structures. *Neuron* **2004**, 41, (6), 907-14.
30. Hansen, S. B.; Sulzenbacher, G.; Huxford, T.; Marchot, P.; Taylor, P.; Bourne, Y., Structures of Aplysia AChBP complexes with nicotinic agonists and antagonists reveal distinctive binding interfaces and conformations. *EMBO J* **2005**, 24, (20), 3635-46.
31. Talley, T. T.; Yalda, S.; Ho, K. Y.; Tor, Y.; Soti, F. S.; Kem, W. R.; Taylor, P., Spectroscopic analysis of benzylidene anabaseine complexes with acetylcholine binding proteins as models for ligand-nicotinic receptor interactions. *Biochemistry* **2006**, 45, (29), 8894-902.
32. Cashin, A. L.; Petersson, E. J.; Lester, H. A.; Dougherty, D. A., Using physical chemistry to differentiate nicotinic from cholinergic agonists at the nicotinic acetylcholine receptor. *J Am Chem Soc* **2005**, 127, (1), 350-6.
33. Deechongkit, S.; Nguyen, H.; Powers, E. T.; Dawson, P. E.; Gruebele, M.; Kelly, J. W., Context-dependent contributions of backbone hydrogen bonding to beta-sheet folding energetics. *Nature* **2004**, 430, (6995), 101-5.
34. England, P. M.; Zhang, Y.; Dougherty, D. A.; Lester, H. A., Backbone mutations in transmembrane domains of a ligand-gated ion channel: implications for the mechanism of gating. *Cell* **1999**, 96, (1), 89-98.
35. Koh, J. T.; Cornish, V. W.; Schultz, P. G., An experimental approach to evaluating the role of backbone interactions in proteins using unnatural amino acid mutagenesis. *Biochemistry* **1997**, 36, (38), 11314-22.
36. Grutter, T.; Prado de Carvalho, L.; Le Novere, N.; Corringer, P. J.; Edelstein, S.; Changeux, J. P., An H-bond between two residues from different loops of the acetylcholine binding site contributes to the activation mechanism of nicotinic receptors. *EMBO J* **2003**, 22, (9), 1990-2003.
37. Sine, S. M.; Ohno, K.; Bouzat, C.; Auerbach, A.; Milone, M.; Pruitt, J. N.; Engel, A. G., Mutation of the acetylcholine receptor alpha subunit causes a slow-channel myasthenic syndrome by enhancing agonist binding affinity. *Neuron* **1995**, 15, (1), 229-39.
38. Saks, M. E.; Sampson, J. R.; Nowak, M. W.; Kearney, P. C.; Du, F.; Abelson, J. N.; Lester, H. A.; Dougherty, D. A., An engineered Tetrahymena tRNA<sup>Gln</sup> for in vivo incorporation of unnatural amino acids into proteins by nonsense suppression. *J Biol Chem* **1996**, 271, (38), 23169-75.

## *Chapter 3*

### **Probing the Effects of Residues Located Outside the Agonist Binding Site on Drug-Receptor Selectivity in the Nicotinic Receptor**

#### **3.1 ABSTRACT**

The nicotinic acetylcholine receptors (nAChRs) are a family of closely related but pharmacologically distinct neurotransmitter-gated ion channels. They are therapeutic targets for a wide range of neurological disorders, and a key issue in drug development is selective targeting among the greater than 20 subtypes of nAChRs that are known. The present work evaluates a proposed hydrogen bonding interaction involving a residue known as the “loop B glycine” that distinguishes receptors that are highly responsive to ACh and nicotine from those that are much less so. We have performed structure-function studies on the loop B site, including unnatural amino acid mutagenesis, in three different nAChR subtypes and found that the correlation between agonist potency and this residue is strong. Low-potency receptor subtypes have a glycine at this key site, and mutation to a residue with a side chain converts a low-potency receptor to a high-potency receptor. Innately high-potency receptors have a lysine at the loop B site and show a decrease in potency for the reverse mutation (*i.e.*, introducing a glycine). This residue lies outside of the agonist binding site, and the details of how changes at the site impact agonist potency vary for differing receptor subtypes. This suggests a model in which the loop B residue influences the global shape of the agonist binding site rather than modulating any specific interaction.

### 3.2 INTRODUCTION

Nicotinic acetylcholine receptors (nAChRs) are a diverse family of pentameric, neurotransmitter-gated ion channels responsible for rapid synaptic transmission throughout the central and peripheral nervous systems.<sup>1-3</sup> Among the roughly two dozen subtypes that have been characterized as important in mammals,<sup>4</sup> a clear pharmacological distinction is observed. nAChRs can be categorized into two groups: receptors that display relatively lower potency for the natural agonist ACh as well as nicotine and related agonists, and receptors that exhibit much greater agonist potency.<sup>5</sup> Prototypes of the low-potency family include the nAChR of the neuromuscular junction, with a subunit composition of  $(\alpha 1)_2\beta 1\gamma\delta$  (*i.e.*, muscle-type), and the homopentameric CNS receptor  $(\alpha 7)_5$ . The prototype high-potency receptors are the  $\alpha 4$ -containing receptors of the CNS that play a prominent role in nicotine addiction.<sup>6</sup> All nAChRs show sequence *identity* among residues that are thought to make direct contact with bound agonists (**Figure 3.1**), and so the pharmacological selectivity must result from residues that are formally located outside of the agonist binding site.

	<u>Loop A</u>	<u>Loop B</u>	<u>Loop C</u>		<u>Loop D</u>
AChBP	W V P D L A A Y	W T H H S R E I	Y S C C P E - A Y E D	AChBP	W Q Q T T W
$\alpha 1$	W R P D V V L Y	W T Y D G S V V	Y S C C P T T P Y L D	$\gamma$	W I E M Q W
$\alpha 2$	W I P D I V L Y	W T Y D K A K I	Y D C C A E - I Y P D	$\delta$	W I D H A W
$\alpha 3$	W K P D I V L Y	W S Y D K A K I	Y N C C E E - I Y P D		
$\alpha 4$	W R P D I V L Y	W T Y D K A K I	Y E C C A E - I Y P D	$\beta 2$	W L T Q E W
$\alpha 6$	W K P D I V L Y	W T Y D K A E I	Y N C C E E - I Y T D	$\beta 4$	W L K Q E W
$\alpha 7$	W K P D I L L Y	W S Y G G W S L	Y E C C K E - P Y P D	$\alpha 7$	W L Q M S W
$\alpha 9$	W R P D I V L Y	W T Y N G N Q V	Y G C C S E - P Y P D	$\alpha 9$	W I R Q I W
$\alpha 10$	W R P D I V L Y	W T H G G H Q L	Y G C C S E - P Y P D	$\alpha 10$	W I R Q E W

**Figure 3.1.** Sequence alignment of the nAChR agonist binding site. AChBP sequence is from *Lymnaea stagnalis*.  $\alpha 1$ ,  $\gamma$ , and  $\delta$  are from mouse; the human sequence differs from mouse at only one residue in loop C: CCPTT (mouse) *vs.* CCPDT (human).  $\alpha 4$ ,  $\beta 2$ , and  $\alpha 7$  are rat; which are identical to human for the residues shown. All other sequences are human. The five conserved residues of the “aromatic box”: TyrA, TrpB, TyrC1, TyrC2, and TrpD are shown in blue. The loop B Gly/Lys site is shown in pink. The backbone carbonyl that hydrogen bonds to the N<sup>H</sup> of agonists is shown in yellow.

One such discriminating site is in the  $\alpha$  subunit on loop B of the agonist binding site (**Figure 3.2**).<sup>5</sup> In  $\alpha 1$  subunit numbering this is position G153, and we will refer to the site generically as the “loop B glycine.” It lies four residues from W149 (TrpB), which has been shown to make a cation- $\pi$  interaction to most agonists.<sup>7, 8</sup> In crystal structures of AChBPs, soluble proteins that have provided an excellent structural model of the nAChR agonist binding site,<sup>9, 10</sup> there is a backbone hydrogen bond between loop B and loop C formed by the NH of G153 and the CO of residue 197 (muscle-type numbering). Residue 198 is TyrC2, another conserved aromatic amino acid of the agonist binding site. This interesting interaction is also present in the recently reported crystal structure of the invertebrate GluCl channel,<sup>11</sup> another member of the superfamily of Cys-loop (pentameric) receptors for which the nAChR is the prototype. The loop B glycine is conserved in the low-potency  $(\alpha 7)_5$  receptor with the aligning residue G152, but not in the higher potency  $(\alpha 4)_2(\beta 2)_3$  receptor, where the aligning residue is K158 (**Figure 3.1**). MD simulations have suggested that this sequence difference contributes to the distinction between low- vs. high-potency receptors.<sup>5</sup> Having a side chain at the loop B residue (as in  $\alpha 4$  K158) facilitates the loop B-loop C hydrogen bond. However, the presence of glycine at this site weakens the hydrogen bond, and this impacts potency. Known mutations of the muscle-type receptor support this model.<sup>12</sup>

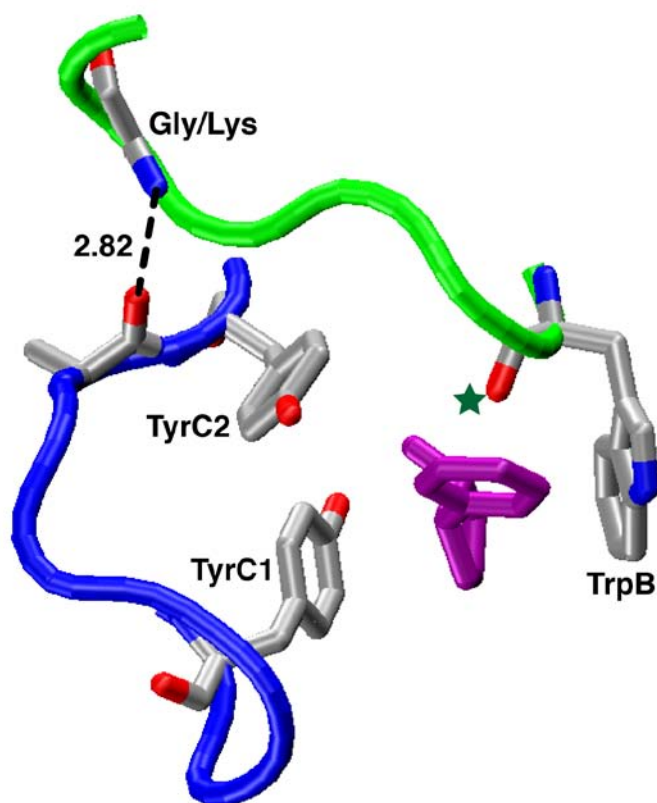


**Figure 3.2.** nAChR agonist binding site, based on the structure of AChBP (pdb: 1UW6).<sup>13</sup> Loop B is in green, loop C is in blue, nicotine is in purple, three of the five residues that form the “aromatic box” of the agonist binding site are highlighted. The backbone carbonyl (green star) that hydrogen bonds to the N<sup>+</sup>H of agonists, and the proposed loop B–loop C hydrogen bond is highlighted.

We recently showed that, indeed, a G153K mutation in the muscle-type receptor greatly increased potency of both ACh and nicotine.<sup>7</sup> The cause of the increased potency was a cation- $\pi$  interaction to TrpB that was absent or weak in the wild type muscle-type receptor, but was strong in both  $\alpha 4$ -containing receptors and in the muscle-type receptor with the G153K mutation.

In the present work we evaluate the role of the loop B glycine in both the muscle-type and  $(\alpha 7)_5$  receptors. G-to-K mutations enhance potency substantially, but the details of how the potency is enhanced differ in the two subtypes. We also evaluate whether the reverse K-to-G mutation has the opposite effect on the high-potency  $(\alpha 4)_2(\beta 2)_3$  receptor. Finally, we use unnatural amino acid mutagenesis to disrupt the proposed hydrogen bond in the  $(\alpha 4)_2(\beta 2)_3$  receptor and evaluate the functional consequences.

### 3.3 RESULTS AND DISCUSSION

#### 3.3.1 Probing the G153 Site in the Low-Potency $(\alpha 1)_2\beta 1\gamma\delta$ (Muscle-type) Receptor

In the  $(\alpha 1)_2\beta 1\gamma\delta$  receptor, we have previously shown<sup>7</sup> that the  $\alpha 1$  G153K mutation produces a significant gain-of-function for both ACh and nicotine, with  $EC_{50}$  increasing 44- and 74-fold, respectively (**Table 3.1**). We also showed that the G153K mutation strengthened the cation- $\pi$  interaction between each agonist and TrpB. We now report the effect of the G153K mutation on epibatidine (**Figure 3.3A**) at  $(\alpha 1)_2\beta 1\gamma\delta$ . Note that unlike nicotine, epibatidine is fairly potent at the wild type muscle-type nAChR, and it does show a cation- $\pi$  interaction to TrpB in the wild type receptor.<sup>14</sup> Nevertheless, the G153K mutation produces a 75-fold increase in epibatidine potency, comparable to what is seen for nicotine (**Table 3.1**). Fluorination of the TrpB position (**Figure 3.3B**) was examined in the background of the G153K mutant. Consistent with previous ACh and nicotine data,<sup>7</sup> our results indicate that the G153K mutation also strengthens the cation- $\pi$  interaction between epibatidine and TrpB of the receptor (**Table 3.2**). This is indicated by an increase in sensitivity to progressive fluorination of the key Trp residue, as illustrated in a “fluorination plot” (**Figure 3.4**).

**Table 3.1.** Mutation of the loop B Gly/Lys site.  $EC_{50}$  values ( $\mu\text{M}$ ) for  $(\alpha 1)_2\beta 1\gamma\delta$ ,  $(\alpha 7)_5$ , and  $(\alpha 4)_2(\beta 2)_3$ . Values in brackets represent the ratio of wild type  $EC_{50}$  to mutant  $EC_{50}$ , such that ratios of  $>1$  represent gain-of-function, and ratios of  $<1$  represent loss-of-function. For the K158Lah mutant, the reference “wild type” receptor is K158L. Complete data tables with Hill coefficients and standard errors are given in Tables 3.2, 3.4-3.6. WT = wild type; ND = not determined.

	$(\alpha 1)_2\beta 1\gamma\delta$		$(\alpha 7)_5$		$(\alpha 4)_2(\beta 2)_3$				
	WT	G153K	WT	G152K	WT	K158G	K158L	K158Lah	Y202Yah
<b>ACh</b>	1.2	0.027 [44]	66	3.7 [18]	0.42	1.3 [0.32]	0.13	0.060 [2.2]	0.73 [0.58]
<b>Nic</b>	56	0.76 [74]	23	0.76 [30]	0.08	0.30 [0.27]	0.035	0.011 [3.2]	0.42 [0.19]
<b>Epi</b>	0.83	0.011 [75]	0.26	0.016 [16]	0.00035	ND	ND	ND	ND



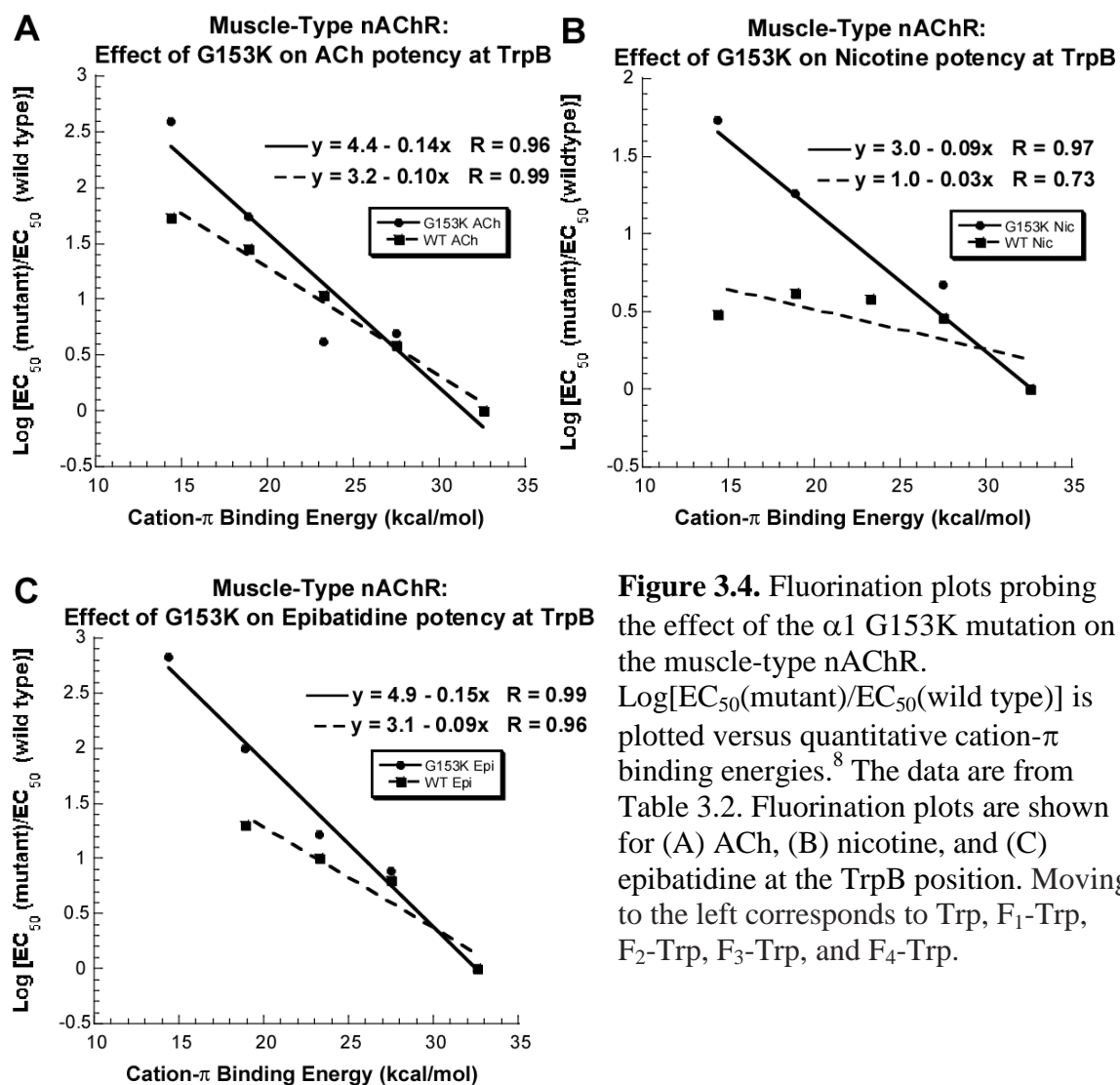


**Figure 3.4.** Fluorination plots probing the effect of the  $\alpha 1$  G153K mutation on the muscle-type nAChR.  $\text{Log}[\text{EC}_{50}(\text{mutant})/\text{EC}_{50}(\text{wild type})]$  is plotted versus quantitative cation- $\pi$  binding energies.<sup>8</sup> The data are from Table 3.2. Fluorination plots are shown for (A) ACh, (B) nicotine, and (C) epibatidine at the TrpB position. Moving to the left corresponds to Trp, F<sub>1</sub>-Trp, F<sub>2</sub>-Trp, F<sub>3</sub>-Trp, and F<sub>4</sub>-Trp.

The AChBP crystal structure suggested that the backbone carbonyl of the TrpB residue can serve as a hydrogen bond acceptor for agonist molecules that possess an available hydrogen bond donor, such as nicotine and epibatidine (**Figure 3.2**). We have confirmed the importance of this interaction in nAChRs by using backbone ester substitution, converting the contributing carbonyl from an amide to an ester, the latter being a much poorer hydrogen bond acceptor (**Figure 3.3C**).<sup>14</sup> In the high affinity  $(\alpha 4)_2(\beta 2)_3$  receptor this mutation has a large effect,<sup>7</sup> but previous studies on the

$(\alpha 1)_2\beta 1\gamma\delta$  receptor revealed that both nicotine and epibatidine make modest backbone hydrogen bonds to the carbonyl (1.6- and 3.7-fold shifts, respectively).<sup>14</sup> To monitor if this hydrogen bonding interaction is affected by the loop B glycine, we performed the same backbone mutation in combination with the G153K mutation in  $(\alpha 1)_2\beta 1\gamma\delta$ . The G153K mutation strengthens the hydrogen bond between both nicotine and epibatidine to the TrpB carbonyl (**Table 3.2, Table 3.3**). The amide-to-ester/G153K mutant results in 15- and 11-fold loss-of-function for nicotine and epibatidine, respectively. As anticipated, ACh is unperturbed by the backbone mutation, since ACh is a quaternary ammonium lacking a hydrogen bond donor.

**Table 3.3.** Amide-to-ester experiments for the backbone carbonyl of TrpB residue for  $(\alpha 1)_2\beta 1\gamma\delta$ ,  $(\alpha 7)_5$ , and  $(\alpha 4)_2(\beta 2)_3$ . EC<sub>50</sub> values ( $\mu\text{M}$ ). Values in brackets represent ratio of wild type EC<sub>50</sub> to mutant EC<sub>50</sub>, such that ratios of >1 represent gain-of-function, and ratios of <1 represent loss-of-function. Complete data tables with Hill coefficients and standard errors are given Tables 3.2, 3.4-3.5. ND = not determined.

	$(\alpha 1 \text{ G153K})_2\beta 1\gamma\delta$		$(\alpha 7 \text{ G152K})_5$		$(\alpha 4 \text{ K158G})_2(\beta 2)_3$	
	Thr	Tah	Thr	Tah	Thr	Tah
<b>ACh</b>	0.024	0.028 [0.86]	1.7	0.58 [2.9]	0.99	0.53 [1.9]
<b>Nic</b>	0.62	9.0 [0.069]	0.29	2.3 [0.13]	0.25	3.4 [0.074]
<b>Epi</b>	0.012	0.13 [0.092]	0.012	0.031 [0.39]	ND	ND

The MD simulations noted above suggested that the substantial increase in potency observed for G153K-containing receptors was not specific to lysine, but simply required a side chain at the loop B glycine. We find that, indeed, mutation of G153 to either alanine or threonine produced receptors with a substantial gain-of-function phenotype, similar to the G153K phenotype (**Table 3.2**).

### 3.3.2 Probing the G152 Site in the Low-Potency ( $\alpha 7$ )<sub>5</sub> Receptor

The homopentameric ( $\alpha 7$ )<sub>5</sub> receptor is distinctive in many ways, including its mode of agonist binding. While most nAChR subtypes employ a cation- $\pi$  interaction between TrpB and the agonist, the ( $\alpha 7$ )<sub>5</sub> receptor eschews this common ligand binding mechanism.<sup>16</sup> Instead, in ( $\alpha 7$ )<sub>5</sub>, ACh forms a cation- $\pi$  interaction to TyrA, and epibatidine forms a cation- $\pi$  interaction to TyrC2 of the agonist binding site. It is a “low-potency” receptor, with a G152 aligning at the loop B glycine site. Given the unusual binding pattern observed in ( $\alpha 7$ )<sub>5</sub>, it was interesting to investigate whether changing the side chain of the loop B glycine would increase agonist potency through a mechanism similar to that observed in ( $\alpha 1$ )<sub>2</sub> $\beta 1\gamma\delta$ . Introduction of lysine at this position (G152K) in ( $\alpha 7$ )<sub>5</sub> did result in a significant gain-of-function when tested with ACh, nicotine, and epibatidine (**Table 3.1**).

To determine whether an amplification of the cation- $\pi$  interaction analogous to that seen in the muscle-type receptor would occur in ( $\alpha 7$ )<sub>5</sub>, we incorporated either F<sub>3</sub>Trp at TrpB or F<sub>3</sub>Phe at TyrA and TyrC2 in the background of the G152K mutant. In contrast to ( $\alpha 1$ )<sub>2</sub> $\beta 1\gamma\delta$ , the consequences of fluorination at TrpB in the G152K mutant did not differ from wild type ( $\alpha 7$ )<sub>5</sub> for ACh, nicotine, or epibatidine (**Table 3.4**). Similarly, introduction of G152K in ( $\alpha 7$ )<sub>5</sub> does not enhance the naturally occurring cation- $\pi$  interaction between ACh and TyrA.

**Table 3.4.** EC<sub>50</sub> values ( $\mu\text{M}$ ) and Hill coefficients for mutant ( $\alpha 7$ )<sub>5</sub> nAChRs. The EC<sub>50</sub> values are  $\pm$  S.E.

<b>(<math>\alpha 7</math>)<sub>5</sub> nAChR</b>							
<b>Residue</b>	<b>Mutation</b>	<b>ACh</b>	<b>n<sub>H</sub></b>	<b>Nicotine</b>	<b>n<sub>H</sub></b>	<b>Epibatidine</b>	<b>n<sub>H</sub></b>
<b>Wild type</b>		66 $\pm$ 1	2.9 $\pm$ 0.1	23 $\pm$ 1	3.1 $\pm$ 0.1	0.26 $\pm$ 0.01	3.3 $\pm$ 0.2
<b>G152K</b>		3.7 $\pm$ 0.1	1.8 $\pm$ 0.1	0.76 $\pm$ 0.03	2.4 $\pm$ 0.2	0.016 $\pm$ 0.001	2.9 $\pm$ 0.4
<b>(<math>\alpha 7</math> G152K)<sub>5</sub></b>							
<b>TyrA (Y92)</b>	<b>Tyr</b>	5.1 $\pm$ 0.3	2.1 $\pm$ 0.3	0.55 $\pm$ 0.01	3.3 $\pm$ 0.3	0.017 $\pm$ 0.001	2.8 $\pm$ 0.3
	<b>F<sub>3</sub>-Phe</b>	240 $\pm$ 11	2.9 $\pm$ 0.4	10 $\pm$ 1	2.8 $\pm$ 0.5	0.47 $\pm$ 0.01	3.4 $\pm$ 0.2
<b>TrpB (W148)</b>	<b>Trp</b>	4.1 $\pm$ 0.2	2.7 $\pm$ 0.3	0.77 $\pm$ 0.03	2.9 $\pm$ 0.3	0.016 $\pm$ 0.001	3.6 $\pm$ 0.5
	<b>F<sub>3</sub>-Trp</b>	9.0 $\pm$ 0.3	1.9 $\pm$ 0.1	1.2 $\pm$ 0.1	2.4 $\pm$ 0.2	0.23 $\pm$ 0.02	2.1 $\pm$ 0.2
<b>TyrC2 (Y194)</b>	<b>Tyr</b>	3.9 $\pm$ 0.1	3.2 $\pm$ 0.2	0.61 $\pm$ 0.01	3.5 $\pm$ 0.3	0.015 $\pm$ 0.001	3.8 $\pm$ 0.2
	<b>F<sub>1</sub>-Phe</b>	8.0 $\pm$ 0.5	1.9 $\pm$ 0.2	3.5 $\pm$ 0.1	2.9 $\pm$ 0.1	0.079 $\pm$ 0.001	3.4 $\pm$ 0.2
	<b>F<sub>3</sub>-Phe</b>	170 $\pm$ 8	2.2 $\pm$ 0.2	60 $\pm$ 2	2.1 $\pm$ 0.1	2.2 $\pm$ 0.1	2.6 $\pm$ 0.3
	<b>4-Br-Phe</b>	3.0 $\pm$ 0.2	1.9 $\pm$ 0.2	1.1 $\pm$ 0.1	3.4 $\pm$ 0.3	0.021 $\pm$ 0.001	2.6 $\pm$ 0.2
	<b>4-CN-Phe</b>	10 $\pm$ 1	2.0 $\pm$ 0.2	15 $\pm$ 1	2.6 $\pm$ 0.2	0.12 $\pm$ 0.01	3.4 $\pm$ 0.3
<b>Ser(B+1) (S149)</b>	<b>4-MeO-Phe</b>	6.0 $\pm$ 0.4	2.3 $\pm$ 0.3	2.5 $\pm$ 0.1	3.2 $\pm$ 0.1	0.025 $\pm$ 0.001	3.0 $\pm$ 0.2
	<b>S149T</b>	1.8 $\pm$ 0.1	2.1 $\pm$ 0.1	0.29 $\pm$ 0.01	4.1 $\pm$ 0.4	0.009 $\pm$ 0.001	3.1 $\pm$ 0.4
	<b>Thr</b>	1.7 $\pm$ 0.1	2.0 $\pm$ 0.1	0.29 $\pm$ 0.01	4.6 $\pm$ 0.4	0.012 $\pm$ 0.001	3.5 $\pm$ 0.4
	<b>Tah</b>	0.6 $\pm$ 0.1	1.7 $\pm$ 0.2	2.3 $\pm$ 0.1	2.0 $\pm$ 0.1	0.031 $\pm$ 0.002	2.7 $\pm$ 0.5

A large perturbation, however, was observed for incorporating F<sub>3</sub>Phe at TyrC2 in the G152K mutant. Full fluorination plots were produced for ACh and epibatidine, and compared to wild type ( $\alpha 7$ )<sub>5</sub> plots (**Figure 3.5**). For ACh as agonist, the G152K mutant enhanced this binding interaction. A similar but less pronounced trend was observed for epibatidine as agonist.

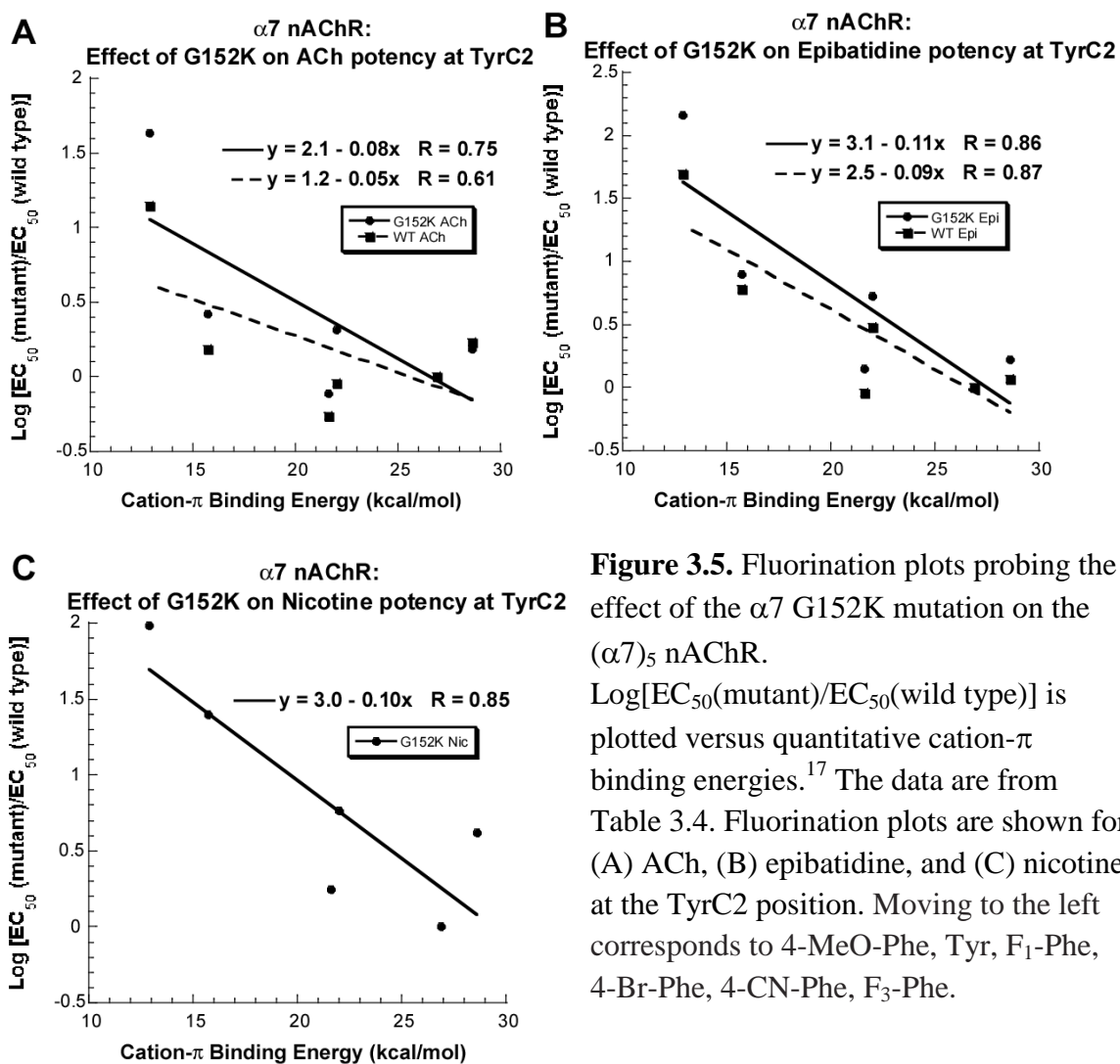


**Figure 3.5.** Fluorination plots probing the effect of the  $\alpha 7$  G152K mutation on the  $(\alpha 7)_5$  nAChR. Log $[EC_{50}(\text{mutant})/EC_{50}(\text{wild type})]$  is plotted versus quantitative cation- $\pi$  binding energies.<sup>17</sup> The data are from Table 3.4. Fluorination plots are shown for (A) ACh, (B) epibatidine, and (C) nicotine at the TyrC2 position. Moving to the left corresponds to 4-MeO-Phe, Tyr, F<sub>1</sub>-Phe, 4-Br-Phe, 4-CN-Phe, F<sub>3</sub>-Phe.

Additionally, we probed the effect of the G152K mutation on the backbone hydrogen bond to the carbonyl of TrpB using the amide-to-ester strategy. In wild type  $(\alpha 7)_5$ , epibatidine participates in a modest backbone hydrogen bond (2.1-fold shift).<sup>16</sup> Interestingly, the G152K mutation does not affect the backbone hydrogen bond, displaying a 2.6-fold loss-of-function for epibatidine (**Table 3.3**). Consistent with previous trends, the backbone mutation had no effect on ACh binding.

Nicotine is not very potent at the  $(\alpha 7)_5$  receptor, which limits the kinds of studies we have been able to perform in the past. Introduction of the G152K mutation in  $(\alpha 7)_5$  produced hypersensitive receptors sufficient for examining nicotine as the agonist. As such,  $(\alpha 7\text{G152K})_5$  mutant receptors allowed accurate measurement of nicotine-induced currents even after incorporation of highly fluorinated Phe derivatives. For such receptors, nicotine participates in a cation- $\pi$  interaction with TyrC2, as indicated by a fluorination plot (**Figure 3.5C**). For the backbone hydrogen bond, nicotine displayed a 7.8-fold loss-of-function in the background of the G152K mutation (**Table 3.3**).

### 3.3.3 Probing the K158 Site in the High-Potency $(\alpha 4)_2(\beta 2)_3$ Receptor

A G-to-K mutation significantly increases potency of agonists in both the muscle-type and  $(\alpha 7)_5$  receptors. It seemed possible that the reverse mutation, K158G, in the high-potency  $(\alpha 4)_2(\beta 2)_3$  receptor would diminish potency. We now report that the K158G mutation in  $(\alpha 4)_2(\beta 2)_3$  receptors is, indeed, a loss-of-function mutation (**Table 3.1**). However, the magnitude of the impact is significantly less than that seen for the G-to-K mutations in the low-potency receptors.

For  $(\alpha 4)_2(\beta 2)_3$  receptors containing the K158G mutation, fluorinated tryptophan derivatives were incorporated at TrpB, the site of a cation- $\pi$  interaction for ACh and nicotine (**Table 3.5**).<sup>7</sup> Note that epibatidine also participates in a cation- $\pi$  interaction and hydrogen bond at TrpB in  $\alpha 4\beta 2$  (**Table 3.5**), but we chose not to test the effect of the K158G mutation on epibatidine binding as it would likely mimic that of nicotine. As such, the K158G mutation attenuated but did not completely abolish the existing cation- $\pi$  interaction for both ACh and nicotine (**Figure 3.6**).

**Table 3.5.** EC<sub>50</sub> values (μM) and Hill coefficients for mutant (α4)<sub>2</sub>(β2)<sub>3</sub> nAChRs. The EC<sub>50</sub> values are ± S.E. †Previously reported in Xiu 2009.<sup>7</sup> All other values in this table were determined in the present work.

<b>α4β2 nAChR</b>					
<b>Mutation</b>	<b>ACh</b>	<b>n<sub>H</sub></b>	<b>Nicotine</b>	<b>n<sub>H</sub></b>	<b>Norm. I (+70mV)</b>
(α4) <sub>3</sub> (β2) <sub>2</sub>	0.023 ± 0.001 <sup>†</sup>	1.3 ± 0.1 <sup>†</sup>	0.01 ± 0.001 <sup>†</sup>	1.7 ± 0.2 <sup>†</sup>	0.297 ± 0.041 <sup>†</sup>
(α4) <sub>2</sub> (β2) <sub>3</sub>	0.42 ± 0.01 <sup>†</sup>	1.2 ± 0.1 <sup>†</sup>	0.08 ± 0.01 <sup>†</sup>	1.2 ± 0.1 <sup>†</sup>	0.041 ± 0.005 <sup>†</sup>
(α4) <sub>3</sub> (β2) <sub>2</sub> K158G	0.11 ± 0.01	0.99 ± 0.05	0.045 ± 0.001	1.5 ± 0.1	0.268 ± 0.015
(α4) <sub>2</sub> (β2) <sub>3</sub> K158G	1.3 ± 0.1	1.1 ± 0.1	0.30 ± 0.02	1.6 ± 0.1	0.015 ± 0.006
<b>(α4 K158G)<sub>2</sub>(β2)<sub>3</sub> – TrpB (W154)</b>					
Trp	1.3 ± 0.1	1.2 ± 0.1	0.27 ± 0.02	1.6 ± 0.2	0.014 ± 0.006
F <sub>1</sub> -Trp	3.7 ± 0.1	1.2 ± 0.1	0.50 ± 0.04	1.4 ± 0.1	0.034 ± 0.005
F <sub>2</sub> -Trp	5.4 ± 0.2	1.2 ± 0.1	0.67 ± 0.06	1.3 ± 0.1	0.024 ± 0.008
F <sub>3</sub> -Trp	23 ± 1	1.3 ± 0.1	2.6 ± 0.2	1.2 ± 0.1	0.017 ± 0.009
F <sub>4</sub> -Trp	25 ± 3	0.99 ± 0.08	4.5 ± 0.5	1.2 ± 0.1	0.021 ± 0.010
<b>(α4 K158G)<sub>2</sub>(β2)<sub>3</sub> – Thr (B+1) (T155)</b>					
Thr	0.99 ± 0.03	1.1 ± 0.1	0.25 ± 0.01	1.5 ± 0.1	0.023 ± 0.004
Tah	0.53 ± 0.02	1.2 ± 0.1	3.4 ± 0.2	1.2 ± 0.1	0.024 ± 0.006
<b>(α4)<sub>2</sub>(β2)<sub>3</sub> – Side Chain Mutations in the α4 Subunit</b>					
D157A	0.58 ± 0.02	1.3 ± 0.1	0.18 ± 0.01	1.4 ± 0.1	0.013 ± 0.009
D157N	0.61 ± 0.03	1.2 ± 0.1	0.14 ± 0.01	1.5 ± 0.1	0.032 ± 0.004
D157E	0.86 ± 0.02	1.2 ± 0.1	0.19 ± 0.01	1.5 ± 0.1	0.017 ± 0.005
D157K	6.0 ± 0.2	1.3 ± 0.1	0.39 ± 0.01	1.7 ± 0.1	-0.023 ± 0.015
K158A	0.57 ± 0.01	1.2 ± 0.1	0.21 ± 0.01	1.4 ± 0.1	0.032 ± 0.008
K160A	0.37 ± 0.01	1.1 ± 0.1	0.081 ± 0.005	1.5 ± 0.1	0.039 ± 0.006
E200A	1.1 ± 0.1	1.1 ± 0.1	0.44 ± 0.02	1.4 ± 0.1	0.037 ± 0.006
E200Q	0.93 ± 0.05	1.3 ± 0.1	0.34 ± 0.01	1.5 ± 0.1	0.019 ± 0.004
E200D	0.32 ± 0.02	1.2 ± 0.1	0.11 ± 0.01	1.5 ± 0.1	0.025 ± 0.003
E200K	0.96 ± 0.03	1.2 ± 0.1	0.36 ± 0.01	1.5 ± 0.1	0.025 ± 0.008
D157AK158A	1.3 ± 0.1	1.2 ± 0.1	0.22 ± 0.02	1.4 ± 0.1	0.032 ± 0.008
D157AK160A	0.63 ± 0.03	1.3 ± 0.1	0.14 ± 0.01	1.4 ± 0.1	0.031 ± 0.007
D157AE200A	4.1 ± 0.1	1.3 ± 0.1	1.1 ± 0.1	1.4 ± 0.1	0.024 ± 0.006
D157NE200Q	1.2 ± 0.1	1.2 ± 0.1	0.41 ± 0.03	1.5 ± 0.1	0.029 ± 0.010
K158AK160A	0.58 ± 0.02	1.2 ± 0.1	0.096 ± 0.004	1.6 ± 0.1	0.021 ± 0.004
K158AE200A	1.3 ± 0.1	1.2 ± 0.1	0.63 ± 0.03	1.5 ± 0.1	0.031 ± 0.004
K160AE200A	1.2 ± 0.1	1.2 ± 0.1	0.40 ± 0.02	1.4 ± 0.1	0.026 ± 0.003
D157NK158QE200Q	1.1 ± 0.1	1.2 ± 0.1	0.31 ± 0.02	1.5 ± 0.1	0.049 ± 0.007
D157NK160QE200Q	0.93 ± 0.05	1.3 ± 0.1	0.24 ± 0.02	1.5 ± 0.1	0.035 ± 0.005
<b>(α4)<sub>2</sub>(β2)<sub>3</sub> – TrpB (W154)</b>					
<b>Mutation</b>	<b>±Epibatidine</b>	<b>n<sub>H</sub></b>	<b>Norm. I (+70mV)</b>		
Trp	0.58 ± 0.03	1.6 ± 0.1	0.036 ± 0.008		
F <sub>1</sub> -Trp	6.8 ± 1.1	1.1 ± 0.2	0.039 ± 0.005		
F <sub>2</sub> -Trp	12 ± 2	1.1 ± 0.1	0.062 ± 0.006		
F <sub>3</sub> -Trp	35 ± 2	1.1 ± 0.1	0.032 ± 0.006		
F <sub>4</sub> -Trp	23 ± 1	1.0 ± 0.1	0.021 ± 0.007		
<b>(α4)<sub>2</sub>(β2)<sub>3</sub> – Thr (B+1) (T155)</b>					
Thr	0.67 ± 0.04	1.4 ± 0.1	0.022 ± 0.004		
Tah	3.7 ± 0.1	1.5 ± 0.1	0.026 ± 0.004		

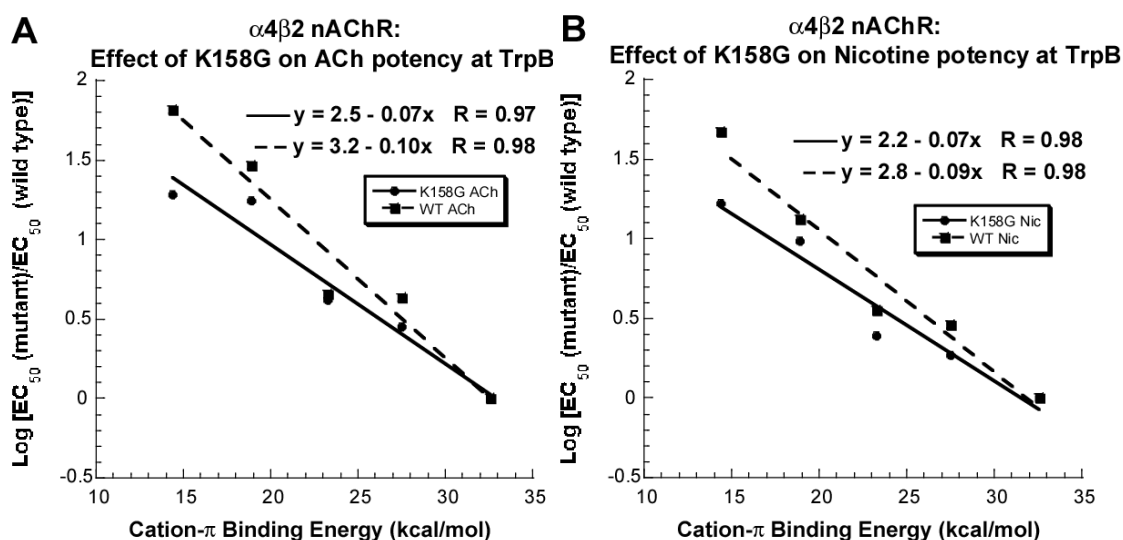


**Figure 3.6.** Fluorination plots probing the effect of the  $\alpha 4$  K158G mutation on the  $(\alpha 4)_2(\beta 2)_3$  nAChR.  $\text{Log}[\text{EC}_{50}(\text{mutant})/\text{EC}_{50}(\text{wild type})]$  is plotted versus quantitative cation- $\pi$  binding energies.<sup>8</sup> The data are from Table 3.5. Fluorination plots are shown for (A) ACh and (B) nicotine at the TrpB position. Moving to the left corresponds to Trp, F<sub>1</sub>-Trp, F<sub>2</sub>-Trp, F<sub>3</sub>-Trp, and F<sub>4</sub>-Trp.

In wild type  $(\alpha 4)_2(\beta 2)_3$ , nicotine forms a strong hydrogen bond to the backbone carbonyl of TrpB, revealed by a 19-fold shift for the backbone ester mutation.<sup>7</sup> In  $(\alpha 4)_2(\beta 2)_3$  receptors containing K158G, the amide-to-ester mutation revealed a 14-fold shift for nicotine (**Table 3.3**) indicating that this mutation has minimal impact on the backbone hydrogen bond.

It is possible that other residues positioned outside the immediate binding site could play a role in reshaping the agonist binding site. Taking into consideration the primary sequence of the  $\alpha 4$  subunit and the crystal structure of AChBP, several residues were identified near the agonist binding site that could participate in ionic interactions with cationic agonists (D157, K158, K160, and E200). Alanine substitution, side chain charge neutralization, and charge reversal were used to probe the importance of these residues in affecting agonist binding interactions. Residues were examined individually

and in combination. While each mutation produced a modest loss-of-function, no significant trend was observed (Figure 3.7, Table 3.5).

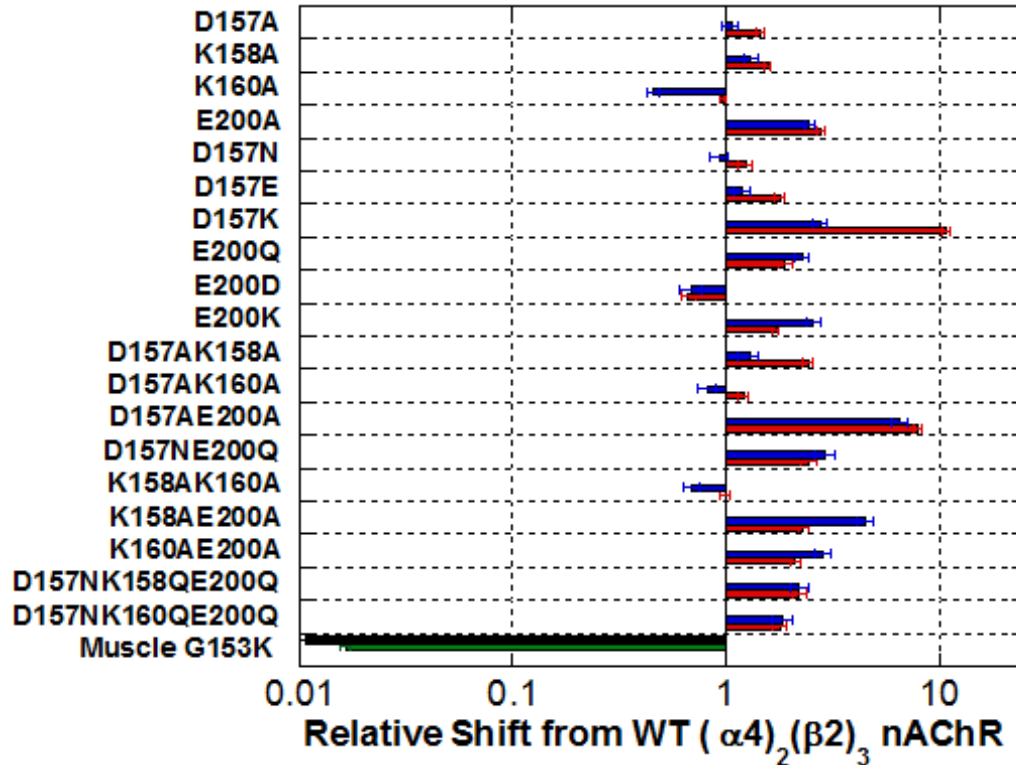


**Figure 3.7.** Comparing the effect on agonist potency of mutating select residues located outside of the  $(\alpha 4)_2(\beta 2)_3$  agonist binding site. The data are from Table 3.5. For each mutation, the relative shift in agonist potency from the wild type  $(\alpha 4)_2(\beta 2)_3$  receptor is shown for ACh (red) and nicotine (blue). The effect of  $\alpha 1$  G153K on ACh (green) and nicotine (black) potency for the muscle receptor are shown for reference.

### 3.3.4 Probing the Proposed Loop B–Loop C Hydrogen Bond

The present results have confirmed the influence of the loop B glycine site on agonist potency. These studies were inspired by the AChBP structure and simulations that indicated a hydrogen bond between loop B and loop C of the agonist binding site is formed to the backbone NH of the loop B glycine. Thus far, however, only side chain modifications have been considered, and these can only indirectly impact the putative hydrogen bond. As described above, backbone mutagenesis can directly probe hydrogen

bonding, and so we have applied that strategy to the proposed hydrogen bond. We chose to study the  $(\alpha 4)_2(\beta 2)_3$ , high-potency receptor, since this is the form for which the hydrogen bond is predicted to be stronger. We can mutate both components of the hydrogen bond by backbone mutagenesis: replacing the NH of K158 with an O by incorporating an  $\alpha$ -hydroxy acid at position 158, and altering the backbone carbonyl acceptor of residue 201 by incorporating an  $\alpha$ -hydroxy acid at position 202.

As established above, the identity of the side chain at position 158 is not crucial, as long as it is not glycine, and we anticipated technical challenges in incorporating the  $\alpha$ -hydroxy analog of lysine. As such, we chose to start from the K158L mutant, since Lah (leucine,  $\alpha$ -hydroxy) is readily available and incorporates well by nonsense suppression. As expected, the K158L mutation has a very modest effect on receptor function (**Table 3.1, Table 3.6**). Referenced to K158L, the K158Lah mutation also has a small effect on receptor function (**Table 3.1**), and it is actually a slight gain-of-function for both ACh and nicotine. Similarly, the Y202Yah mutation produced a relatively small perturbation, but it is now a loss-of-function. It may be that the perturbation with nicotine as agonist is significant, but still the effect is smaller than comparable perturbations we have seen at other hydrogen bonding sites.

**Table 3.6.** EC<sub>50</sub> values ( $\mu$ M) and Hill coefficients for mutant  $(\alpha 4)_2(\beta 2)_3$  nAChRs probing the Loop B-Loop C hydrogen bond. The EC<sub>50</sub> values are  $\pm$ S.E.

<b><math>(\alpha 4)_2(\beta 2)_3</math> – K158</b>					
<b>Mutation</b>	<b>ACh</b>	<b>n<sub>H</sub></b>	<b>Nicotine</b>	<b>n<sub>H</sub></b>	<b>Norm. I (+70mV)</b>
<b>K158L</b>	0.13 $\pm$ 0.01	1.2 $\pm$ 0.1	0.035 $\pm$ 0.003	1.5 $\pm$ 0.1	-0.005 $\pm$ 0.023
<b>Leu</b>	0.15 $\pm$ 0.01	1.3 $\pm$ 0.1	0.031 $\pm$ 0.001	1.3 $\pm$ 0.1	0.038 $\pm$ 0.010
<b>Lah</b>	0.060 $\pm$ 0.001	1.2 $\pm$ 0.1	0.011 $\pm$ 0.001	1.3 $\pm$ 0.1	0.026 $\pm$ 0.004
<b><math>(\alpha 4)_2(\beta 2)_3</math> – TyrC2 (Y202)</b>					
<b>Tyr</b>	0.44 $\pm$ 0.01	1.2 $\pm$ 0.1	0.096 $\pm$ 0.006	1.5 $\pm$ 0.1	0.035 $\pm$ 0.007
<b>Yah</b>	0.73 $\pm$ 0.03	1.2 $\pm$ 0.1	0.42 $\pm$ 0.03	1.4 $\pm$ 0.1	-0.008 $\pm$ 0.026

### 3.3.5 Implications for nAChR Function and Subtype Selectivity

A number of lines of evidence have established an important role for the loop B glycine in nAChR function. AChBP structures show its involvement in a loop B-loop C hydrogen bond,<sup>9, 10</sup> and MD simulations indicate that the strength of the hydrogen bond has an impact on the potency of ACh and nicotine at nAChR receptor subtypes.<sup>5</sup> A mutation at this site in the muscle-type nAChR produces a myasthenic syndrome.<sup>12</sup> Furthermore, in the muscle-type receptor, the G153K mutation reshapes the agonist binding site, allowing nicotine to approach the key TrpB residue of the agonist binding site more closely, amplifying both a cation- $\pi$  interaction<sup>7</sup> and a hydrogen bonding interaction.

In the present work we have further probed the loop B glycine in three different nAChR subtypes: muscle-type,  $(\alpha 7)_5$ , and  $(\alpha 4)_2(\beta 2)_3$ . In the muscle-type receptor, ACh, nicotine, and the nicotine analog epibatidine all show substantial increases in potency in response to the G153K mutation, which can be ascribed to an increased interaction with TrpB. As seen previously with nicotine, the cation- $\pi$  interaction is strengthened for epibatidine when the G153K mutation is present. It has been proposed that the G153K mutation should not be unique; any amino acid with a side chain should have a similar impact. Indeed, we find in the muscle-type receptor that G153A and G153T show similar phenotypes to G153K. Also, in the high-potency  $(\alpha 4)_2(\beta 2)_3$  receptor, a K158L mutation, which in most contexts would be expected to be strongly perturbing, has a minimal impact, indicating that there is nothing special about the lysine side chain.

The  $(\alpha 7)_5$  nAChR is low-potency like the muscle-type nAChR, but it shows a distinct pattern of agonist binding. As such, it was interesting to see if it would respond

to mutations of the loop B glycine in a similar manner. Indeed, the G152K mutation does significantly enhance the potency of ACh, nicotine, and epibatidine in the  $(\alpha 7)_5$  nAChR, however, the effects are generally smaller than seen for the muscle-type receptor.

Agonists do not make a cation- $\pi$  interaction to TrpB in  $(\alpha 7)_5$ , and the G152K mutation does not change this. Similarly, the hydrogen bond to the carbonyl of TrpB is weak in both the wild type and the G152K mutant. However, the G152K mutation does amplify a cation- $\pi$  interaction between agonists and TyrC2. A weak interaction with ACh becomes stronger in the mutant, and a strong interaction with epibatidine is further enhanced. Recall that TyrC2 is adjacent to the carbonyl that acts as the acceptor to the proposed critical hydrogen bond. However, in the muscle-type receptor it is interactions with TrpB, which lies across the agonist binding site from TyrC2, that are impacted by mutations at the loop B glycine site. This suggests that mutation of the glycine site globally alters the shape of the agonist binding site, such that agonists that interact strongly with TrpB see that interaction enhanced, and agonists that interact with TyrC2 see that interaction enhanced.

Given these results it was reasonable to ask whether a high-potency receptor could be converted to a low-potency receptor by the reverse (K-to-G) mutation at the key loop B site. The binding interactions in the  $(\alpha 4)_2(\beta 2)_3$  receptor are well characterized, and so we chose it as the target of such studies. We find that the K158G mutation does indeed diminish potency, but the effect is much less substantial than seen with the two G-to-K mutations. This suggests that in the optimized high-potency receptor there are other modifications that contribute to the high-potency. Conversely, in a low-potency receptor

the G-to-K mutation enhances potency considerably, and there may be other potential changes that could make the receptor even more “ $\alpha 4$ -like” and thus higher potency still.

Although these and other studies of the loop B glycine have probed the effects of side chain mutations, the key proposed interaction actually involves interactions with the backbone. This is an attractive model because, as noted above, the residue contributing the carbonyl is adjacent to TyrC2, a conserved contributor to the “aromatic box” of the agonist binding site. The unnatural amino acid methodology allows us to probe such backbone hydrogen bonds, replacing the NH donor with an O or replacing the amide (peptide) carbonyl with an ester carbonyl, a much weaker hydrogen bond acceptor.

We have performed both mutations in the high-potency  $(\alpha 4)_2(\beta 2)_3$  receptor, which is predicted to have a strong hydrogen bond, probing the response to both ACh and nicotine. In all cases, the impact is small, ranging from a 2-fold to a 5-fold change in potency. This is consistent with the argument given above that, in the optimized high-potency  $(\alpha 4)_2(\beta 2)_3$  receptor, features other than just the backbone hydrogen bond contribute to increasing potency. Furthermore, it is possible that these features are able to compensate for single disruptions in agonist binding (*i.e.*, disrupting the proposed loop B-loop C hydrogen bond). It is surprising that the two approaches to modulate the hydrogen bond have opposite effects: one is a loss-of-function and one is actually a gain-of-function. Again, the effects are small, and we hesitate to attempt to provide detailed interpretation.

Overall, these results provide strong support for the notion that the identity of the side chain at the loop B glycine site strongly influences nAChR function. With any residue other than glycine (and likely proline), the agonist binding site is shaped properly

to allow strong interactions with agonists. However, when this key residue is glycine, the agonist binding site is distorted such that optimal drug-receptor interactions cannot occur. This happens regardless of whether key drug-receptor interactions involve TrpB or TyrC2, and so we prefer a model that emphasizes a global reorganization of the agonist binding site, rather than just the repositioning of a single residue. Interestingly, although the model is based on the behavior of a proposed hydrogen bond, directly modifying that hydrogen bond has a smaller effect on receptor function than presumed indirect effects brought about by side chain modifications.

### 3.4 METHODS

#### *Molecular Biology*

All nAChR subunit genes were in the pAMV vector (mouse  $\alpha$ 1,  $\beta$ 1,  $\gamma$ , and  $\delta$ ; rat  $\alpha$ 4,  $\beta$ 2, and  $\alpha$ 7). Site-directed mutagenesis was performed using the QuikChange protocol (Stratagene). For nonsense suppression experiments,<sup>18</sup> the site of interest within the nAChR subunit was mutated to an amber stop codon (TAG). Circular DNA was linearized with Not I. After purification (Qiagen), linearized DNA was used as a template for runoff *in vitro* transcription using T7 mMessage mMachine kit (Ambion). hRIC-3 cDNA in pGEM vector was obtained from Dr. Miller Treinin at Hebrew University.<sup>19</sup> Circular hRIC-3 DNA was linearized with Xho I, and mRNA was prepared as previously described.

THG73<sup>20</sup> was used as the amber suppressor tRNA. Nitroveratryloxycarbonyl (NVOC) protected cyanomethyl esters of unnatural amino acids and  $\alpha$ -hydroxy amino acid cyanomethyl esters were synthesized, coupled to dinucleotide dCA, and

enzymatically ligated to 74-nucleotide THG73 tRNA<sub>CUA</sub> as previously reported.<sup>18</sup> Crude tRNA-amino acid product was used without desalting, and the product was confirmed by MALDI-TOF MS on 3-hydroxypicolinic acid (3-HPA) matrix. Deprotection of the NVOC group on the tRNA-amino acid was carried out by photolysis for 5 minutes prior to coinjection with mRNA containing the UAG mutation at the site of interest.

### ***Microinjection***

Stage V-VI *Xenopus laevis* oocytes were employed. For muscle-type nAChR experiments,  $\alpha 1:\beta 1:\gamma:\delta$  mRNA was injected at a ratio of 2:1:1:1 by mass for wild type protein. Note that for all experiments reported, we use a previously reported L9'S mutation in the  $\beta 1$  subunit to increase receptor sensitivity.<sup>7, 8</sup> If an unnatural amino acid was to be incorporated into the  $\alpha 1$  subunit, then an mRNA ratio of 10:1:1:1 was employed. For wild type and nonsense suppression experiments, the total mRNA injected was 30-65 ng/oocyte.

All studies of the  $(\alpha 7)_5$  receptor contain a T6'S mutation in the M2 transmembrane helix, which serves to decrease desensitization without altering other aspects of receptor pharmacology.<sup>21</sup> For  $(\alpha 7)_5$  experiments, 10 ng  $\alpha 7$  mRNA was coinjected with 10 ng of hRIC-3 mRNA per oocyte. In the case of nonsense suppression experiments, 20 ng  $\alpha 7$  mRNA was co-injected with 25 ng of hRIC-3 mRNA per oocyte.<sup>16</sup>

In accordance with previously reported protocols,<sup>7</sup> all  $\alpha 4\beta 2$  receptors contain a L9'A mutation in the  $\alpha 4$  subunit to increase receptor expression. Coinjection of  $\alpha 4:\beta 2$  mRNA at a ratio of 1:1 by mass yielded wild type  $(\alpha 4)_2(\beta 2)_3$  receptors. For  $(\alpha 4)_2(\beta 2)_3$

nAChRs with conventional mutations located outside the immediate binding site (*i.e.*, K158G, D157N, etc.), an injection ratio of 1:1 for  $\alpha 4$ : $\beta 2$  mRNA by mass was employed (Table 3.7). For wild type recovery experiments incorporating a tryptophan into the  $\alpha 4$  subunit to produce  $(\alpha 4)_2(\beta 2)_3$  receptors, a mass ratio of 1:1 for  $\alpha 4$ : $\beta 2$  mRNA was injected into each oocyte. However, for subsequent nonsense suppression experiments incorporating fluorinated tryptophan derivatives into the  $\alpha 4$  subunit, a mass ratio of 3:1 for  $\alpha 4$ : $\beta 2$  mRNA was injected into each oocyte to account for decreased suppression efficiency. The total  $\alpha 4\beta 2$  mRNA injected was 30-72 ng/oocyte depending on the relative expression level. All  $(\alpha 4)_2(\beta 2)_3$  nAChR stoichiometries were confirmed by voltage jump experiments.<sup>7</sup>

**Table 3.7.** Injection ratios of  $\alpha 4$  K158G: $\beta 2$  mRNA used to control  $\alpha 4\beta 2$  receptor stoichiometry in *Xenopus* oocytes.  $EC_{50}$  values ( $\mu M$ ) and Hill coefficients are shown. The  $EC_{50}$  values are  $\pm$  S.E. ND, not determined.

<b><math>\alpha 4</math> K158G:<math>\beta 2</math> mRNA Ratios</b>					
<b>Ratio</b>	<b>ACh</b>	<b><math>n_H</math></b>	<b>Nicotine</b>	<b><math>n_H</math></b>	<b>Norm. I (+70mV)</b>
<b>100:1</b>	0.11 $\pm$ 0.01	1.0 $\pm$ 0.1	0.045 $\pm$ 0.001	1.5 $\pm$ 0.1	0.268 $\pm$ 0.015
<b>30:1</b>	0.08 $\pm$ 0.01	1.0 $\pm$ 0.1	ND	ND	0.248 $\pm$ 0.027
<b>10:1</b>	0.35 $\pm$ 0.04	0.71 $\pm$ 0.05	ND	ND	0.242 $\pm$ 0.021
<b>6:1</b>	0.49 $\pm$ 0.02	0.80 $\pm$ 0.02	ND	ND	0.215 $\pm$ 0.016
<b>3:1</b>	0.68 $\pm$ 0.02	1.1 $\pm$ 0.1	ND	ND	0.045 $\pm$ 0.008
<b>1:1</b>	1.3 $\pm$ 0.1	1.1 $\pm$ 0.1	0.30 $\pm$ 0.02	1.7 $\pm$ 0.2	0.015 $\pm$ 0.006
<b>1:3</b>	1.1 $\pm$ 0.1	1.3 $\pm$ 0.1	0.26 $\pm$ 0.02	2.1 $\pm$ 0.3	0.059 $\pm$ 0.006
<b>1:10</b>	1.0 $\pm$ 0.1	1.2 $\pm$ 0.1	0.26 $\pm$ 0.03	1.7 $\pm$ 0.3	0.043 $\pm$ 0.032

For all suppression experiments, approximately 15 ng/oocyte of tRNA was used. Each oocyte was injected with 50 nL of RNA solution, and the oocytes were incubated for 24-48 hours at 18 °C in ND96 buffer (96 mM NaCl, 2 mM KCl, 1 mM MgCl<sub>2</sub>, 1.8 mM CaCl<sub>2</sub>, and 5 mM HEPES, pH 7.5) with 0.005% (w/v) gentamycin and 2% (v/v) horse serum. In the case of low-expressing mutant receptors, a second injection of

mRNA/tRNA was required 24 hour after the first injection. As a negative control for all suppression experiments, 76-nucleotide tRNA (dCA ligated to 74-nucleotide tRNA) was coinjected with mRNA in the same manner as fully charged tRNA.

### ***Electrophysiology***

Acetylcholine chloride and (-)-nicotine tartrate were purchased from Sigma/Aldrich/RBI (St. Louis, MO) and drug dilutions were prepared from 1M *aq* stock solutions. ( $\pm$ )-Epibatidine was purchased from Tocris and drug dilutions were prepared from a 50 mM stock solution (1:1 H<sub>2</sub>O:EtOH). For ( $\alpha$ 1)<sub>2</sub> $\beta$ 1 $\gamma$  $\delta$  and ( $\alpha$ 4)<sub>2</sub>( $\beta$ 2)<sub>3</sub> experiments, drug dilutions were prepared in Ca<sup>2+</sup>-free ND96 buffer. For ( $\alpha$ 7)<sub>5</sub> experiments, drug dilutions were prepared in Ca<sup>2+</sup>-containing ND96 buffer.

Ion channel function was assayed using the OpusXpress 6000A (Molecular Devices Axon Instruments) in two-electrode voltage clamp mode. Oocytes were clamped at a holding potential of -60mV. For ( $\alpha$ 1)<sub>2</sub> $\beta$ 1 $\gamma$  $\delta$  and ( $\alpha$ 4)<sub>2</sub>( $\beta$ 2)<sub>3</sub> receptors, 1 mL of each drug solution was applied to the clamped oocytes for 12 seconds, followed by a 2 minute wash with Ca<sup>2+</sup>-free ND96 buffer between each concentration. In the case of hypersensitive ( $\alpha$ 1G153K)<sub>2</sub> $\beta$ 1 $\gamma$  $\delta$  receptors, a 1.5 minute drug application was used to ensure maximum peak response when using very low concentrations of agonist. For ( $\alpha$ 7)<sub>5</sub> receptors, 1 mL of each drug solution was applied for 30 seconds, followed by a 5 minute wash step with Ca<sup>2+</sup>-containing ND96 buffer between each concentration. Data were sampled at 50 Hz and filtered at 20 Hz. Voltage jump experiments were sampled at 5000 Hz and filtered at 180 Hz.

### *Data Analysis*

Dose-response data were obtained for at least 6 concentrations of agonists and for a minimum of 5 oocytes (from two different batches). Mutants with  $I_{\max}$  of at least 100 nA of current were defined as functional.  $EC_{50}$  and Hill coefficients ( $n_H$ ) were calculated by fitting the averaged, normalized dose-response relation to the Hill equation. All data are reported as mean  $\pm$ S.E.

### **3.5 ACKNOWLEDGEMENTS**

This work was supported by the NIH (NS 34407 and NS 11756).

### 3.6 REFERENCES

1. Corringer, P. J.; Le Novère, N.; Changeux, J. P., Nicotinic receptors at the amino acid level. *Annu Rev Pharmacol Toxicol* **2000**, 40, 431-58.
2. Grutter, T.; Changeux, J. P., Nicotinic receptors in wonderland. *Trends Biochem Sci* **2001**, 26, (8), 459-63.
3. Karlin, A., Emerging structure of the nicotinic acetylcholine receptors. *Nat Rev Neurosci* **2002**, 3, (2), 102-14.
4. Jensen, A. A.; Frolund, B.; Lijefors, T.; Krogsgaard-Larsen, P., Neuronal nicotinic acetylcholine receptors: Structural revelations, target identifications, and therapeutic inspirations. *J. Med. Chem.* **2005**, 48, (15), 4705-4745.
5. Grutter, T.; de Carvalho, L. P.; Le Novère, N.; Corringer, P. J.; Edelstein, S.; Changeux, J. P., An H-bond between two residues from different loops of the acetylcholine binding site contributes to the activation mechanism of nicotinic receptors. *EMBO J.* **2003**, 22, (9), 1990-2003.
6. Gotti, C.; Zoli, M.; Clementi, F., Brain nicotinic acetylcholine receptors: native subtypes and their relevance. *Trends Pharm. Sci.* **2006**, 27, (9), 482-491.
7. Xiu, X.; Puskar, N. L.; Shanata, J. A.; Lester, H. A.; Dougherty, D. A., Nicotine binding to brain receptors requires a strong cation- $\pi$  interaction. *Nature* **2009**, 458, (7237), 534-7.
8. Zhong, W.; Gallivan, J. P.; Zhang, Y.; Li, L.; Lester, H. A.; Dougherty, D. A., From ab initio quantum mechanics to molecular neurobiology: a cation- $\pi$  binding site in the nicotinic receptor. *Proc Natl Acad Sci U S A* **1998**, 95, (21), 12088-93.
9. Brejc, K.; van Dijk, W. J.; Klaassen, R. V.; Schuurmans, M.; van Der Oost, J.; Smit, A. B.; Sixma, T. K., Crystal structure of an ACh-binding protein reveals the ligand-binding domain of nicotinic receptors. *Nature* **2001**, 411, (6835), 269-76.
10. Sixma, T. K.; Smit, A. B., Acetylcholine binding protein (AChBP): a secreted glial protein that provides a high-resolution model for the extracellular domain of pentameric ligand-gated ion channels. *Annu Rev Biophys Biomol Struct* **2003**, 32, 311-34.
11. Hibbs, R. E.; Gouaux, E., Principles of activation and permeation in an anion-selective Cys-loop receptor. *Nature* **2011**, 474, (7349), 54-U80.
12. Sine, S. M.; Ohno, K.; Bouzat, C.; Auerbach, A.; Milone, M.; Pruitt, J. N.; Engel, A. G., Mutation of the acetylcholine receptor  $\alpha$  subunit causes a slow-channel myasthenic syndrome by enhancing agonist binding affinity. *Neuron* **1995**, 15, (1), 229-239.
13. Celie, P. H.; van Rossum-Fikkert, S. E.; van Dijk, W. J.; Brejc, K.; Smit, A. B.; Sixma, T. K., Nicotine and carbamylcholine binding to nicotinic acetylcholine receptors as studied in AChBP crystal structures. *Neuron* **2004**, 41, (6), 907-914.
14. Cashin, A. L.; Petersson, E. J.; Lester, H. A.; Dougherty, D. A., Using physical chemistry to differentiate nicotinic from cholinergic agonists at the nicotinic acetylcholine receptor. *J. Am. Chem. Soc.* **2005**, 127, (1), 350-356.
15. Cashin, A. L.; Petersson, E. J.; Lester, H. A.; Dougherty, D. A., Using physical chemistry to differentiate nicotinic from cholinergic agonists at the nicotinic acetylcholine receptor. *J Am Chem Soc* **2005**, 127, (1), 350-6.

16. Puskar, N. L.; Xiu, X.; Lester, H. A.; Dougherty, D. A., Two Neuronal Nicotinic Acetylcholine Receptors, alpha 4 beta 4 and alpha 7, Show Differential Agonist Binding Modes. *Journal of Biological Chemistry* **2011**, 286, (16), 14618-14627.
17. Lummis, S. C.; D, L. B.; Harrison, N. J.; Lester, H. A.; Dougherty, D. A., A cation-pi binding interaction with a tyrosine in the binding site of the GABAC receptor. *Chem Biol* **2005**, 12, (9), 993-7.
18. Nowak, M. W.; Gallivan, J. P.; Silverman, S. K.; Labarca, C. G.; Dougherty, D. A.; Lester, H. A., *In vivo* incorporation of unnatural amino acids into ion channels in a *Xenopus* oocyte expression system. *Methods Enzymol* **1998**, 293, 504-529.
19. Williams, M. E.; Burton, B.; Urrutia, A.; Shcherbatko, A.; Chavez-Noriega, L. E.; Cohen, C. J.; Aiyar, J., Ric-3 promotes functional expression of the nicotinic acetylcholine receptor alpha7 subunit in mammalian cells. *J Biol Chem* **2005**, 280, (2), 1257-63.
20. Saks, M. E.; Sampson, J. R.; Nowak, M. W.; Kearney, P. C.; Du, F.; Abelson, J. N.; Lester, H. A.; Dougherty, D. A., An engineered *Tetrahymena* tRNAGln for *in vivo* incorporation of unnatural amino acids into proteins by nonsense suppression. *J. Biol. Chem* **1996**, 271, 23169-75.
21. Placzek, A. N.; Grassi, F.; Meyer, E. M.; Papke, R. L., An alpha7 nicotinic acetylcholine receptor gain-of-function mutant that retains pharmacological fidelity. *Mol Pharmacol* **2005**, 68, (6), 1863-76.

## Chapter 4

### Contrasting Drug-Receptor Interactions at Neuronal vs. Muscle-Type Nicotinic Acetylcholine Receptors: The Neuronal $\alpha 4\beta 4$ Receptor\*

*\*This chapter is adapted in part from: Puskar, N. L.; Xiu, X.; Lester, H. A.; Dougherty, D. A. Two neuronal nicotinic acetylcholine receptors,  $\alpha 4\beta 4$  and  $\alpha 7$ , show differential agonist binding modes. *The Journal of Biological Chemistry*. **2011**; 286: 14618-14627. © The American Society for Biochemistry and Molecular Biology.*

#### 4.1 ABSTRACT

Nicotinic acetylcholine receptors (nAChR) are pentameric, neurotransmitter-gated ion channels responsible for rapid excitatory neurotransmission in the central and peripheral nervous systems, resulting in skeletal muscle tone and various cognitive effects in the brain. These complex proteins are activated by the endogenous neurotransmitter acetylcholine (ACh) as well as by nicotine and structurally related agonists. Activation and modulation of nAChRs have been implicated in the pathology of multiple neurological disorders, and as such, these proteins are established therapeutic targets. Our lab has reported that the muscle-type,  $\alpha 4\beta 2$ , and  $\alpha 7$  receptors bind agonist molecules via a cation- $\pi$  interaction.<sup>1-3</sup> This chapter describes our efforts to elucidate the agonist binding mechanism of the  $\alpha 4\beta 4$  receptor. Unnatural amino acid mutagenesis and chimeric  $\beta$  subunits were used to probe the respective contributions of the  $\alpha 4\beta 4$  principal and complementary binding components to agonist binding and receptor pharmacology. Here, we report that the  $\alpha 4\beta 4$  receptor utilizes a strong cation- $\pi$  interaction to a conserved tryptophan (TrpB) of the receptor for both ACh and nicotine, and nicotine participates in a strong hydrogen bond with a backbone carbonyl contributed by TrpB.

## 4.2 INTRODUCTION

Nicotinic acetylcholine receptors (nAChRs) belong to the Cys-loop superfamily of neurotransmitter-gated ion channels, which includes  $\gamma$ -aminobutyric acid (GABA<sub>A</sub> and GABA<sub>C</sub>), glycine (Gly), and serotonin type 3 (5-HT<sub>3</sub>) receptors. These transmembrane proteins are critical to proper rapid synaptic transmission in the central and peripheral nervous systems.<sup>4</sup> In fact, several nAChRs have been implicated in pathophysiology and/or therapy of multiple neurological and psychiatric disorders including addiction, schizophrenia, Parkinson's disease, Alzheimer's disease, pain, ADHD, epilepsy, depression, and congenital myasthenic syndromes.<sup>5,6</sup>

The nAChR is the longest-known, most-studied neuroreceptor. nAChRs are pentameric, integral membrane proteins whose overall structure has been roughly determined by cryo-electron microscopy images of the *Torpedo californica* nAChR (**Figure 4.1**).<sup>7</sup> Each subunit contains a large, principally  $\beta$ -sheet extracellular N-terminal domain, four transmembrane  $\alpha$ -helices (M1-M4), and a small extracellular C-terminal domain. Five homologous subunits are arranged pseudosymmetrically around a central ion conducting pore formed by the M2 helices of each subunit.<sup>8</sup> To date, 16 mammalian genes have been identified that encode nAChR subunits, termed  $\alpha$ 1- $\alpha$ 7,  $\alpha$ 9,  $\alpha$ 10,  $\beta$ 1- $\beta$ 4,  $\delta$ ,  $\gamma$ , and  $\epsilon$ .

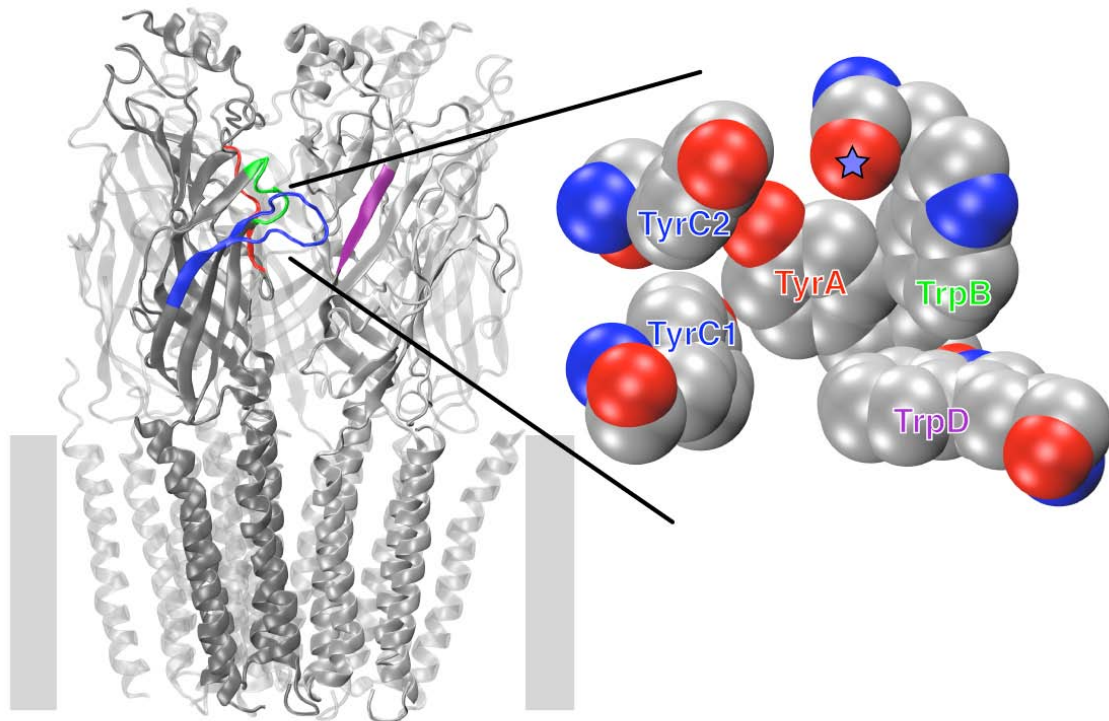


**Figure 4.1.** nAChR structure. *Left panel*, global layout of the nAChR based on cryo-electron microscopy of the *Torpedo* receptor (pdb: 2BG9).<sup>7</sup> The position of the membrane is denoted by gray bars. A large intracellular domain that is only partly observed in the structure is omitted. *Right panel*, enlargement of agonist binding site from AChBP (pdb: 1I9B).<sup>9</sup> Aromatic residues forming the ligand binding site are indicated. TyrA, TrpB, TyrC1, and TyrC2 are contributed by the  $\alpha$  subunit, and TrpD is contributed by the non- $\alpha$  subunit. Coloring of the residue labels matches that of the corresponding loops in the full structure. Backbone carbonyl contributed by TrpB is denoted by a star.

The “muscle-type” nAChR is postsynaptically located at the neuromuscular junction and has a uniquely precise stoichiometry of  $(\alpha 1)_2\beta 1\gamma\delta$  (fetal form; the adult form is  $(\alpha 1)_2\beta 1\epsilon\delta$ ). Neuronal nAChRs, however, are formed from various combinations of  $\alpha 2$ - $\alpha 10$  and  $\beta 2$ - $\beta 4$  subunits and current estimates indicate that as many as 25 active subtypes occur in humans.<sup>10, 11</sup> These receptors are mostly located post- and presynaptically in autonomic ganglia and cholinergic neurons of the CNS, but can also occur in non-neuronal cells.<sup>5, 10</sup> Given this large collection of closely related receptors, it

seems certain that therapeutics directed toward specific neurological disorders will require selectivity in terms of which nAChR subtype(s) is targeted.

Early work established a nicotinic pharmacophore comprised of a cationic N and a hydrogen bond accepting group separated by an appropriate distance.<sup>12, 13</sup> This report focuses on critical drug-receptor interactions occurring at the agonist binding site. The cationic moiety of ACh interacts with a cluster of aromatic amino acids first identified by photoaffinity labeling and mutagenesis experiments of the full receptor.<sup>4, 9</sup> Crystal structures of the acetylcholine binding proteins (AChBP) provided a structural template for the N-terminal, extracellular, ligand binding domain (LBD) of the nAChR, as it shares 20%-25% sequence identity with the extracellular domain of the much larger ion channel protein.<sup>9, 14</sup> Five aromatic residues (labeled according to their respective loop) form the agonist binding site, and these five aromatics are completely conserved across the nAChR family (**Figure 4.1**). The principal binding site contributes loop A (TyrA), loop B (TrpB), and loop C (TyrC1 and TyrC2), and the complementary binding site contributes loop D (TrpD), loop E, and loop F. In recent work, it was confirmed that the hydrogen bond acceptor of the agonist interacts with residues from the complementary subunits ( $\beta$  in neuronal nAChRs;  $\gamma$ ,  $\delta$ ,  $\varepsilon$  in the muscle-type nAChR).<sup>15</sup>

In the Dougherty group, we have used the nonsense suppression methodology to probe the molecular determinants for agonist binding in several nAChR subtypes, such as the muscle-type and neuronal  $\alpha 4\beta 2$  and  $\alpha 7$  receptors.<sup>1-3, 16, 17</sup> From these studies, the cation- $\pi$  interaction proved a common component of agonist affinity in each of the aforementioned receptors. Preliminary studies of the neuronal  $\alpha 4\beta 4$  nAChR, however, proved inconclusive.<sup>18</sup> Interestingly, the  $\alpha 4$  and  $\beta 4$  subunits colocalize in brain regions

implicated in behavioral responses to nicotine, and  $\beta 4^{-/-}$  knockout mice are more resistant to nicotine-induced seizures when compared to wild type mice.<sup>5, 19</sup> Given the significance of the  $\alpha 4\beta 4$  subtype in nicotine addiction and its similar structure to  $\alpha 4\beta 2$ , we were interested in elucidating the agonist binding mode of the  $\alpha 4\beta 4$  receptor.

The primary goal of the present work is described in two parts: (1) to use unnatural amino acid mutagenesis to probe the  $\alpha 4\beta 4$  principal binding site and determine the contribution of each residue (*e.g.*, TyrA, TrpB, TyrC1, and TyrC2) to agonist binding, and (2) to employ chimeric  $\beta$  subunits to identify which region(s) of the complementary binding site contributes to the divergent pharmacologies observed for the  $\alpha 4\beta 2$  and  $\alpha 4\beta 4$  receptors.

## 4.3 RESULTS

### 4.3.1 Part 1: Using Unnatural Amino Acid Mutagenesis to Probe the Principal Binding Site of the Neuronal $\alpha 4\beta 4$ Receptor

#### *Challenges in Studying Neuronal nAChRs with Unnatural Amino Acids*

The nonsense suppression methodology for incorporating unnatural amino acids into receptors and ion channels expressed in *Xenopus* oocytes has proven to be broadly applicable, including studies of serotonin (5-HT<sub>3</sub>) receptors, GABA receptors, glycine receptors, K<sup>+</sup> and Na<sup>+</sup> channels, and GPCRs.<sup>16, 20-24</sup> Studies of the muscle-type nAChR have long been straightforward, but attempts to apply the methodology to neuronal nAChRs were initially frustrated by several factors. These issues include poor expression in *Xenopus* oocytes as well as expression of variable stoichiometries. Here, we report the strategies used to overcome these obstacles in the  $\alpha 4\beta 4$  receptor.

Human  $\alpha 4$  and  $\beta 4$  subunit genes were in plasmid Bluescript (pBluescript). Injection of mRNA transcribed from pBluescript into oocytes produced moderate expression of wild type protein and low expression for nonsense suppression experiments. As such, both  $\alpha 4$  and  $\beta 4$  subunit genes were subcloned into pGEMhe facilitating *in vitro* transcription of mRNA for expression in *Xenopus* oocytes. Using mRNA transcribed from the pGEMhe vector, we successfully incorporated several unnatural amino acids into the  $\alpha 4\beta 4$  nAChR.

An additional issue concerning the expression of neuronal nAChRs in *Xenopus* oocytes is the tendency of these receptors to exist in variable stoichiometries. This can be problematic, since interpretation of subtle structure-function studies requires a homogeneous collection of receptors. Several studies of other receptor subtypes have shown that biasing the ratios of subunit mRNAs injected into the oocyte can influence subunit stoichiometry,<sup>2, 25</sup> and we have found similar results in our previous studies of unnatural amino acids in the  $\alpha 4\beta 2$  receptor.<sup>2</sup> For the  $\alpha 4\beta 2$  nAChR, the  $(\alpha 4)_2(\beta 2)_3$  form is the higher sensitivity form for nicotine, and chronic exposure to nicotine leads to upregulation of this form at the expense of  $(\alpha 4)_3(\beta 2)_2$  in a variety of cell types.<sup>25, 26</sup>

In initial studies of the  $\alpha 4\beta 4$  receptor, we observed variable dose-response curves and anomalously low Hill coefficients, indicating a mixed population of receptors. By biasing the subunit mRNA ratios, we observed two dominant  $\alpha 4\beta 4$  receptor populations, which we have assigned as  $(\alpha 4)_2(\beta 4)_3$  and  $(\alpha 4)_3(\beta 4)_2$ . In order to facilitate comparisons and to emphasize the critical role of the  $\beta$  subunit in defining drug selectivity at nAChRs, our studies of the  $\alpha 4\beta 4$  nAChR have focused on the  $(\alpha 4)_2(\beta 4)_3$  form. We found that injection of an mRNA ratio  $\alpha 4:\beta 4$  of 1:1 or lower produces a pure population of

$(\alpha 4)_2(\beta 4)_3$ , while a ratio greater than 30:1 is necessary to produce pure populations of  $(\alpha 4)_3(\beta 4)_2$  (**Table 4.1**).

**Table 4.1.** Stoichiometries of  $\alpha 4\beta 4$  nAChRs expressed in *Xenopus* oocytes injected with different ratios of human  $\alpha 4:\beta 4$  subunit mRNA.  $EC_{50}$  ( $\mu M$ ) and  $n_H$  values are  $\pm SEM$ .

<b>Ratio</b>	<b>ACh</b>	<b><math>n_H</math></b>	<b>Stoichiometry</b>
<b>100:1</b>	$58 \pm 3$	$1.9 \pm 0.2$	A3B2
<b>30:1</b>	$51 \pm 3$	$1.9 \pm 0.2$	Mixture
<b>10:1</b>	$41 \pm 2$	$1.4 \pm 0.1$	Mixture
<b>3:1</b>	$26 \pm 1$	$1.1 \pm 0.1$	Mixture
<b>1:1</b>	$11 \pm 1$	$1.3 \pm 0.1$	A2B3
<b>1:3</b>	$13 \pm 1$	$1.3 \pm 0.1$	A2B3
<b>Ratio</b>	<b>Nicotine</b>	<b><math>n_H</math></b>	<b>Stoichiometry</b>
<b>100:1</b>	$12 \pm 2$	$1.7 \pm 0.3$	A3B2
<b>1:3</b>	$2.4 \pm 0.1$	$1.3 \pm 0.1$	A2B3

With the above strategies, unnatural amino acid mutagenesis studies of the  $\alpha 4\beta 4$  receptor proceeded smoothly (**Figure 4.2**). In the present work, we report  $EC_{50}$  measurements, the effective concentration of agonist required to induce half-maximal response.  $EC_{50}$  is a functional measure that can be altered by changes in agonist affinity and/or receptor gating. All of our previous studies of the nAChR agonist binding site have employed this metric, and so using  $EC_{50}$  values allows direct comparisons between different subtypes. In addition, an earlier study of the  $\alpha 4\beta 2$  receptor employed single-channel analysis to establish that shifts in  $EC_{50}$  caused by subtle mutations at TrpB, a major focus of the present work, result from changes in agonist affinity, not receptor gating.<sup>2</sup>

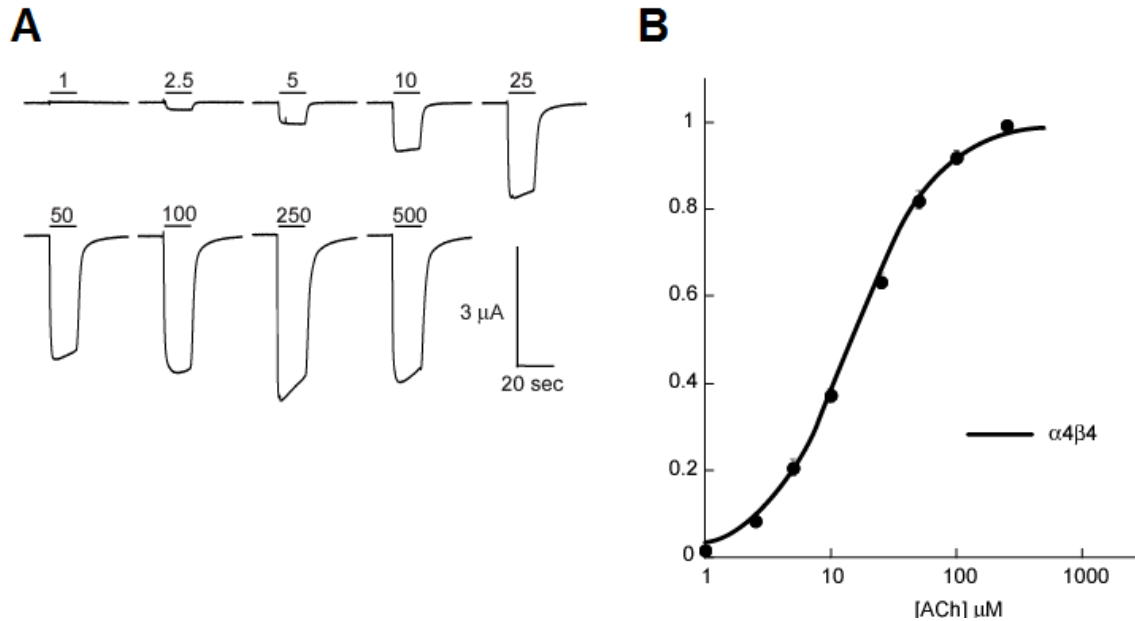


**Figure 4.2.** Wild type recovery experiments for the  $\alpha 4\beta 4$  nAChR. A. Representative voltage-clamp current traces from oocytes with Trp incorporated by nonsense suppression at position TrpB. Bars indicate application of ACh at concentrations ( $\mu\text{M}$ ) noted. B. Dose-response curve and fit of data in A to the Hill equation. Error bars indicate SEM.;  $n = 10\text{-}13$ .

### *Ligand Binding Mechanism of the $\alpha 4\beta 4$ Receptor*

Our lab has previously established that the muscle-type and  $\alpha 4\beta 2$  nAChRs interact with agonists (**Figure 4.3A**) through cation- $\pi$  interactions at TrpB.<sup>2, 3</sup> We therefore focused on TrpB in the  $\alpha 4\beta 4$  receptor using strategies that are now well established for identifying a cation- $\pi$  interaction. In particular, we systematically fluorinate a side chain (**Figure 4.3B**) and determine whether the progressive diminution of the cation- $\pi$  binding ability of the residue induced by fluorination is manifested in receptor function. The fluorination approach can be augmented with other substitutions, such as the highly deactivating cyano (CN) substituent, and is compared to the much less deactivating but sterically similar bromo (Br) substituent. With ACh as agonist, both the CN-Trp/Br-Trp effect (9-fold ratio of  $\text{EC}_{50}$ ; **Table 4.2**) and the fluorination effect (**Figure**

**4.4A)** establish that a cation- $\pi$  interaction is present at TrpB. We were unable to achieve adequate incorporation of F<sub>3</sub>-Trp or F<sub>4</sub>-Trp, so we incorporated 7-aza-Trp, which is structurally very similar to Trp but shows a diminished cation- $\pi$  binding ability. When all the data are combined (Trp, F<sub>1</sub>-Trp, F<sub>2</sub>-Trp, 7-aza-Trp, Br-Trp, and CN-Trp) into one plot, we observe a linear correlation with *ab initio* calculated cation- $\pi$  binding energies. The slope of this cation- $\pi$  binding plot resembles that reported for other nAChRs. A much more thorough study was possible with nicotine as the agonist, producing compelling evidence for a cation- $\pi$  interaction to TrpB (**Figure 4.4B**). Considering the effects of nicotine at TrpB, the cation- $\pi$  slope resembles that of the  $\alpha$ 4 $\beta$ 2 receptor rather than the muscle-type receptor, which shows no consistent fluorination effect with nicotine as the agonist. Hence, in the  $\alpha$ 4 $\beta$ 4 receptor, similar to the  $\alpha$ 4 $\beta$ 2 receptor,<sup>2</sup> nicotine mimics ACh at TrpB with regard to the cation- $\pi$  interaction.

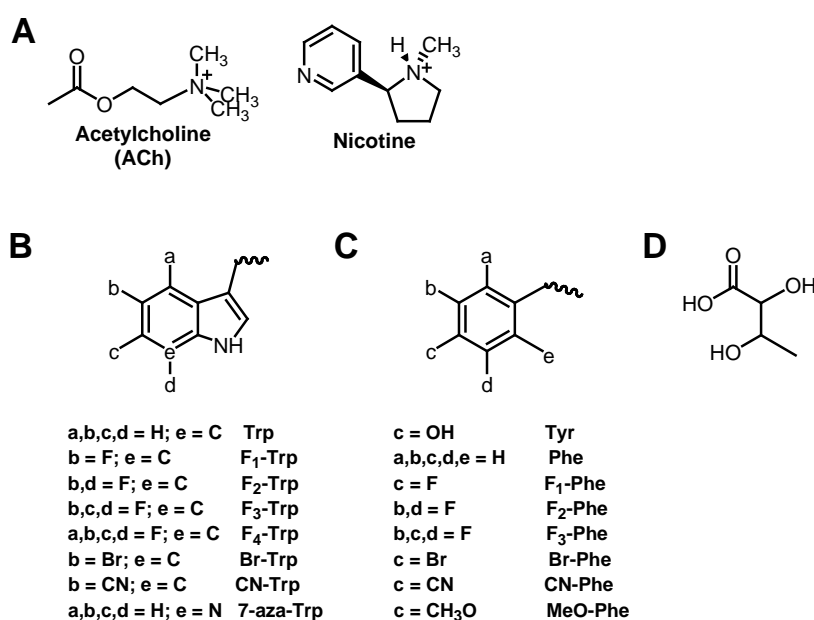


**Figure 4.3.** Key structures employed in this study. A. Structures of ACh and nicotine. B. Tryptophan derivatives; F<sub>1</sub>-Trp, 5-fluoro-tryptophan; F<sub>2</sub>-Trp, 5,7-difluoro-tryptophan; F<sub>3</sub>-Trp, 5,6,7-trifluoro-tryptophan; F<sub>4</sub>-Trp, 4,5,6,7-tetrafluoro-tryptophan; Br-Trp, 5-bromo-tryptophan; CN-Trp, 5-cyano-tryptophan; 7-aza-Trp, 7-aza-tryptophan. C. Phenylalanine

derivatives; F<sub>1</sub>-Phe, 4-fluoro-phenylalanine; F<sub>2</sub>-Phe, 3,5-difluoro-phenylalanine; F<sub>3</sub>-Phe, 3,4,5-trifluoro-phenylalanine; Br-Phe, 4-bromo-phenylalanine; CN-Phe, 4-cyano-phenylalanine; MeO-Phe, 4-methoxy-phenylalanine. If not indicated, a, b, c, or d group is H. D. Tah, threonine- $\alpha$ -hydroxy.

**Table 4.2.** Data for mutant  $\alpha 4\beta 4$  (A2B3) nAChRs.  $EC_{50}$  ( $\mu M$ ) and  $n_H$  values are  $\pm SEM$ . NR = No response.

<b>Mutation</b>	<b>ACh</b>	<b><math>n_H</math></b>	<b>Nicotine</b>	<b><math>n_H</math></b>
<b>(<math>\alpha 4</math>)<sub>3</sub>(<math>\beta 4</math>)<sub>2</sub></b>	58 $\pm$ 3	1.9 $\pm$ 0.2	12 $\pm$ 2	1.7 $\pm$ 0.3
<b>(<math>\alpha 4</math>)<sub>2</sub>(<math>\beta 4</math>)<sub>3</sub></b>	13 $\pm$ 1	1.3 $\pm$ 0.1	2.4 $\pm$ 0.1	1.3 $\pm$ 0.1
<b>TyrA</b>				
<b>Tyr</b>	17 $\pm$ 1	1.2 $\pm$ 0.1	3.1 $\pm$ 0.2	1.3 $\pm$ 0.1
<b>Phe</b>	260 $\pm$ 11	1.3 $\pm$ 0.1	11 $\pm$ 0.4	1.6 $\pm$ 0.1
<b>F<sub>1</sub>-Phe</b>	254 $\pm$ 21	1.3 $\pm$ 0.1	6.6 $\pm$ 0.6	1.5 $\pm$ 0.2
<b>F<sub>2</sub>-Phe</b>	159 $\pm$ 16	1.3 $\pm$ 0.1	7.1 $\pm$ 0.4	1.4 $\pm$ 0.1
<b>F<sub>3</sub>-Phe</b>	158 $\pm$ 14	1.4 $\pm$ 0.1	7.7 $\pm$ 0.5	1.4 $\pm$ 0.1
<b>Br-Phe</b>	49 $\pm$ 1	1.6 $\pm$ 0.1	3.5 $\pm$ 0.2	1.5 $\pm$ 0.1
<b>CN-Phe</b>	855 $\pm$ 63	1.4 $\pm$ 0.1	80 $\pm$ 6	1.4 $\pm$ 0.1
<b>MeO-Phe</b>	50 $\pm$ 2	1.4 $\pm$ 0.1	4.2 $\pm$ 0.2	1.4 $\pm$ 0.1
<b>TrpB</b>				
<b>Trp</b>	15 $\pm$ 1	1.3 $\pm$ 0.1	2.0 $\pm$ 0.1	1.2 $\pm$ 0.1
<b>F<sub>1</sub>-Trp</b>	41 $\pm$ 2	1.5 $\pm$ 0.1	5.6 $\pm$ 0.5	1.4 $\pm$ 0.1
<b>F<sub>2</sub>-Trp</b>	51 $\pm$ 2	1.6 $\pm$ 0.1	8.1 $\pm$ 0.9	1.5 $\pm$ 0.2
<b>F<sub>3</sub>-Trp</b>	NR	NR	73 $\pm$ 6	1.2 $\pm$ 0.1
<b>F<sub>4</sub>-Trp</b>	NR	NR	190 $\pm$ 116	0.8 $\pm$ 0.2
<b>Br-Trp</b>	28 $\pm$ 1	1.5 $\pm$ 0.1	7.1 $\pm$ 0.5	1.5 $\pm$ 0.1
<b>CN-Trp</b>	254 $\pm$ 27	1.2 $\pm$ 0.1	46 $\pm$ 3	1.6 $\pm$ 0.1
<b>7-aza-Trp</b>	162 $\pm$ 17	1.6 $\pm$ 0.2	28 $\pm$ 2	2.0 $\pm$ 0.2
<b>TyrC1</b>				
<b>Tyr</b>	11 $\pm$ 1	1.2 $\pm$ 0.1	1.8 $\pm$ 0.1	1.3 $\pm$ 0.1
<b>Phe</b>	1100 $\pm$ 126	1.8 $\pm$ 0.3	60 $\pm$ 2	2.0 $\pm$ 0.1
<b>Br-Phe</b>	1400 $\pm$ 140	2.0 $\pm$ 0.3	65 $\pm$ 9	1.3 $\pm$ 0.2
<b>CN-Phe</b>	2700 $\pm$ 500	1.5 $\pm$ 0.2	156 $\pm$ 13	1.8 $\pm$ 0.2
<b>MeO-Phe</b>	550 $\pm$ 37	1.6 $\pm$ 0.1	75 $\pm$ 9	1.5 $\pm$ 0.2
<b>TyrC2</b>				
<b>Tyr</b>	11 $\pm$ 1	1.2 $\pm$ 0.1	2.2 $\pm$ 0.1	1.3 $\pm$ 0.1
<b>Phe</b>	26 $\pm$ 1	1.6 $\pm$ 0.1	2.0 $\pm$ 0.2	1.6 $\pm$ 0.2
<b>Br-Phe</b>	4.5 $\pm$ 0.3	1.4 $\pm$ 0.1	0.36 $\pm$ 0.01	1.7 $\pm$ 0.1
<b>CN-Phe</b>	11 $\pm$ 1	1.2 $\pm$ 0.1	2.5 $\pm$ 0.1	1.4 $\pm$ 0.1
<b>MeO-Phe</b>	13 $\pm$ 1	1.3 $\pm$ 0.1	1.3 $\pm$ 0.1	1.5 $\pm$ 0.2
<b>Thr(B+1)</b>				
<b>Thr</b>	15 $\pm$ 1	1.3 $\pm$ 0.1	1.7 $\pm$ 0.1	1.3 $\pm$ 0.1
<b>Tah</b>	12 $\pm$ 1	1.3 $\pm$ 0.1	23 $\pm$ 1	1.6 $\pm$ 0.1

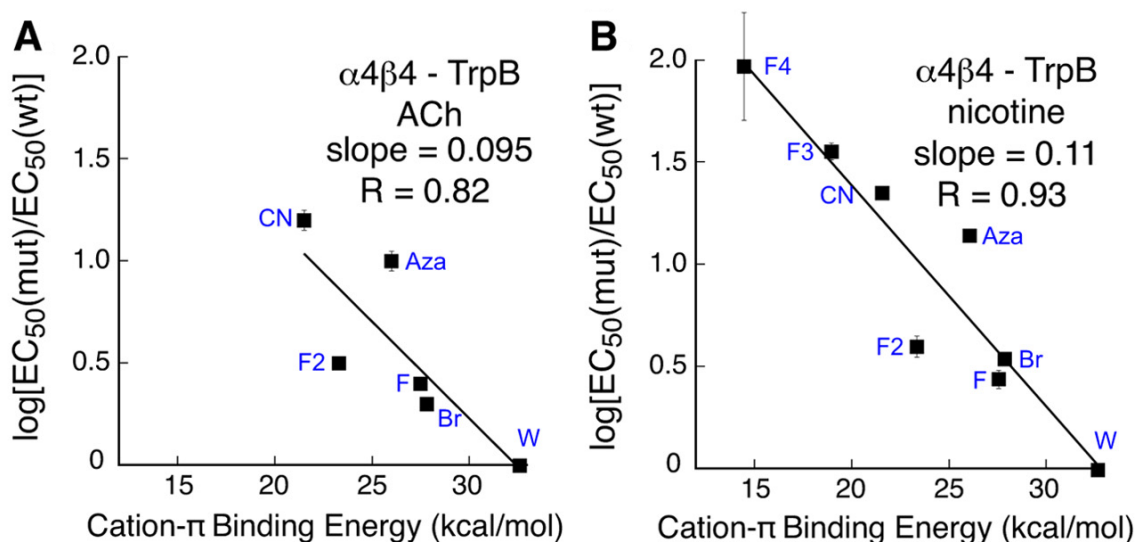


**Figure 4.4.** Cation- $\pi$  binding plots for  $\alpha 4\beta 4$  nAChR at position TrpB with ACh (A) and nicotine (B).  $\text{Log}[EC_{50}(\text{mut})/EC_{50}(\text{wt})]$  is plotted *vs.* quantitative cation- $\pi$  binding energies.<sup>3</sup> Data are from Table 4.2. Where not visible, error bars are smaller than the data marker.

We performed extensive studies of the remaining components of the aromatic box contributed by the principal face of the ligand binding domain (TyrA, TyrC1, and TyrC2). Historically, nonsense suppression with tyrosine derivatives has proven more challenging than tryptophan derivatives when probing for a cation- $\pi$  interaction. Direct fluorination of tyrosine progressively lowers the  $\text{pK}_a$  of the side chain hydroxyl group, such that the  $\text{pK}_a$  for tetrafluorotyrosine is  $\sim 5.3$  (lowered from  $\sim 10$  for tyrosine). This decrease in  $\text{pK}_a$  can lead to ionization of the hydroxyl in unnatural tyrosine analogues. Thus observed shifts in  $EC_{50}$  could result from ionization of the hydroxyl group rather than changes in the cation- $\pi$  binding ability, complicating analysis. In other receptors, we have circumvented this potential problem by first incorporating phenylalanine, followed by successively fluorinated phenylalanine derivatives (**Figure 4.3C**), thereby avoiding the  $\text{pK}_a$  complication.<sup>27</sup>

In the  $\alpha 4\beta 4$  receptor, we found that for TyrA deletion of the hydroxyl group (to give Phe) severely impacts receptor function for both ACh and nicotine (**Table 4.2**). Incorporation of either MeO-Phe or Br-Phe perturbs receptor function minimally, while CN-Phe is strongly perturbing. This represents a distinction in the behavior of TyrA when comparing  $\alpha 4\beta 4$  to the  $\alpha 4\beta 2$  and muscle-type receptors. For proper receptor function in  $\alpha 4\beta 4$ , it appears that TyrA requires only steric bulk at this position. However, MeO-Phe is highly deleterious in the  $\alpha 4\beta 2$  and muscle-type receptors, suggesting a hydrogen bond donor is required. Successive fluorination of phenylalanine does not result in progressively reduced channel function; we conclude that neither ACh nor nicotine participates in a cation- $\pi$  interaction with TyrA.

The remaining two residues, TyrC1 and TyrC2, are both contributed by loop C, a very mobile component of the binding site.<sup>28</sup> We probed both of these residues for possible hydrogen bonding and cation- $\pi$  interactions, and we find that TyrC1 and TyrC2 display opposite effects. TyrC1 is highly sensitive to any mutation that obliterates hydrogen bond donating ability, as evidenced by a rightward shift in  $EC_{50}$  of over 50-fold for ACh and 30-fold for nicotine in response to the Phe, MeO-Phe, Br-Phe, and CN-Phe mutations (**Table 4.2**). Given the small CN-Phe/Br-Phe ratio, TyrC1 is not likely to interact with either ACh or nicotine through a cation- $\pi$  interaction. If this position served as a hydrogen bond acceptor, then incorporation of MeO-Phe would have rescued normal channel function. Rather, MeO-Phe incorporation resulted in a substantial loss of channel function; therefore, we conclude that TyrC1 is an important hydrogen bond donor.

In contrast, TyrC2 is quite receptive to mutations of the 4-position hydroxyl group, with many types of substituents accepted and no obvious structure-function relationship. The fact that CN-Phe gives essentially wild type behavior for both ACh and nicotine would appear to rule out a strong cation- $\pi$  interaction at this site. These results suggest that TyrC2 participates structurally in shaping the ligand-binding site rather than directly in ligand recognition. Again, the results for both TyrC1 and TyrC2 are similar to what is seen for muscle-type and  $\alpha 4\beta 2$ .

In  $\alpha 4\beta 4$ , we also investigated the hydrogen bonding capability of the backbone carbonyl of TrpB (**Figure 4.1**), because this site is known to behave differently in the muscle-type and  $\alpha 4\beta 2$  nAChRs.<sup>2, 17</sup> By replacing the amino acid at the  $i+1$  position with the analogous  $\alpha$ -hydroxy acid, one converts the carbonyl associated with residue  $i$  to an ester carbonyl rather than an amide (peptide) carbonyl (**Figure 4.5, Figure 4.3D**).<sup>17</sup> It is well established that ester carbonyls are poorer hydrogen bond acceptors than amide carbonyls, and so if a hydrogen bond to this carbonyl is essential, the backbone ester mutation should influence agonist potency. With nicotine as the agonist, the backbone ester mutation causes a 14-fold increase in  $EC_{50}$  in  $\alpha 4\beta 4$  (**Table 4.2**). Importantly, the potency of ACh, which cannot make a conventional hydrogen bond to the carbonyl, is essentially unperturbed by the backbone ester mutation. This establishes that the mutation does not globally alter the binding/gating characteristics of the receptor, supporting the notion that we are modulating a hydrogen bonding interaction between the receptor and nicotine. As with TrpB, the behavior of  $\alpha 4\beta 4$  is more similar to that of  $\alpha 4\beta 2$  rather than muscle-type.

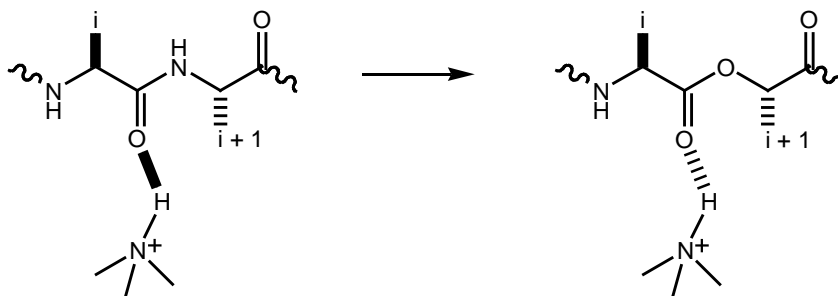


**Figure 4.5.** The backbone ester strategy for modulating a hydrogen bond;  $\alpha$ -hydroxy acid incorporation.

### 4.3.2 Part 2: Using Chimeric $\beta$ Subunits to Examine the Contribution of the Complementary Binding Site to Subtype-Specific Receptor Pharmacology

We have now established that  $\alpha 4\beta 2^2$  and  $\alpha 4\beta 4$  utilize the same drug-receptor interactions to bind agonists (*e.g.*, a cation- $\pi$  interaction and a hydrogen bond). However, several studies have suggested that the subtle pharmacological differences observed for these neuronal nAChRs are determined by the identities of both the  $\alpha$  and  $\beta$  subunits.<sup>29-31</sup> Given that both  $\alpha 4\beta 2$  and  $\alpha 4\beta 4$  receptors contain an identical principal binding site contributed by the  $\alpha 4$  subunit, the complementary subunit (*i.e.*,  $\beta 4$  vs.  $\beta 2$ ) is likely the discriminating factor amongst these two receptors. In fact, studies by Parker *et al.* confirmed that  $\beta 2$ -containing receptors consistently display higher affinities for agonists compared to  $\beta 4$ -containing receptors, and identified loop D as a major determinant for agonist affinity.<sup>31</sup> In part 2 of this chapter, we use chimeric  $\beta$  subunits to identify which loop(s) of the complementary binding site influences agonist binding and receptor pharmacology.

#### **General Strategy**

The complementary binding site was partitioned into discrete sections according to loops D-F, and several chimeric  $\beta$  subunits were designed, replacing portions of the  $\beta 2$

subunit with the corresponding region from the  $\beta 4$  subunit (**Figure 4.6**). Chimera D converted loop D of the  $\beta 2$  subunit to that of the  $\beta 4$  subunit via a single semiconserved threonine to lysine mutation. Similarly, chimeras E and F replaced either loop E or F to the analogous  $\beta 4$  region to examine their respective effects on agonist affinity. As shown in **Figure 4.6**, there is considerable residue variety among the sequences of loops E and F. In combination, these mutations may account for subtle changes in the ligand binding site and ultimately affect pharmacological properties of the receptor. The four remaining chimeras (DE, DF, EF, and DEF) replaced multiple loops of the  $\alpha 4\beta 2$  complementary binding site with the corresponding  $\beta 4$  loops. Chimera DEF completely converts the  $\alpha 4\beta 2$  agonist binding site to that of  $\alpha 4\beta 4$ .

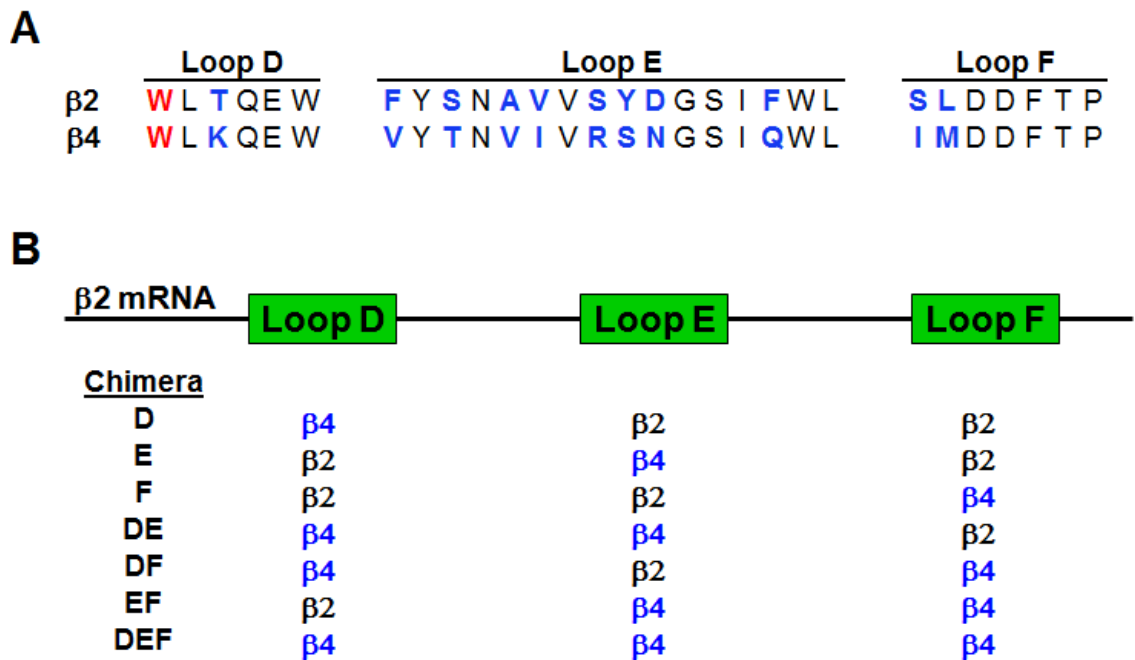


**Figure 4.6.** Design of chimeric  $\beta$  subunits. A. Complementary LBD loop sequences for rat  $\beta 2$  and  $\beta 4$  subunits. TrpD is highlighted in red. Differences in the sequences are highlighted in blue. B. Depiction of chimeras constructed from various combinations  $\beta 2$  and  $\beta 4$  regions.

All chimeric  $\beta$  subunits were coexpressed with the  $\alpha 4$  subunit. In accordance with previous studies of  $\alpha 4\beta 2$  and  $\alpha 4\beta 4$ ,<sup>1, 2</sup> a  $\alpha 4$ :chimeric  $\beta$  mRNA ratio of 1:3 ratio was coinjected into oocytes to ensure a homogeneous population of  $(\alpha 4)_2(\beta 2/\beta 4)_3$  receptors. In both  $\alpha 4\beta 2$  and  $\alpha 4\beta 4$ , TrpB is the key residue that interacts with both ACh and nicotine via a cation- $\pi$  interaction, a key component of agonist binding.<sup>2</sup> We therefore incorporated F<sub>3</sub>-Trp at TrpB in each chimeric receptor and evaluated the impact on the cation- $\pi$  interaction. For chimeras that experienced a functional change in response F<sub>3</sub>-Trp incorporation when compared to  $\alpha 4\beta 2$ , additional tryptophan derivatives were incorporated at TrpB (**Figure 4.3B**).

#### ***Functional Scan of Chimeric $\alpha 4\beta 2/\beta 4$ Receptors***

EC<sub>50</sub> was used to evaluate receptor function as discussed in Part 1. Although EC<sub>50</sub> is composed of both binding and gating parameters, we anticipate that shifts in EC<sub>50</sub> caused by subtle mutations at TrpB result from changes in agonist binding, not receptor gating, based on previous single-channel analysis of  $\alpha 4\beta 2$ .<sup>2</sup> Using either ACh or nicotine as the agonist, a dose-response relationship was determined for each chimera. EC<sub>50</sub> values of chimeric receptors were compared to  $\alpha 4\beta 2$  values (**Table 4.3**). Each chimera was functional and EC<sub>50</sub> values were slightly shifted from  $\alpha 4\beta 2$ , with chimera DE experiencing the greatest perturbation.

**Table 4.3.** EC<sub>50</sub> values (μM) and Hill coefficients for α4β2/β4 chimeras. All values are ±S.E. †Previously reported in Xiu 2009.<sup>2</sup> All other values in this table were determined in the present work.

		ACh	n <sub>H</sub>	Nicotine	n <sub>H</sub>	Norm. I (+70mV)
(α4) <sub>3</sub> (β2) <sub>2</sub> <sup>†</sup>		0.023 ± 0.001	1.3 ± 0.1	0.01 ± 0.001	1.7 ± 0.2	0.297 ± 0.041
(α4) <sub>2</sub> (β2) <sub>3</sub> <sup>†</sup>		0.42 ± 0.01	1.2 ± 0.1	0.08 ± 0.01	1.2 ± 0.1	0.041 ± 0.005
Chimera	Mutation					
<b>D</b>	Wild Type ( <b>D</b> )	0.31 ± 0.01	1.4 ± 0.1	0.09 ± 0.01	1.5 ± 0.1	0.022 ± 0.005
	Trp	0.39 ± 0.01	1.4 ± 0.1	0.09 ± 0.01	1.4 ± 0.1	-0.006 ± 0.017
	F <sub>3</sub> -Trp	30 ± 1	1.6 ± 0.1	2.1 ± 0.1	1.2 ± 0.1	0.031 ± 0.010
<b>E</b>	Wild type ( <b>E</b> )	0.69 ± 0.02	1.4 ± 0.1	0.23 ± 0.02	1.9 ± 0.2	0.019 ± 0.004
	Trp	0.83 ± 0.03	1.3 ± 0.1	0.23 ± 0.02	1.6 ± 0.2	0.006 ± 0.011
	F <sub>3</sub> -Trp	46 ± 3	1.3 ± 0.1	10 ± 1	1.2 ± 0.2	0.015 ± 0.006
<b>F</b>	Wild type ( <b>F</b> )	0.11 ± 0.01	1.1 ± 0.1	0.09 ± 0.01	1.3 ± 0.1	0.018 ± 0.011
	Trp	0.10 ± 0.01	1.2 ± 0.1	0.06 ± 0.01	1.3 ± 0.1	0.040 ± 0.003
	F <sub>3</sub> -Trp	6.5 ± 0.3	1.1 ± 0.1	0.54 ± 0.03	1.5 ± 0.1	0.047 ± 0.008
<b>DE</b>	Wild type ( <b>DE</b> )	1.8 ± 0.1	1.4 ± 0.1	0.68 ± 0.03	1.6 ± 0.1	0.018 ± 0.005
	Trp	2.3 ± 0.1	1.3 ± 0.1	0.49 ± 0.03	1.7 ± 0.1	0.018 ± 0.004
	F <sub>3</sub> -Trp	130 ± 10	1.1 ± 0.1	20 ± 3	1.9 ± 0.4	0.018 ± 0.012
<b>DF</b>	Wild type ( <b>DF</b> )	0.21 ± 0.01	1.2 ± 0.1	0.07 ± 0.01	1.1 ± 0.1	0.021 ± 0.004
	Trp	0.16 ± 0.01	1.2 ± 0.1	0.04 ± 0.01	1.5 ± 0.1	0.039 ± 0.006
	F <sub>3</sub> -Trp	13 ± 1	1.4 ± 0.1	1.1 ± 0.1	1.4 ± 0.1	0.043 ± 0.003
<b>EF</b>	Wild type ( <b>EF</b> )	0.22 ± 0.01	1.4 ± 0.1	0.24 ± 0.01	1.8 ± 0.1	0.041 ± 0.006
	Trp	0.23 ± 0.01	1.1 ± 0.1	0.30 ± 0.01	1.8 ± 0.1	0.037 ± 0.006
	F <sub>3</sub> -Trp	46 ± 2	1.4 ± 0.1	15 ± 1	1.9 ± 0.2	0.071 ± 0.009
<b>DEF</b>	Wild type ( <b>DEF</b> )	0.55 ± 0.03	1.4 ± 0.1	0.39 ± 0.02	1.9 ± 0.1	0.005 ± 0.009
	Trp	0.5 ± 0.02	1.1 ± 0.1	0.42 ± 0.02	1.5 ± 0.1	0.035 ± 0.004
	F <sub>3</sub> -Trp	73 ± 3	1.5 ± 0.1	20 ± 1	1.8 ± 0.2	0.019 ± 0.003

For each chimeric receptor, F<sub>3</sub>-Trp was incorporated at TrpB to evaluate the impact of the altered complementary binding site on the native cation-π interaction (a key component of the agonist binding mode) (**Table 4.3**). The F<sub>3</sub>-Trp/Trp fold shifts reported for α4β2 and α4β4 were compared to the fold shift for each chimera (**Figure 4.7**). A fold shift for ACh at α4β4 was unavailable due to inadequate incorporation of F<sub>3</sub>-Trp at TrpB. With ACh as agonist, all chimeras exhibited a F<sub>3</sub>-Trp/Trp fold shift greater than that observed for α4β2. A similar trend was observed for nicotine, with one exception – chimera F. Here, the F<sub>3</sub>-Trp/Trp fold shift for chimera F was less than values observed for both α4β2 and α4β4. This result was interesting; suggesting that chimera F disrupted

the cation- $\pi$  interaction as evidenced by a smaller perturbation in response to incorporation of F<sub>3</sub>-Trp (**Figure 4.7**). Although the effect was not large, chimera F was the obvious target for additional suppression experiments.

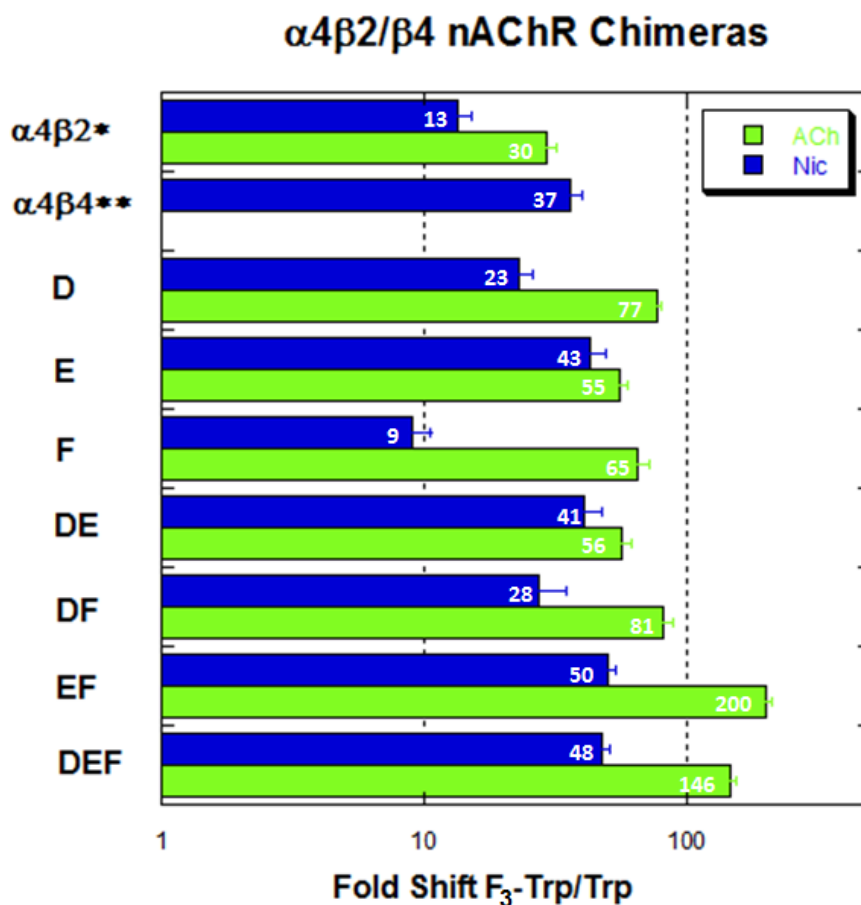


**Figure 4.7.** Bar graph comparing F<sub>3</sub>-Trp/Trp fold shifts for chimeric receptors. Fold shifts for ACh (green) and nicotine (blue) are indicated in white lettering. \*Previously reported in Xiu 2009.<sup>2</sup> \*\*Previously reported in Puskar 2011.<sup>1</sup> All other values in this table were determined in the present work.

#### *Using the Fluorination Approach to Explore the Effect of Loop F on Agonist Binding*

Given that ACh and nicotine responded differently to incorporation of F<sub>3</sub>-Trp at TrpB in chimera F, we used the fluorination approach to further examine the effect of chimera F on the cation- $\pi$  interaction at TrpB (as described in Part 1) (**Figure 4.3B**). The  $\log(\text{EC}_{50}(\text{mutant})/\text{EC}_{50}(\text{wild type}))$  was plotted against *ab initio* calculated cation- $\pi$

binding energies (Table 4.4).<sup>3</sup> Typically, we interpret the slope of a cation- $\pi$  binding plot to indicate the relative strength of a cation- $\pi$  interaction, and as such, we compared the slope obtained for chimera F to values observed for  $\alpha 4\beta 2$  and  $\alpha 4\beta 4$ .

**Table 4.4.** EC<sub>50</sub> values ( $\mu\text{M}$ ) and Hill coefficients for chimera F. All values are  $\pm$ S.E. F<sub>1</sub>-Trp, 5-fluoro-tryptophan; F<sub>2</sub>-Trp, 5,7-difluoro-tryptophan; F<sub>3</sub>-Trp, 5,6,7-trifluoro-tryptophan; F<sub>4</sub>-Trp, 4,5,6,7-tetrafluoro-tryptophan; Br-Trp, 5-bromo-tryptophan; CN-Trp, 5-cyano-tryptophan.

Mutation	ACh	n <sub>H</sub>	Nic	n <sub>H</sub>	Norm I (+70mV)
Trp	0.10 $\pm$ 0.01	1.2 $\pm$ 0.1	0.06 $\pm$ 0.01	1.3 $\pm$ 0.1	0.040 $\pm$ 0.003
F <sub>1</sub> -Trp	0.51 $\pm$ 0.02	1.3 $\pm$ 0.1	0.27 $\pm$ 0.01	1.4 $\pm$ 0.1	0.031 $\pm$ 0.011
F <sub>2</sub> -Trp	1.2 $\pm$ 0.1	1.1 $\pm$ 0.1	0.27 $\pm$ 0.01	1.3 $\pm$ 0.1	0.051 $\pm$ 0.009
F <sub>3</sub> -Trp	6.5 $\pm$ 0.3	1.1 $\pm$ 0.1	0.54 $\pm$ 0.03	1.5 $\pm$ 0.1	0.047 $\pm$ 0.008
F <sub>4</sub> -Trp	15 $\pm$ 1	1.1 $\pm$ 0.1	3.6 $\pm$ 0.3	1.0 $\pm$ 0.1	0.025 $\pm$ 0.007
Br-Trp	0.35 $\pm$ 0.02	1.4 $\pm$ 0.1	0.20 $\pm$ 0.01	1.6 $\pm$ 0.1	0.035 $\pm$ 0.005
CN-Trp	4.7 $\pm$ 0.2	1.3 $\pm$ 0.1	1.9 $\pm$ 0.2	1.4 $\pm$ 0.2	0.032 $\pm$ 0.005

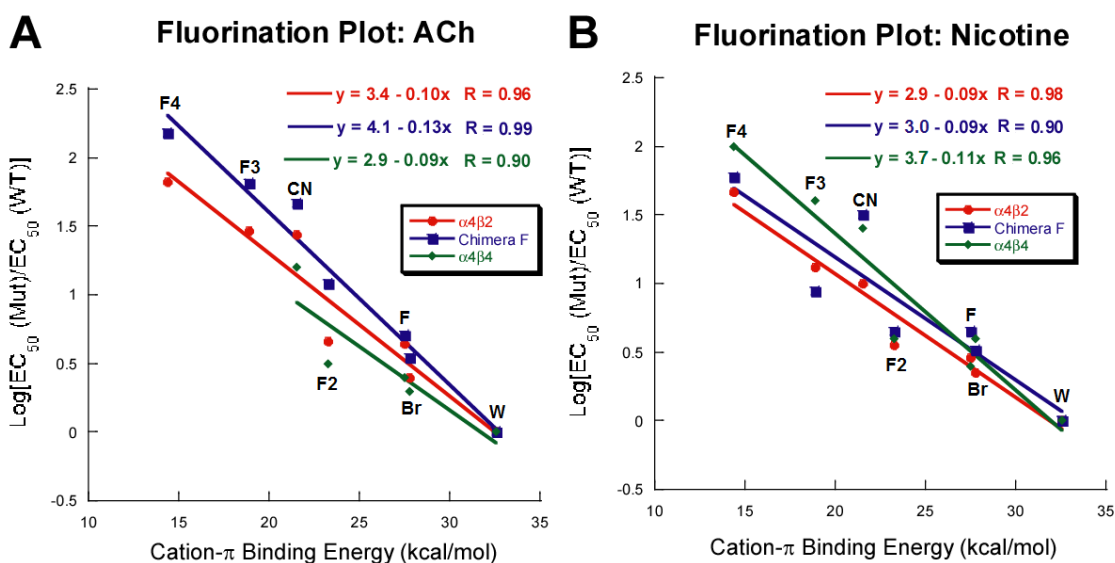


**Figure 4.8.** Cation- $\pi$  binding (fluorination) plots monitor the relative strength of a cation- $\pi$  interaction at TrpB. Data are from Table 4.4. Chimera F (blue) is compared to  $\alpha 4\beta 2$  (red) and  $\alpha 4\beta 4$  (green) for ACh (A) and nicotine (B).

Compared to both  $\alpha 4\beta 2$  and  $\alpha 4\beta 4$ , chimera F strengthened the cation- $\pi$  interaction between ACh and TrpB of the receptor. This was indicated by an increase in

sensitivity to progressive fluorination of TrpB illustrated in the cation- $\pi$  binding plot (**Figure 4.8A**). Nicotine, however, displayed a more variable effect (**Figure 4.8B**). Some mutations displayed an increase in sensitivity to fluorination of TrpB, while others showed a decrease in sensitivity (**Table 4.5**). As such, no significant trend was observed.

**Table 4.5.** Ratios of mutant EC<sub>50</sub> to wild type EC<sub>50</sub>, such that ratios >1 represent loss-of-function. Chimera F (blue) is compared to  $\alpha 4\beta 2$  (red) and  $\alpha 4\beta 4$  (green) for ACh and nicotine. \*Previously reported in Xiu 2009.<sup>2</sup> \*\*Previously reported in Puskar 2011.<sup>1</sup> All other values in this table were determined in the present work. NR = not response.

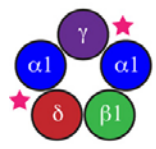
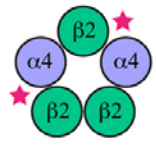
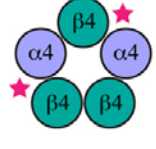
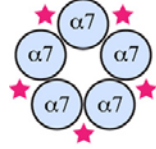
Mutation	Ratio of EC <sub>50</sub> (mutant)/EC <sub>50</sub> (wild type recovery)					
	ACh			Nicotine		
	$\alpha 4\beta 2$ *	Chimera F	$\alpha 4\beta 4$ **	$\alpha 4\beta 2$ *	Chimera F	$\alpha 4\beta 4$ **
Trp	1.0	1.0	1.0	1.0	1.0	1.0
F <sub>1</sub> -Trp	4.3	5.1	2.7	2.9	4.5	2.8
F <sub>2</sub> -Trp	4.5	12	3.4	3.6	4.5	4.1
F <sub>3</sub> -Trp	30	65	NR	13	9	36.5
F <sub>4</sub> -Trp	66	150	NR	47	60	95.0
Br-Trp	2.5	3.5	1.9	2.2	3.3	3.6
CN-Trp	27	47	16.9	10	32	23.0

#### 4.4 DISCUSSION

With >20 nAChR subtypes, these neurotransmitter-gated ion channels are essential for proper brain function and provide a wide array of targets for pharmaceutical development.<sup>4, 5</sup> Given the considerable sequence similarity, especially in the region of the agonist binding site, it becomes quite challenging to discern the mechanisms for differential activation of homologous receptors. Our lab uses unnatural amino acid mutagenesis to address such questions. This method enables subtle and systematic modifications that can isolate specific binding interactions and provide qualitative guidance on the relative magnitudes of specific interactions.

Here, we establish the agonist binding mode for the  $\alpha 4\beta 4$  receptor and contrast drug-receptor interactions for four members of the nAChR family: muscle-type,  $\alpha 4\beta 2$ ,  $\alpha 7$ , and  $\alpha 4\beta 4$  (**Figure 4.9**). Note that the side chains within the aromatic box are identical in all the receptors considered: three tyrosines and two tryptophans. Thus, differences among the receptors must result from subtle structural effects.

**Figure 4.9.** Summary of ligand-receptor interactions present for the muscle-type,  $\alpha 4\beta 2$ ,  $\alpha 4\beta 4$ , and  $\alpha 7$  nAChRs. Stars indicate relevant binding site interfaces.

	ACh	nicotine epibatidine	
	Cation- $\pi$	Cation- $\pi$	H-bond
	TrpB	none TrpB	weak weak
	TrpB	TrpB	strong
	TrpB	TrpB	strong
	TyrA	TyrC2 TyrA	weak

Considering the  $\alpha 4\beta 4$  receptor, the binding of ACh is similar to what has been previously observed for the muscle-type and  $\alpha 4\beta 2$  receptors, but not  $\alpha 7$ . The quaternary ammonium ion of ACh makes a cation- $\pi$  interaction to the face of the aromatic residue TrpB, providing an unambiguous anchor point for ACh docking. The slopes of the cation- $\pi$  binding plots are as follows: 0.095, 0.10, and 0.095 for the  $\alpha 4\beta 4$ ,  $\alpha 4\beta 2$ , and muscle-type nAChRs, respectively.<sup>2, 3</sup> We interpret such similarity in slopes to indicate that the three receptors participate in equally strong cation- $\pi$  interactions between ACh and TrpB. Further, we find that the roles of the other residues of the aromatic box (TyrA, TyrC1, and TyrC2) are similar to those seen in the muscle-type and  $\alpha 4\beta 2$  receptors when

binding ACh. Results for  $\alpha 4\beta 4$  are strikingly different from the  $\alpha 7$  receptor, which uses agonist specific cation- $\pi$  interactions at TyrA and TyrC2.

An interesting result is observed when nicotine is the agonist; now the neuronal  $\alpha 4\beta 4$  receptor acts similarly to the  $\alpha 4\beta 2$  receptor rather than to the muscle-type receptor. In  $\alpha 4\beta 4$ , nicotine makes the same cation- $\pi$  interaction to TrpB as ACh, consistent with the long-accepted nicotinic pharmacophore, but an interaction that is absent in the muscle-type receptor. Interestingly, the slope of the cation- $\pi$  binding plot for  $\alpha 4\beta 4$  is 0.11, which could suggest a moderately stronger cation- $\pi$  interaction at this position than observed for  $\alpha 4\beta 2$  (slope = 0.089).<sup>2</sup> Thus, a cation- $\pi$  interaction to TrpB serves as a discriminator between receptors with higher sensitivity to nicotine ( $\alpha 4\beta 4$  and  $\alpha 4\beta 2$ ) and those with lower sensitivity (muscle-type).

Concerning the hydrogen bond to the backbone carbonyl associated with TrpB,  $\alpha 4\beta 4$  also behaves like  $\alpha 4\beta 2$ , not muscle-type or  $\alpha 7$ . At  $\alpha 4\beta 4$ , nicotine displays a 14-fold decrease in receptor function in response to the backbone ester mutation, comparable to 19-fold for  $\alpha 4\beta 2$ .<sup>2</sup> This contrasts the 1.6-fold shift for muscle-type or 2.1-fold shift for epibatidine at  $\alpha 7$ .<sup>1, 17</sup> Note that when the agonist is ACh – a molecule unable to make a conventional hydrogen bond to a carbonyl – essentially wild type receptor behavior is observed. This indicates that the backbone mutation did not alter receptor function downstream from binding, *i.e.*, gating. We conclude that nicotine is able to make a hydrogen bond to the carbonyl in question in all three receptors considered, but that the interaction is much stronger in  $\alpha 4\beta 4$  and  $\alpha 4\beta 2$ . This is an additional contributor to the enhanced potency of nicotine at the neuronal  $\alpha 4\beta 4$  and  $\alpha 4\beta 2$  receptors. Previous studies

of neuronal nAChRs have indicated that large differences in agonist affinity are primarily determined by the nature of the complementary subunit.<sup>31</sup> Our results provide a molecular rationale indicating that both  $\alpha 4$ -containing neuronal receptors make the same ligand-receptor interactions, but the magnitudes of the two interactions examined differ depending on the receptor, reflecting the nature of the  $\beta$  subunit. For nicotine, the cation- $\pi$  interaction is stronger in the  $\alpha 4\beta 4$  receptor, whereas the hydrogen bond interaction is stronger in the  $\alpha 4\beta 2$  nAChR.

Chimeric  $\beta$  subunits were used to further examine the role of the complementary binding site in defining subtype-specific receptor pharmacology. Using the cation- $\pi$  interaction at TrpB as a probe for agonist binding, we found that most chimeras experienced a modest increase in the  $F_3$ -Trp/Trp ratio compared to  $\alpha 4\beta 2$  and  $\alpha 4\beta 4$ . One exception, however, was nicotine at chimera F, which showed a decreased  $F_3$ -Trp/Trp ratio compared to  $\alpha 4\beta 2$ . Further analysis revealed that chimera F experienced a variable effect in response to additional tryptophan derivatives, and no significant trend was observed. Given that the core residues of the principal binding site are conserved in all nAChRs and chimera studies of the complementary binding site appear less informative, the question remains as to what features of the nAChR are responsible for differences in receptor pharmacology. It is possible that the variable residues flanking the conserved core residues may be the key to understanding the pharmacological diversity of nAChRs. Further experiments are underway to probe both the non- $\alpha$  subunits and residues within the  $\alpha$  subunit that are located outside the aromatic box (Chapter 3).

Here we identify structural features of the nAChR that discriminate among these four receptors and are likely to contribute to differential receptor pharmacology. In the

muscle-type receptor, TrpB makes a cation- $\pi$  interaction to ACh and to epibatidine, but not to nicotine.<sup>3, 16, 17</sup> In the neuronal  $\alpha 4\beta 4$  and  $\alpha 4\beta 2$  receptors, the TrpB cation- $\pi$  interaction to ACh remains, but now nicotine also makes a strong cation- $\pi$  interaction.<sup>2</sup> The  $\alpha 7$  receptor eschews the cation- $\pi$  interaction to TrpB, as agonists have moved their cationic center across the aromatic box to TyrA and TyrC2.<sup>1</sup> The nAChR family also uses a backbone hydrogen bonding interaction as a second discriminating feature for drug-receptor interactions. This interaction is modest in the muscle-type and  $\alpha 7$  receptors,<sup>1, 17</sup> but it is much stronger in  $\alpha 4\beta 4$  and  $\alpha 4\beta 2$ <sup>2</sup> – the higher sensitivity receptors. Taken as a whole, the data support the view that the energy of the cation- $\pi$  and hydrogen bond interactions studied here underlies the higher sensitivity of both  $\alpha 4\beta 2$  and  $\alpha 4\beta 4$ .

## 4.5 METHODS

### *Molecular Biology*

For ligand binding studies of the  $\alpha 4\beta 4$  nAChR (Part 1), human  $\alpha 4$  and  $\beta 4$  subunit genes were in pGEMhe. For chimera experiments (Part 2), rat  $\alpha 4$  and  $\beta 2$  nAChR subunit genes were in the pAMV vector, and as such, chimeras replaced loop regions of the rat  $\beta 2$  subunit with the corresponding regions of the rat  $\beta 4$  subunit. In accordance with previously reported protocols,<sup>2</sup> all  $\alpha 4\beta 2/\beta 4$  chimeric receptors contained a L9'A mutation in the  $\alpha 4$  subunit to increase receptor expression. Site-directed mutagenesis was performed using the QuikChange protocol (Stratagene). For nonsense suppression experiments, the site of interest within the nAChR subunit was mutated to an amber stop codon. Circular DNA for nAChR subunit genes in pAMV were linearized with Not I and nAChR subunit genes in pGEMhe were linearized with Nhe I. After purification

(Qiagen), linearized DNA was used as a template for runoff *in vitro* transcription using T7 mMessage mMachine kit (Ambion).

THG73<sup>32</sup> was used as the amber suppressor tRNA. Nitroveratryloxycarbonyl (NVOC) protected cyanomethyl ester form of unnatural amino acids and  $\alpha$ -hydroxythreonine cyanomethyl ester were synthesized, coupled to dinucleotide dCA, and enzymatically ligated to 74-nucleotide THG73 tRNA<sub>CUA</sub> as previously reported.<sup>20</sup> Crude tRNA-amino acid product was used without desalting, and the product was confirmed by MALDI-TOF MS on 3-hydroxypicolinic acid (3-HPA) matrix. Deprotection of the NVOC group on the tRNA-amino acid was carried out by photolysis for 5 minutes prior to coinjection with mRNA containing the UAG mutation at the site of interest.

### ***Microinjection***

Stage V-VI *Xenopus laevis* oocytes were employed. For experiments in Part 1, coinjection of  $\alpha 4$ : $\beta 4$  mRNA at a ratio of 1:1 by mass or lower yielded wild type ( $\alpha 4$ )<sub>2</sub>( $\beta 4$ )<sub>3</sub> receptors, while a ratio greater than 30:1 by mass produced pure populations of ( $\alpha 4$ )<sub>3</sub>( $\beta 4$ )<sub>2</sub>. If an unnatural amino acid was to be incorporated into the  $\alpha 4$  subunit to produce a ( $\alpha 4$ )<sub>2</sub>( $\beta 4$ )<sub>3</sub> receptor, then a mass ratio of 2:1 for  $\alpha 4$ : $\beta 4$  mRNA was injected into each oocyte.

In Part 2,  $\alpha 4\beta 2/\beta 4$  chimeric receptors were expressed using a co injection of  $\alpha 4$ : $\beta 2/\beta 4$  chimera mRNA at a ratio of 1:3 by mass. This ratio consistently produced chimeric receptors with the stoichiometry of ( $\alpha 4$ )<sub>2</sub>( $\beta 2/\beta 4$ )<sub>3</sub>. For nonsense suppression experiments incorporating an unnatural amino acid into the  $\alpha 4$  subunit, a mass ratio of 3:1 for  $\alpha 4$ : $\beta 2/\beta 4$  chimera mRNA was injected into each oocyte to produce ( $\alpha 4$ )<sub>2</sub>( $\beta 2/\beta 4$ )<sub>3</sub>

receptors. To ensure  $(\alpha 4)_2(\beta 2/\beta 4)_3$  stoichiometry, all receptor stoichiometries were confirmed by voltage jump experiments.<sup>2</sup>

For all experiments (Part 1 and 2), the total mRNA injected was 25-65 ng/oocyte depending on the relative expression level, and approximately 15 ng of tRNA per cell was used for suppression experiments. Each oocyte was injected with 50 nL of RNA solution, and the oocytes were incubated for 24-48 hours at 18 °C in ND96 buffer (96 mM NaCl, 2 mM KCl, 1 mM MgCl<sub>2</sub>, 1.8 mM CaCl<sub>2</sub>, and 5 mM HEPES, pH 7.5) with 0.005% (w/v) gentamycin and 2% (v/v) horse serum. In the case of low-expressing mutant receptors, a second injection was required 24 hours after the first injection. As a negative control for all suppression experiments, 76-nucleotide tRNA (dCA ligated to 74-nucleotide tRNA) was coinjected with mRNA in the same manner as fully charged tRNA.

### ***Electrophysiology***

Acetylcholine chloride and (-)-nicotine tartrate were purchased from Sigma/Aldrich/RBI (St. Louis, MO) and drug dilutions were prepared from 1M *aq* stock solutions. Drug dilutions were prepared in calcium-free ND96 buffer. Ion channel function was assayed using the OpusXpress 6000A (Molecular Devices Axon Instruments) in two-electrode voltage clamp mode. Oocytes were clamped at a holding potential of -60 mV. One mL of each drug solution was applied to the clamped oocytes for 12 sec and followed by a 2 minute wash with calcium-free ND96 buffer between each concentration. Data were sampled at 125 Hz and filtered at 50 Hz. Voltage jump experiments were sampled at 5000 Hz and filtered at 180 Hz.

### ***Data Analysis***

Dose-response data were obtained for at least 6 concentrations of agonists and for a minimum of 5 oocytes (from two different batches). Mutants with  $I_{\max}$  of at least 100 nA of current were defined as functional.  $EC_{50}$  and Hill coefficient ( $n_H$ ) were calculated by fitting the averaged, normalized dose-response relation to the Hill equation. All data are reported as means  $\pm$ S.E.

### **4.6 ACKNOWLEDGEMENTS**

We thank Ariele P. Hanek helpful discussions. This work was supported, in whole or in part, by National Institutes of Health Grants NS34407 and NS11756 and by Grant MH086383 (to H. A. L.). This work was also supported by California Tobacco-Related Disease Research Program Grant 19XT-0102 from the University of California (to D. A. D.).

## 4.7 REFERENCES

1. Puskar, N. L.; Xiu, X.; Lester, H. A.; Dougherty, D. A., Two neuronal nicotinic acetylcholine receptors,  $\alpha 4\beta 4$  and  $\alpha 7$ , show differential agonist binding modes. *J Biol Chem* **286**, (16), 14618-27.
2. Xiu, X.; Puskar, N. L.; Shanata, J. A.; Lester, H. A.; Dougherty, D. A., Nicotine binding to brain receptors requires a strong cation- $\pi$  interaction. *Nature* **2009**, *458*, (7237), 534-7.
3. Zhong, W.; Gallivan, J. P.; Zhang, Y.; Li, L.; Lester, H. A.; Dougherty, D. A., From ab initio quantum mechanics to molecular neurobiology: a cation- $\pi$  binding site in the nicotinic receptor. *Proc Natl Acad Sci U S A* **1998**, *95*, (21), 12088-93.
4. Corringer, P. J.; Le Novere, N.; Changeux, J. P., Nicotinic receptors at the amino acid level. *Annu Rev Pharmacol Toxicol* **2000**, *40*, 431-58.
5. Jensen, A. A.; Frolund, B.; Liljefors, T.; Krosgaard-Larsen, P., Neuronal nicotinic acetylcholine receptors: structural revelations, target identifications, and therapeutic inspirations. *J Med Chem* **2005**, *48*, (15), 4705-45.
6. Romanelli, M. N.; Gratteri, P.; Guandalini, L.; Martini, E.; Bonaccini, C.; Gualtieri, F., Central nicotinic receptors: structure, function, ligands, and therapeutic potential. *ChemMedChem* **2007**, *2*, (6), 746-67.
7. Unwin, N., Refined structure of the nicotinic acetylcholine receptor at 4 Å resolution. *J Mol Biol* **2005**, *346*, (4), 967-89.
8. Miyazawa, A.; Fujiyoshi, Y.; Unwin, N., Structure and gating mechanism of the acetylcholine receptor pore. *Nature* **2003**, *423*, (6943), 949-55.
9. Brejc, K.; van Dijk, W. J.; Klaassen, R. V.; Schuurmans, M.; van Der Oost, J.; Smit, A. B.; Sixma, T. K., Crystal structure of an ACh-binding protein reveals the ligand-binding domain of nicotinic receptors. *Nature* **2001**, *411*, (6835), 269-76.
10. Gotti, C.; Clementi, F., Neuronal nicotinic receptors: From structure to pathology. *Prog Neurobiol* **2004**, *74*, (6), 363-96.
11. Romanelli, M. N.; Gratteri, P.; Guandalini, L.; Martini, E.; Bonaccini, C.; Gualtieri, F., Central Nicotinic Receptors: Structure, Function, Ligands, and Therapeutic Potential. *ChemMedChem* **2007**, *2*, (6), 746-767.
12. Beers, W. H.; Reich, E., Structure and activity of acetylcholine. *Nature* **1970**, *228*, (5275), 917-22.
13. Glennon, R. A.; Dukat, M., Central nicotinic receptor ligands and pharmacophores. *Pharm Acta Helv* **2000**, *74*, (2-3), 103-14.
14. Sixma, T. K.; Smit, A. B., Acetylcholine binding protein (AChBP): a secreted glial protein that provides a high-resolution model for the extracellular domain of pentameric ligand-gated ion channels. *Annu Rev Biophys Biomol Struct* **2003**, *32*, 311-34.
15. Blum, A. P.; Lester, H. A.; Dougherty, D. A., Inaugural article: Nicotinic pharmacophore: the pyridine N of nicotine and carbonyl of acetylcholine hydrogen bond across a subunit interface to a backbone NH. *Proc Natl Acad Sci U S A* **107**, (30), 13206-11.
16. Beene, D. L.; Brandt, G. S.; Zhong, W.; Zacharias, N. M.; Lester, H. A.; Dougherty, D. A., Cation- $\pi$  interactions in ligand recognition by serotonergic (5-

- HT3A) and nicotinic acetylcholine receptors: the anomalous binding properties of nicotine. *Biochemistry* **2002**, 41, (32), 10262-9.
17. Cashin, A. L.; Petersson, E. J.; Lester, H. A.; Dougherty, D. A., Using physical chemistry to differentiate nicotinic from cholinergic agonists at the nicotinic acetylcholine receptor. *J Am Chem Soc* **2005**, 127, (1), 350-6.
  18. Xiu, J. Structure-Function Studies of Nicotinic Acetylcholine Receptors Using Unnatural Amino Acids. The California Institute of Technology, Ph.D. Thesis, Pasadena, 2007.
  19. Wu, J.; Liu, Q.; Yu, K.; Hu, J.; Kuo, Y. P.; Segerberg, M.; St John, P. A.; Lukas, R. J., Roles of nicotinic acetylcholine receptor beta subunits in function of human alpha4-containing nicotinic receptors. *J Physiol* **2006**, 576, (Pt 1), 103-18.
  20. Nowak, M. W.; Gallivan, J. P.; Silverman, S. K.; Labarca, C. G.; Dougherty, D. A.; Lester, H. A., In vivo incorporation of unnatural amino acids into ion channels in *Xenopus* oocyte expression system. *Methods Enzymol* **1998**, 293, 504-29.
  21. Padgett, C. L.; Hanek, A. P.; Lester, H. A.; Dougherty, D. A.; Lummis, S. C., Unnatural amino acid mutagenesis of the GABA(A) receptor binding site residues reveals a novel cation-pi interaction between GABA and beta 2Tyr97. *J Neurosci* **2007**, 27, (4), 886-92.
  22. Lummis, S. C.; D, L. B.; Harrison, N. J.; Lester, H. A.; Dougherty, D. A., A cation-pi binding interaction with a tyrosine in the binding site of the GABAC receptor. *Chem Biol* **2005**, 12, (9), 993-7.
  23. Mu, T. W.; Lester, H. A.; Dougherty, D. A., Different binding orientations for the same agonist at homologous receptors: a lock and key or a simple wedge? *J Am Chem Soc* **2003**, 125, (23), 6850-1.
  24. Torrice, M. M.; Bower, K. S.; Lester, H. A.; Dougherty, D. A., Probing the role of the cation-pi interaction in the binding sites of GPCRs using unnatural amino acids. *Proc Natl Acad Sci U S A* **2009**, 106, (29), 11919-24.
  25. Moroni, M.; Zwart, R.; Sher, E.; Cassels, B. K.; Bermudez, I., alpha4beta2 nicotinic receptors with high and low acetylcholine sensitivity: pharmacology, stoichiometry, and sensitivity to long-term exposure to nicotine. *Mol Pharmacol* **2006**, 70, (2), 755-68.
  26. Nelson, M. E.; Kuryatov, A.; Choi, C. H.; Zhou, Y.; Lindstrom, J., Alternate stoichiometries of alpha4beta2 nicotinic acetylcholine receptors. *Mol Pharmacol* **2003**, 63, (2), 332-41.
  27. Nowak, M. W.; Kearney, P. C.; Sampson, J. R.; Saks, M. E.; Labarca, C. G.; Silverman, S. K.; Zhong, W.; Thorson, J.; Abelson, J. N.; Davidson, N.; et al., Nicotinic receptor binding site probed with unnatural amino acid incorporation in intact cells. *Science* **1995**, 268, (5209), 439-42.
  28. Espinoza-Fonseca, L. M.; Trujillo-Ferrara, J. G., Fully flexible docking models of the complex between alpha7 nicotinic receptor and a potent heptapeptide inhibitor of the beta-amyloid peptide binding. *Bioorg Med Chem Lett* **2006**, 16, (13), 3519-23.
  29. Hussy, N.; Ballivet, M.; Bertrand, D., Agonist and antagonist effects of nicotine on chick neuronal nicotinic receptors are defined by alpha and beta subunits. *J Neurophysiol* **1994**, 72, (3), 1317-26.

30. Luetje, C. W.; Patrick, J., Both alpha- and beta-subunits contribute to the agonist sensitivity of neuronal nicotinic acetylcholine receptors. *J Neurosci* **1991**, 11, (3), 837-45.
31. Parker, M. J.; Beck, A.; Luetje, C. W., Neuronal nicotinic receptor beta2 and beta4 subunits confer large differences in agonist binding affinity. *Mol Pharmacol* **1998**, 54, (6), 1132-9.
32. Saks, M. E.; Sampson, J. R.; Nowak, M. W.; Kearney, P. C.; Du, F.; Abelson, J. N.; Lester, H. A.; Dougherty, D. A., An engineered Tetrahymena tRNA<sup>Gln</sup> for in vivo incorporation of unnatural amino acids into proteins by nonsense suppression. *J Biol Chem* **1996**, 271, (38), 23169-75.

## *Chapter 5*

### **Optimizing Techniques to Implement Nonsense Suppression in Mammalian Cells\***

*\*This work was done in collaboration with Kristina McCleary.*

#### **5.1 ABSTRACT**

Our lab previously used microelectroporation to incorporate unnatural amino acids into ion channels expressed in mammalian cells. While this work represented major progress, this method still faced several limitations. Specifically, microelectroporation is not robust enough for large-scale cellular imaging techniques and requires significant amounts of aminoacylated tRNA. This chapter describes our efforts to further develop transfection techniques for mammalian cells to increase the expression of mutant protein such that functional analysis of several thousand cells simultaneously can be achieved using the FlexStation3. Using HEK293T cells, we have optimized two protocols to efficiently cotransfect DNA and tRNA. These protocols are termed double electroporation using the Neon transfection system and single transfection using *TransIT* transfection reagent. Both methods successfully suppress an amber stop codon using an *in vivo* aminoacylated tRNA, but fail to achieve suppression using *in vitro* aminoacylated tRNAs. Studies are ongoing to evaluate the cause of the failed suppression experiments using *in vitro* aminoacylated tRNAs. Possible causes include the amino acid falling off the tRNA inside the cell and translational incompetence of the tRNA molecule itself.

## 5.2 INTRODUCTION

The nonsense suppression methodology, developed by Schultz in 1989,<sup>1</sup> has emerged as a powerful biophysical tool facilitating site-specific incorporation of virtually any unnatural amino acid - as long as it can be synthesized in the chemistry lab - into biologically relevant proteins. This method is particularly attractive because it can conceivably generate an infinite number of proteins with novel chemical properties as well as probe protein structure/function relationships.

Our lab has adapted the nonsense suppression methodology to incorporate unnatural amino acids into proteins expressed in *Xenopus laevis* oocytes.<sup>2,3</sup> In doing so, we have successfully determined the ligand binding mechanism and channel gating properties of numerous ion channels and neuroreceptors.<sup>4-9</sup> While heterologous expression in *Xenopus* oocytes has proven an optimal model system to efficiently express hundreds of mutant proteins, we are currently interested in expanding this technology to a mammalian expression system. One advantage of implementing a mammalian expression system is that one can study mammalian proteins in a biologically relevant context (*i.e.*, one can study a *human* protein in a *human* cell line). Additionally, using a mammalian system will allow for the study of cell-specific signal transduction pathways, and one can imagine designing experiments using unnatural amino acids (*e.g.*, photocaged amino acids) to exert temporal control of various signaling cascades.<sup>10</sup>

### ***Progress towards Unnatural Amino Acid Mutagenesis in Mammalian Cells***

One of the key challenges in mammalian protein expression is determining the appropriate transfection method that will maximize protein expression, limit cell toxicity, and consume the least amount of nucleic acid. Several transfection techniques have been

developed to effectively introduce nucleic acids into cells, such as chemical-based methods (*e.g.*, calcium phosphate, cationic polymers, cationic liposomes, and cationic activated dendrimers), non-chemical methods (*e.g.*, electroporation), particle-based methods (*e.g.*, gene gun), and viral transduction. Each transfection technique is accompanied by inherent advantages and disadvantages depending on the cell line of interest and nucleic acid material being delivered.

In recent years, many researchers have contributed major advances towards the types of transfection techniques amenable to introducing both DNA and tRNA into mammalian cells. For example, RajBhandary and workers successfully suppressed a serine site with tyrosine in chloramphenicol acetyltransferase.<sup>11</sup> This experiment utilized a cationic lipid (Effectene) to co-transfect *in vitro* aminoacylated tRNA with DNA into COS cells.<sup>11</sup> Alternatively, Schultz and workers took a different approach employing directed evolution of suppressor tRNA-aminoacyl synthetase pairs to site-specifically incorporate unnatural amino acids into several types of mammalian cells.<sup>12-14</sup> And in 2003, our lab used microelectroporation to cotransfect mRNA and tRNA that had been aminoacylated *in vitro* with an unnatural amino acid to express mutant ion channels in CHO cells and cultured neurons.<sup>15</sup> Whole-cell patch clamp electrophysiology confirmed the presence of functional mutant protein.<sup>15</sup> While this work represents major progress in this field, these methods do not yield robust amounts of mutant protein and require functional analysis on a single cell scale.

We are interested in further developing techniques to increase the expression of mutant protein in mammalian cells to a level that allows functional analysis of several thousand cells simultaneously. This chapter describes our efforts to determine the

optimal transfection protocol for incorporating unnatural amino acids into ion channels expressed in mammalian cells.

## **5.3 METHODS**

### **5.3.1 Molecular Biology**

Human 5HT<sub>3A</sub> subunit gene in pcDNA3.1(+) vector was purchased from Missouri S & T cDNA Research Center. Mouse  $\alpha$ 4,  $\alpha$ 4GFP, and  $\beta$ 2 genes were in pciNEO vector, and the mouse  $\beta$ 4 gene was in pcDNA3.1(+) vector. All mouse constructs were obtained from the Lester lab. All eGFP constructs used in these studies are from Monahan *et al.*<sup>15</sup>

Site-directed mutagenesis was performed using the QuikChange protocol (Stratagene) to incorporate either an amber stop codon (TAG) or a frameshift stop codon (GTTT) at the site of interest within the subunit DNA. THG73<sup>16</sup> was used as the amber suppressor tRNA. Human serine amber suppressor tRNA (HSAS) was used to incorporate serine opposite an amber stop codon.<sup>17</sup> For suppression of the frameshift codon (GTTT), the yeast phenylalanine frameshift suppressor tRNA (YFaFS) was used.<sup>18</sup>

Nitroveratryloxycarbonyl (NVOC) protected cyanomethyl esters of natural or unnatural amino acids and  $\alpha$ -hydroxy acid cyanomethyl esters were prepared as previously reported.<sup>2</sup> Aminoacyl tRNA was confirmed by MALDI-TOF MS on 3-hydroxypicolinic acid (3-HPA) matrix. Prior to transfection, the NVOC protecting group on the aminoacyl tRNA was deprotected by photolysis for 5 minutes.

### **5.3.2 Mammalian Cell Culture**

Human embryonic kidney cells (HEK293T) cells were purchased from American Tissue Culture Collection (ATCC). The HEK293T cell line is optimized for increased

efficiency of transient transfections due to expression of the simian virus 40 (SV40) large tumor antigen in the cell.<sup>19, 20</sup> Therefore, transiently transfected plasmids containing the SV40 origin of replication produce extremely high levels of expression.

All cell culture reagents were obtained from Gibco, except for heat-inactivated fetal bovine serum purchased from Sigma. HEK293T cells were grown on sterile 100 mm culture dishes at 37 °C and 5% CO<sub>2</sub> in a humidified atmosphere. Cells were cultured in DMEM:F12 with Glutamax I<sub>TM</sub> with 10% fetal bovine serum according to literature.<sup>21</sup>

HEK293T cell seeding was optimized for both 100 and 35 mm dishes. **Tables 5.1** and **5.2** indicate the number of cells to seed to achieve the appropriate confluency for day of transfection. According to protocols, 70%-90% confluency is desired to achieve efficient transfection (highlighted in red). 35 mm dishes were used for all transfections and aliquotted into 3 columns of a 96-well plate, unless otherwise specified.

**Table 5.1.** Optimization of HEK293T cell seeding for 100 mm dishes.

Dilution	Dilution Shorthand	24 hr	36 hr	48 hr	72 hr
10 million cells/dish	1:1	80%	n/a	n/a	n/a
7.5 million cells/dish	1:1.5	70%	-	100%	n/a
5 million cells/dish	1:2	70%	90%	n/a	n/a
3.3 million cells/dish	1:3	25%-30%	-	60%	80%-90%
2.5 million cells/dish	1:4	20%-30%	-	50%	80%-90%
2 million cells/dish	1:5	30%	-	70%	90%
1 million cells/dish	1:10	15%	-	30%	70%

**Table 5.2.** Optimization of HEK293T cell seeding for 35 mm dishes.

Dilution	24 hr	48 hr	72 hr
100,000 cells/dish	5%	10%	40%
200,000 cells/dish	10%	20%	50%
300,000 cells/dish	15%	25%	70%
400,000 cells/dish	25%	30%	70%
500,000 cells/dish	35%	50%	100%
600,000 cells/dish	30%	70%	n/a
700,000 cells/dish	30%	80%	n/a
800,000 cells/dish	40%	90%	n/a
900,000 cells/dish	50%	100%	n/a
1,000,000 cells/dish	60%	100%	n/a
1,500,000 cells/dish	70%-100%	n/a	n/a

Cells were transiently transfected using various protocols, such as polyethylenimine (PEI), ExpressFect transfection reagent (Denville Scientific), Neon Transfection System (Life Technologies), *TransIT*-mRNA transfection kit (Mirus), TransMessenger transfection reagent (Qiagen), and Lipofectamine RNAiMAX transfection reagent (Life Technologies). Following transfection, cells were plated ( $\sim 3 \times 10^4$  cells/well) onto black 96-well plates with clear bottoms (BD Falcon), incubated for 1-2 days, and then assayed using the Flexstation 3. Unless otherwise indicated, manufacturers' protocols were followed for each transfection method. For PEI transfections in 35 mm plates, 1.5  $\mu\text{g}$  of DNA was transfected with 0.3 mL of DMEM and 9  $\mu\text{L}$  of PEI (in 3 mL DMEM total). For confocal experiments, ExpressFect transfections were performed in 35 mm plates and 1  $\mu\text{g}$  of DNA was transfected with 4  $\mu\text{L}$  of ExpressFect for 4 hr.

### 5.3.3 The FlexStation 3

The FlexStation 3 is a 96-well fluorescent plate reader used to analyze the functional properties of neurotransmitter-gated ion channels (*e.g.*, human  $5\text{HT}_{3\text{A}}$  and human  $\alpha 4\beta 4$  receptors). This device is comprised of two modules - a fluidics module and a detection module (**Figure 5.1**). The fluidics module contains an 8-channel pipette that delivers solutions of neurotransmitter from the source plate to the 96-well sample plate containing HEK293T cells expressing ion channels. The detection module contains an excitation source and a PMT detector that detects the change in fluorescence in response to neurotransmitter activation.

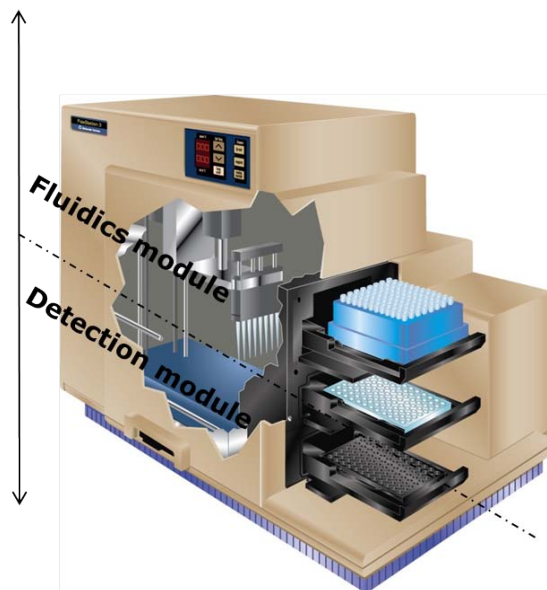


**Figure 5.1.** Schematic of the FlexStation 3 microplate reader. © Molecular Devices.

Following a two day incubation period, transfected cells in a 96-well plate were washed twice with flex buffer (115 mM NaCl, 1 mM KCl, 1 mM CaCl<sub>2</sub>, 1 mM MgCl<sub>2</sub>, 0.9 mM glucose, 10 mM HEPES, pH 7.4) at room temperature.<sup>21</sup> FLIPR membrane potential assay dye (blue kit, Molecular Devices) was diluted 1:10 (unless otherwise specified) in flex buffer and loaded onto washed cells (100 μL/well). Cells were incubated at 37 °C for 45-60 min, and then assayed using the FlexStation. Fluorescence was measured every 1.5 sec for 180 sec, and at 20 sec, 100 μL of neurotransmitter (*e.g.*, 5-HT or ACh) was added to each well. 5-HT and ACh were purchased from Sigma, and neurotransmitter solutions were prepared in flex buffer.

In response to neurotransmitter application, ion channels expressed on the cell membrane bind to the neurotransmitter, undergo a conformational change allowing ions to enter the cell, and cause a change in membrane potential. This change in membrane potential is proportional to the relative fluorescence measurements detected by the FlexStation. Prior to neurotransmitter application, the cell membrane is polarized and the

quenched fluorescent dye is located outside of the cell membrane (**Figure 5.2**). In response to neurotransmitter stimulation, ion channels expressed on the cell membrane open, thereby depolarizing the membrane. The dye enters the cell and fluoresces.

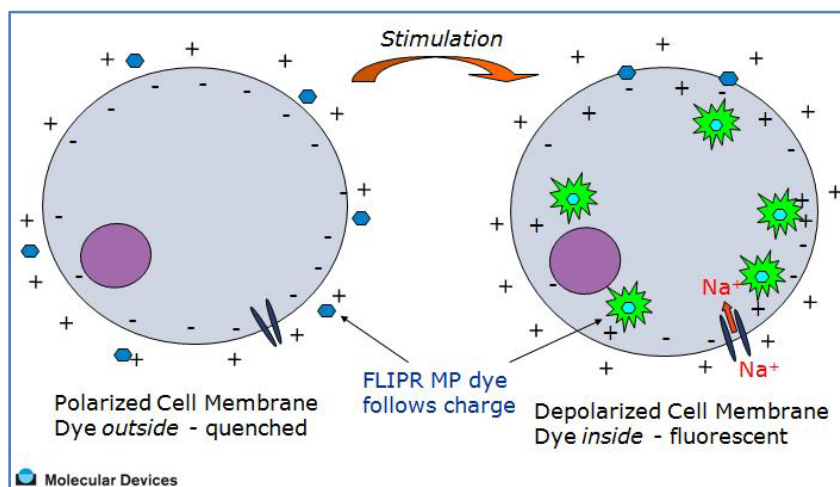


**Figure 5.2.** Membrane potential assay. Schematic depicting the change in fluorescence in response to cell membrane depolarization. © Molecular Devices.

SOFTmax Pro (Molecular Devices) was used for data analysis (**Figure 5.3A**). Dose-response data were obtained for at least 3 columns of cells (unless otherwise specified). For each column, reduction analysis was performed and the baseline fluorescence at 20 sec was subtracted from the peak fluorescence for each concentration of neurotransmitter (**Figure 5.3B**). These values were normalized to the maximum fluorescence (fluorescence at maximal dose of neurotransmitter).  $EC_{50}$  and Hill coefficient ( $n_H$ ) were calculated by fitting the averaged, normalized dose-response relation to the Hill equation.

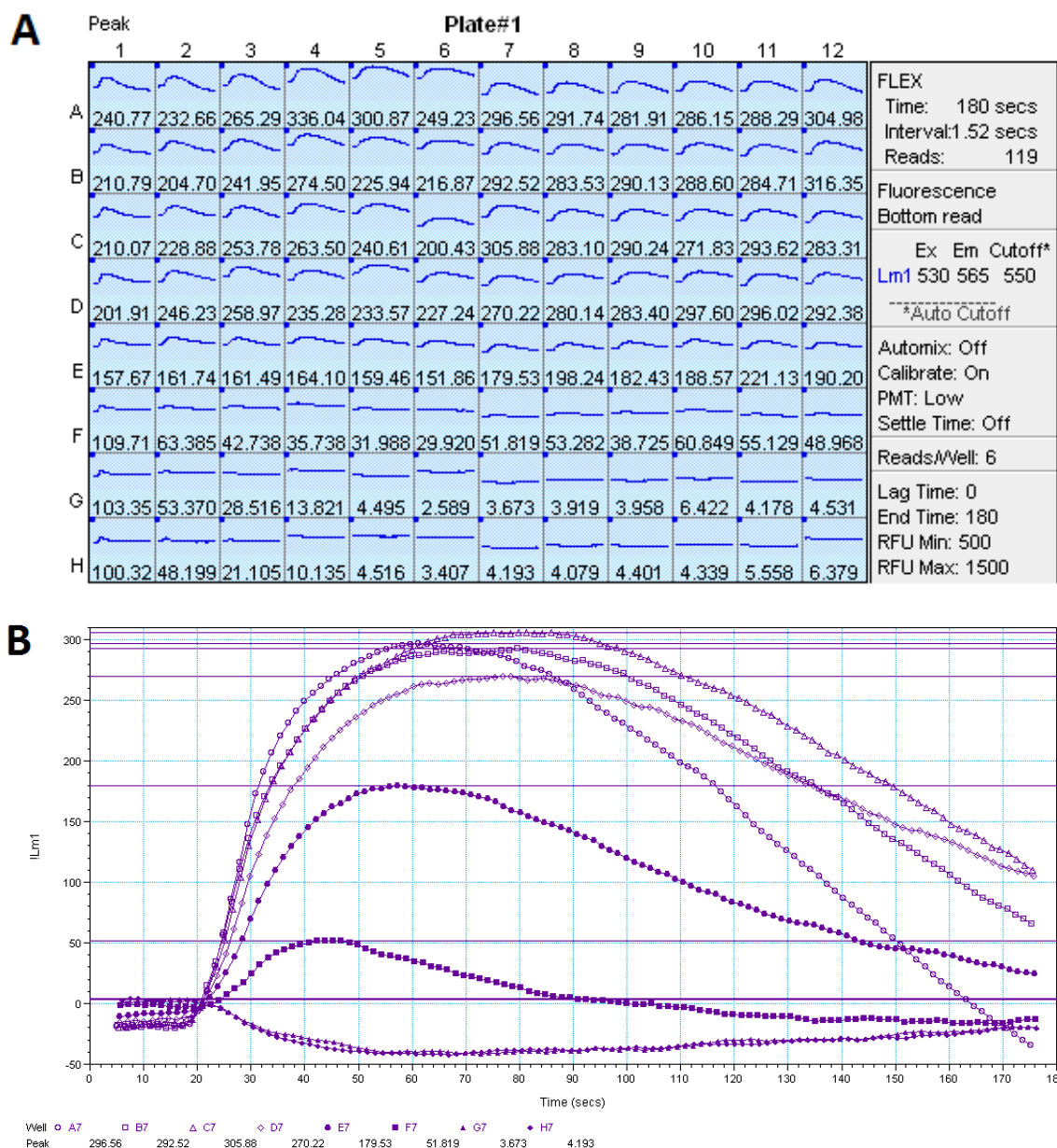


**Figure 5.3.** SOFTmax PRO data analysis of a 96-well plate. A. Example plate containing HEK293T cells expressing human 5HT<sub>3A</sub> receptors is shown (data collected in house). The columns are labeled 1-12 and the rows are labeled A-H. The drug plate is prepared by serial dilution with row A containing the highest drug concentration, and row H containing the lowest. Each row receives a specific drug concentration. The peak relative fluorescence is reported for each well of the plate. B. Reduction analysis of column 7 (from the plate in A), indicating the peak relative fluorescence per drug concentration.

### 5.3.4 Fluorescent Dye Experiments

Several concentrations of rhodamine B (Sigma) were prepared in a drug plate by 1:1 serial dilutions of rhodamine B:water starting with a 50 mM stock of rhodamine B. 100  $\mu$ L of dye was added to 100  $\mu$ L of water in the assay plate for each concentration and the area under the curve of the emission spectrum was measured. This was repeated for each PMT setting (low, medium, high).

Note that eosin Y and fluorescein (purchased from City Chemical Company and Sigma, respectively) were also tested with the low PMT setting. Interestingly, both dyes displayed a maximal RFU of 50,000 indicating that the FlexStation is capable of detecting very high fluorescence signals.

## 5.4 RESULTS AND DISCUSSION

### 5.4.1 Determining the Optimal PMT Setting to Detect Small Fluorescence Signals

It is possible that even under optimal transfection conditions, the fluorescence signal of mutant ion channels containing unnatural amino acids will be significantly lower than for wild type ion channels. Thus, we needed to determine the appropriate FlexStation PMT setting to maximize the relative fluorescence unit (RFU) signal detected. The RFU dependence on PMT setting was measured for a serial dilution of rhodamine B at each of the PMT settings (low, medium, high).

Using the low PMT setting, the FlexStation was unable to detect fluorescence for high rhodamine B concentrations (50 – 0.39 mM), which is likely due to self-quenching of the dye. A maximal signal of 10,000 RFU was detected for 0.19 mM rhodamine B and each subsequent serial dilution produced a fluorescence signal decreased by approximately half (**Table 5.3**). A similar trend was observed for the medium PMT

setting. Here, the maximal signal is 6500 RFU detected for 0.049 mM rhodamine B, followed by a decrease in RFU proportional to dye concentration. Under the high PMT setting, 1.52  $\mu$ M rhodamine B was the highest concentration that produced a fluorescence signal (300 RFU). Similarly, as the dye concentration decreased, so did the RFU.

**Table 5.3.** Comparison of RFU signal detected by the FlexStation 3 for each PMT settings for a serial dilution of rhodamine B.

<b>Rhodamine B Concentration (<math>\mu</math>M)</b>	<b>Low PMT Setting</b>	<b>Medium PMT Setting</b>	<b>High PMT Setting</b>
<b>0.763</b>	191.47	144.91	124.55
<b>0.381</b>	77.67	65.71	47.34
<b>0.191</b>	44.83	27.18	22.21
<b>0.095</b>	20.88	16.13	12.56
<b>0.048</b>	17.04	8.56	6.44
<b>0.024</b>	10.07	5.52	4.34
<b>0.012</b>	7.88	4.64	2.89
<b>0.006</b>	5.87	3.42	2.25

For any given rhodamine B concentration, the low PMT setting produced the greatest RFU signal. As shown in **Table 5.3**, we compared RFU values detected at various PMT settings for very low concentrations of dye. We anticipate that small RFU signals (produced by very low dye concentrations) are likely to mimic those of a mutant ion channel expressing an unnatural amino acid. We, therefore, chose to use the low PMT setting for FlexStation assays of transfected cells.

#### **5.4.2 Transfection of Mammalian Cells**

##### ***ExpressFect and PEI Transfections of Neuronal Nicotinic Acetylcholine Receptors***

To establish a positive control, functional ion channels were expressed in HEK293T cells and detected using the FlexStation. Neuronal  $\alpha 4\beta 2$  and  $\alpha 4\beta 4$  receptors were tested as ion channel targets for FlexStation analysis. Using ExpressFect

transfection reagent, HEK293T cells were transfected with  $\alpha 4$  DNA tagged with green fluorescent protein ( $\alpha 4$ -GFP) and either  $\beta 2$  or  $\beta 4$  wild type DNA. Confocal microscopy revealed robust membrane expression of  $\alpha 4$ GFP $\beta 4$  receptors, but not  $\alpha 4$ GFP $\beta 2$  receptors (**Figure 5.4**). The  $\alpha 4$ GFP $\beta 4$  image clearly shows membrane expression by the rough edges and the bright dots as ER exit sites, both of which are absent in the  $\alpha 4$ GFP $\beta 2$  image. This observation was not surprising since literature supports that  $\alpha 4\beta 2$  receptors become trapped in the endoplasmic reticulum (ER) due to the presence of an ER retention motif and lack of an ER export motif.<sup>22</sup>

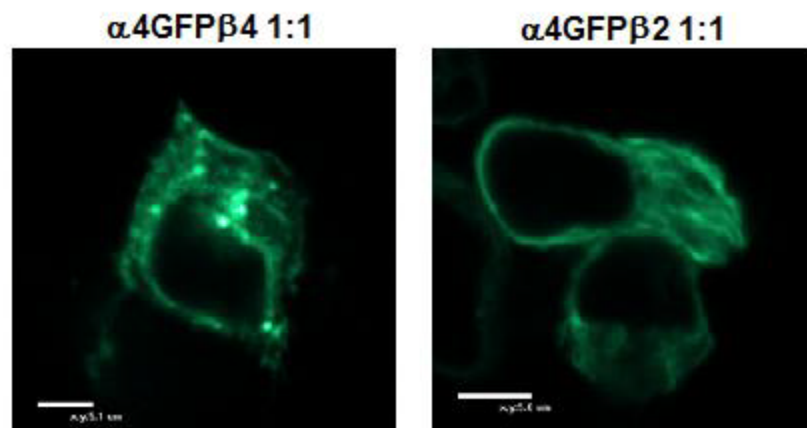


**Figure 5.4.** Confocal images of HEK293T cells expressing mouse  $\alpha 4\beta 4$  or  $\alpha 4\beta 2$  receptors containing GFP in the  $\alpha 4$  subunit.

We previously reported that biasing  $\alpha 4:\beta 4$  subunit mRNA in *Xenopus* oocytes can control  $\alpha 4\beta 4$  receptor stoichiometry shown by electrophysiology (Chapter 4).<sup>7</sup> We therefore tested the ability of the FlexStation to detect changes in receptor stoichiometry using a similar experiment. HEK293T cells were transfected with several ratios of  $\alpha 4:\beta 4$  subunit DNA and functionally analyzed using the FlexStation (**Table 5.4**). Transfections were performed using both PEI and ExpressFect protocols. Consistent results were obtained using both protocols.

**Table 5.4.** Human  $\alpha 4\beta 4$  receptors expressed in HEK293T cells for given ratios of  $\alpha 4:\beta 4$  DNA.  $EC_{50}$  measurements and RFU values were collected using the FlexStation.

$\alpha 4:\beta 4$ Ratio	$EC_{50}$ ( $\mu M$ )	Hill	N	Average Max RFU
<b>2000:1</b>	$1.79 \pm 0.23$	$1.16 \pm 0.14$	6	40.4
<b>1000:1</b>	$1.46 \pm 0.23$	$1.14 \pm 0.17$	5	52.9
<b>500:1</b>	$0.75 \pm 0.04$	$1.67 \pm 0.13$	17	104.4
<b>200:1</b>	$0.70 \pm 0.02$	$1.49 \pm 0.05$	17	106.2
<b>100:1</b>	$0.72 \pm 0.07$	$1.13 \pm 0.10$	20	144.6
<b>50:1</b>	$0.70 \pm 0.05$	$1.24 \pm 0.09$	20	155.4
<b>30:1</b>	$0.65 \pm 0.04$	$1.20 \pm 0.07$	20	163.8
<b>10:1</b>	$0.66 \pm 0.04$	$1.23 \pm 0.07$	21	125.0
<b>3:1</b>	$0.75 \pm 0.07$	$1.14 \pm 0.11$	19	80.1
<b>1:1</b>	$3.14 \pm 0.24$	$0.98 \pm 0.06$	23	67.0
<b>1:3</b>	$5.51 \pm 0.62$	$2.55 \pm 0.48$	2	47.3
<b>1:10</b>	$7.45 \pm 1.60$	$3.83 \pm 3.23$	2	16.1

Multiple stoichiometries of the  $\alpha 4\beta 4$  receptor were observed. The most abundant  $\alpha 4\beta 4$  population was observed for transfection of  $\alpha 4:\beta 4$  DNA ratios ranging from 500:1 to 3:1, which likely represents  $(\alpha 4)_3(\beta 4)_2$ . These receptors displayed a characteristic  $EC_{50}$  of approximately 0.7  $\mu M$  ACh and an average maximal RFU of 100-150. Alternatively,  $(\alpha 4)_2(\beta 4)_3$  receptors were observed for  $\alpha 4:\beta 4$  DNA ratios biasing the  $\beta 4$  subunit, such as 1:1 to 1:10. This second receptor population was accompanied by a right-shifted  $EC_{50}$  and decreased average maximal RFU compared to  $(\alpha 4)_3(\beta 4)_2$ . It appears that agonist sensitivity for these two  $\alpha 4\beta 4$  stoichiometries differs depending on whether the receptors are expressed in HEK293T cells or *Xenopus* oocytes. In HEK293T cells,  $(\alpha 4)_3(\beta 4)_2$  receptors cells display a lower, more sensitive  $EC_{50}$  than  $(\alpha 4)_2(\beta 4)_3$  receptors, while the reverse is observed for oocyte expression.<sup>7</sup> We also note the presence of a third  $\alpha 4\beta 4$  population for DNA ratios extremely biasing  $\alpha 4$  (e.g. 2000:1 and 1000:1), which is probably a physiological irrelevant stoichiometry (e.g.,  $(\alpha 4)_4(\beta 4)_1$ ) resulting from excessive subunit bias.

### *ExpressFect and PEI Transfections of the 5-HT<sub>3A</sub> Receptor*

While the FlexStation can discriminate between receptors that experience variable stoichiometries, we anticipated that attempting nonsense suppression in such a receptor was unnecessarily complicated. We moved forward with the homopentameric serotonin-gated ion channel, the 5HT<sub>3A</sub> receptor. HEK293T cells were transfected with human 5HT<sub>3A</sub> DNA using either ExpressFect or PEI transfection protocols. Both transfection methods produced similar results. EC<sub>50</sub> (0.3  $\mu$ M 5-HT) and average maximal RFU were consistent with each other and literature values (Figure 5.5).<sup>23</sup>

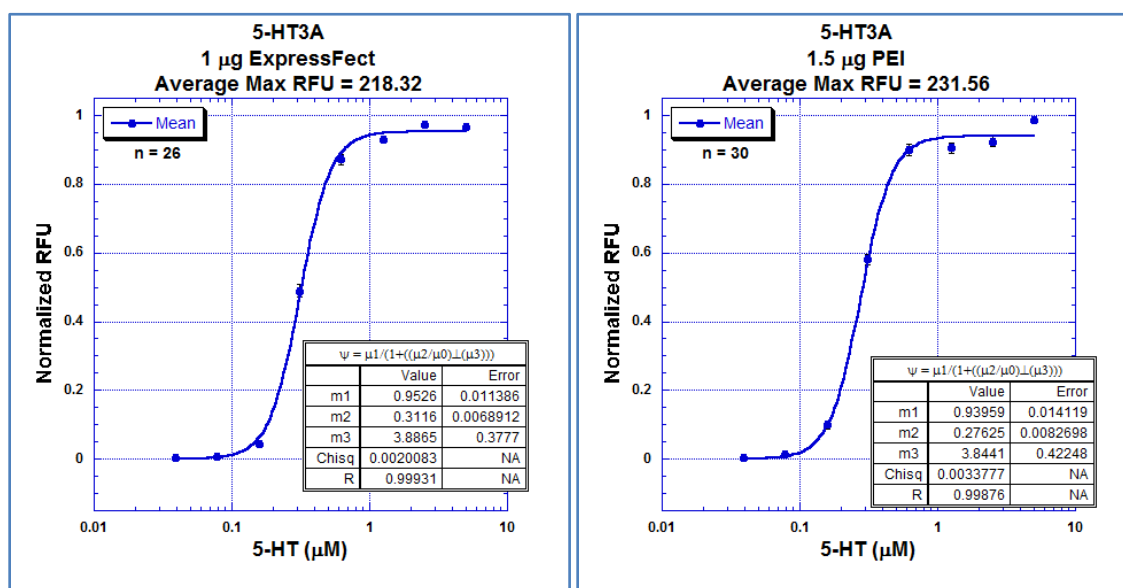


**Figure 5.5.** Dose-reponse curves of human 5HT<sub>3A</sub> receptors expressed in HEK293T cells. Cells were transfected using either ExpressFect transfection reagent (left) or PEI (right).

Expression of conventional mutant 5HT<sub>3A</sub> receptors in HEK293T cells was also examined. Mutation of W183 in the 5HT<sub>3A</sub> receptor was a logical starting point since our lab previously reported that this residue participates in a cation- $\pi$  interaction with serotonin and mutation of this residue results in large shifts in EC<sub>50</sub>.<sup>4, 23</sup> Using either ExpressFect or PEI, 5HT<sub>3A</sub> W183A and W183Y mutant receptors were expressed in cells

and assayed using the FlexStation. Results were consistent with literature values (**Figure 5.6**). The slight differences in absolute  $EC_{50}$  value are likely due to species variation; we used human  $5HT_{3A}$  constructs while the literature values are based on mouse  $5HT_{3A}$  constructs (**Table 5.5**).

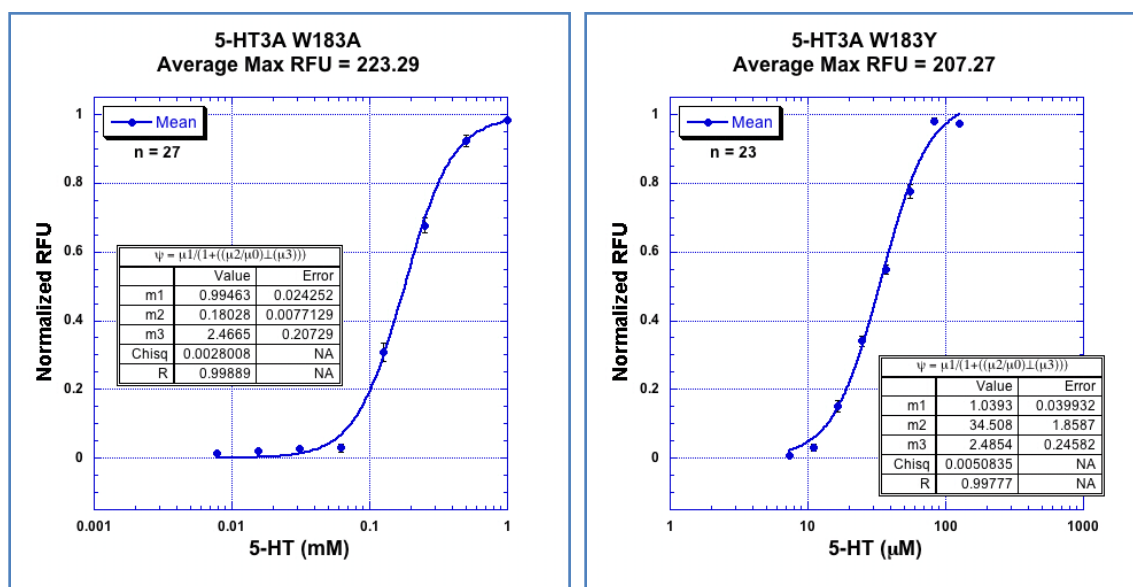


**Figure 5.6.** Dose-response curves of  $5HT_{3A}$  W183A (left) or W183Y (right) mutant receptors expressed in HEK293T cells.

**Table 5.5.** Conventional  $5HT_{3A}$  mutant receptors expressed in HEK293T cells. \*Mouse  $5HT_{3A}$  data is shown for comparison and referenced from Thompson 2008.<sup>23</sup>

	Human $5HT_{3A}$			Mouse $5HT_{3A}$ *	
	$EC_{50}$ (μM)	Fold Shift	Hill	$EC_{50}$ (μM)	Fold Shift
<b>Wild Type</b>	$0.28 \pm 0.01$	-	$3.84 \pm 0.42$	0.24	-
<b>W183A</b>	$180 \pm 7$	652	$2.47 \pm 0.21$	39.8	166
<b>W183Y</b>	$34.5 \pm 1.9$	125	$2.49 \pm 0.25$	5.25	22

Since mRNA injection is routinely used in oocyte experiments and mRNA is one step further in protein translation compared to DNA, we explored the possibility that transfection of mRNA might yield increased receptor expression in HEK293T cells. *In vitro* transcription  $5HT_{3A}$  mRNA from the pcDNA3.1(+) construct was unsuccessful. So the  $5HT_{3A}$  gene was subcloned from pcDNA3.1(+) into the pGEMhe vector, which

facilitates *in vitro* mRNA transcription. Oocytes injected with 5HT<sub>3A</sub> mRNA prepared from the pGEMhe vector expressed functional protein. HEK293T cells were transfected with the same 5HT<sub>3A</sub> mRNA using TransMessenger, a kit developed for efficient mRNA transfection. However, no protein expression was detected. This is likely to reflect an mRNA polyadenylation issue rendering the mRNA less stable in a mammalian cell system. We concluded that transfection of mRNA was inferior to DNA transfection, especially considering that the HEK293T cell line was chosen based on its ability to replicate plasmid DNA and yield increased expression.

***ExpressFect and PEI Transfections: Attempted Suppression in the 5HT<sub>3A</sub> Receptor***

Given that transfection of wild type 5HT<sub>3A</sub> DNA in HEK293T cells proved successful, several attempts were made to incorporate tryptophan at position W183 in the 5HT<sub>3A</sub> receptor. Since W183 makes a cation- $\pi$  interaction to serotonin, lack of W incorporation or incorporation of any other endogenous amino acid (*e.g.*, readthrough) should be easily detected by the FlexStation. 5HT<sub>3A</sub> W183TAG DNA and THG73 tRNA *in vitro* aminoacylated with W (THG73-W) were cotransfected into cells using either ExpressFect or PEI. Despite transfecting various amounts of 5HT<sub>3A</sub> W183TAG DNA and/or THG73-W, no functional receptor expression was detected for either transfection protocol (**Tables 5.6** and **5.7**). Robust expression was detected from wild type 5HT<sub>3A</sub> DNA transfected into the same batch of HEK293T cells establishing cell viability. Additional trials using new reagents and different batches of nucleic acid materials still resulted in no receptor expression. As such, ExpressFect and PEI transfection methods are not suitable for nonsense suppression in mammalian cells.

**Table 5.6.** Using ExpressFect to perform wild type recovery of tryptophan at position W183 in the 5HT<sub>3A</sub> receptor. \*DNA amount is per 3 columns of a 96-well plate.

W183TAG DNA (μg)*	THG73-W (μg)	ExpressFect, Avg Max RFU
0.5	1.25	No Expression
1	1.25	No Expression
2	1.25	No Expression
5	1.25	No Expression

**Table 5.7.** Using PEI to perform wild type recovery of tryptophan at position W183 in the 5HT<sub>3A</sub> receptor. \*DNA amount is per 3 columns of a 96-well plate.

W183TAG DNA (μg)*	THG73-W (μg)	PEI, Avg Max RFU
<i>Vary DNA, wide range of tRNA</i>		
0.5	0.5	No Expression
1	0.5	No Expression
1	2	No Expression
1	3	No Expression
<i>tRNA constant (1 μg)</i>		
0.25	1	No Expression
0.5	1	No Expression
1	1	No Expression
2	1	No Expression
<i>Vary DNA and tRNA, but keep total nucleic acid constant (1 μg)</i>		
0.25	0.75	No Expression
0.75	0.25	No Expression
0.1	0.9	No Expression
0.9	0.1	No Expression

### *Neon Transfections of the 5-HT<sub>3A</sub> Receptor*

Electroporation was explored as an alternative transfection technique amenable to nonsense suppression in mammalian cells. The Neon Transfection System was used to electroporate various amounts of 5HT<sub>3A</sub> DNA. The average maximal RFU was monitored for one- and two-day incubation of transfected cells (**Table 5.8**). Regardless of incubation time, 2 μg of wild type 5HT<sub>3A</sub> DNA per 3 columns of a 96-well plate yielded the highest expression. Cells incubated for two days gave higher expression than for one-day incubations. Several electroporation conditions (*e.g.*, voltage, pulse width, and number of pulses) were tested to determine the most effective transfection protocol

(Table 5.9). Conditions 6, 7, and 8 produced the highest average maximal RFU. Condition 7 (highlighted in red) was selected as the optimal condition for further electroporation transfections.

**Table 5.8.** Optimizing wild type 5HT<sub>3A</sub> DNA transfection using the Neon Transfection System. \*DNA amount is per 3 columns of a 96-well plate.

DNA (µg)*	1 Day Incubation, Avg Max RFU	2 Day Incubation, Avg Max RFU
1	145.0	232.0
2	300.1	359.7
4	137.4	309.3
8	185.1	304.5

**Table 5.9.** Optimization of Neon electroporation protocol. Maximum RFU signals are reported for each of the 24 preprogrammed Neon transfection conditions. 2 µg of DNA was transfected per 3 columns of a 96-well plate.

Condition	Voltage	Width	# Pulses	Max RFU	Condition	Voltage	Width	# Pulses	Max RFU
1	0	20	1	n/a	13	1100	20	2	242
2	1400	20	1	294	14	1200	20	2	311
3	1500	20	1	299	15	1300	20	2	280
4	1600	20	1	174	16	1400	20	2	115
5	1700	20	1	130	17	850	30	2	265
6	1100	30	1	342	18	950	30	2	254
7	1200	30	1	341	19	1050	30	2	301
8	1300	30	1	322	20	1150	30	2	238
9	1400	30	1	216	21	1300	10	3	265
10	1000	40	1	321	22	1400	10	3	273
11	1100	40	1	298	23	1500	10	3	270
12	1200	40	1	256	24	1600	10	3	87

### *Neon Transfections: Attempted Suppression in the 5HT<sub>3A</sub> Receptor*

Using the Neon Transfection System, cells were challenged to incorporate tryptophan at position W183 in the 5HT<sub>3A</sub> receptor. Master mixes containing various amounts of 5HT<sub>3A</sub> W183TAG DNA and THG73-W were prepared, one of which contained THG73-76mer to test for readthrough. HEK293T cells were electroporated with each master mix and the average maximal RFU was monitored (Table 5.10). No

functional receptor expression was detected for any of the DNA/tRNA master mixes tested.

**Table 5.10.** Using Neon electroporation for wild type recovery incorporating tryptophan at position W183 in the 5HT<sub>3A</sub> receptor. \*DNA and tRNA amounts are per 3 columns of a 96-well plate.

W183TAG DNA ( $\mu\text{g}$ )*	THG73-W tRNA ( $\mu\text{g}$ )*	Avg Max RFU
<i>Constant DNA</i>		
2	0	No Expression
2	2 (THG73-76mer)	No Expression
2	0.1	No Expression
2	0.5	No Expression
2	1	No Expression
2	2	No Expression
2	4	No Expression
<i>Constant tRNA</i>		
1	2	No Expression
2	2	No Expression
4	2	No Expression
8	2	No Expression
16	2	No Expression
32	2	No Expression

Here, we show that transfection of DNA containing an amber stop codon and *in vitro* aminoacylated THG73 tRNA does not produce receptor expression for any transfection method employed. These findings differ from previous work by Monahan *et al.* demonstrating that THG73 does in fact incorporate unnatural amino acids into ion channels expressed in mammalian cells.<sup>15</sup> Monahan's studies used whole-cell patch clamp electrophysiology to functionally analyze a single cell,<sup>15</sup> but the FlexStation detects fluorescence signals from thousands of cells in a single well of a 96-well plate. As such, the signal obtained using the FlexStation can be easily diluted by non-expressing cells under conditions of low expression. So it follows that if THG73 is poorly recognized by the mammalian translational machinery resulting in limited protein

expression, this signal might be detected using single-cell detection techniques, but not by the FlexStation.

Given the negative results with THG73, we explored using an alternative suppressor tRNA, the yeast phenylalanine frameshift suppressor tRNA (YFaFS). Cells were electroporated with 2  $\mu\text{g}$  of 5HT<sub>3A</sub> W183GGGT DNA and varying amounts of YFaFS-W tRNA or YFaFS-76mer (**Table 5.11**). Cells appeared healthy by visual inspection, but no expression was detected. Control RFU levels were observed from electroporation of wild type 5HT<sub>3A</sub> DNA. Several trials produced similar results indicating that YFaFS tRNA provides no additional benefit over THG73 tRNA.

**Table 5.11.** Using Neon electroporation for wild type recovery of a frameshift codon at position W183 in the 5HT<sub>3A</sub> receptor. \*DNA and tRNA amounts are per 3 columns of a 96-well plate.

Trial Date	W183GGGT DNA ( $\mu\text{g}$ )*	YFaFS-W tRNA ( $\mu\text{g}$ )*	Avg Max RFU
<b>Trial 1</b>	2 (WT)	0	572.6
	2	8 (YFaFS-76mer)	No Expression
	2	8	No Expression
<b>Trial 2</b>	2 (WT)	0	301.2
	2	8 (YFaFS-76mer)	No Expression
	2	4	No Expression
<b>Trial 3</b>	2	8	No Expression
	2 (WT)	0	443.7
	2	8 (YFaFS-76mer)	No Expression
	2	4	No Expression
	2	8	No Expression

### *Using Human Serine Amber Suppressor tRNA to Suppress an Amber Codon in eGFP*

The endogenous aminoacyl tRNA synthetase in the cells charges the human serine amber suppressor tRNA (HSAS) with serine, which can then be incorporated opposite an amber stop codon.<sup>17</sup> This human-derived tRNA is recognized by the HEK293T cells, and so we explored using HSAS to optimize co-transfection of DNA and tRNA materials.

We targeted residue A37 in the enhanced green fluorescent protein (eGFP) since this site is located well before the chromophore. If suppression does not occur, then even expression of a truncated protein will not give a fluorescent signal. Both electroporation and ExpressFect were used to transfect cells with eGFP A37TAG DNA and HSAS, and suppression efficiency was monitored by confocal microscopy. Wild type recovery of eGFP A37TAG using THG73-Ala was attempted, but results were indistinguishable from 76mer control experiments. Cells transfected with eGFP A37TAG and HSAS revealed improved eGFP expression relative to wild type recovery, however approximate expression was <1% of wild type expression (**Figure 5.7**). Electroporation gave slightly lower expression than ExpressFect. These experiments provided the initial confirmation that successful transfection of tRNA had occurred, but that protein expression was significantly hindered when using a stoichiometric tRNA (*e.g.*, THG73 tRNA).

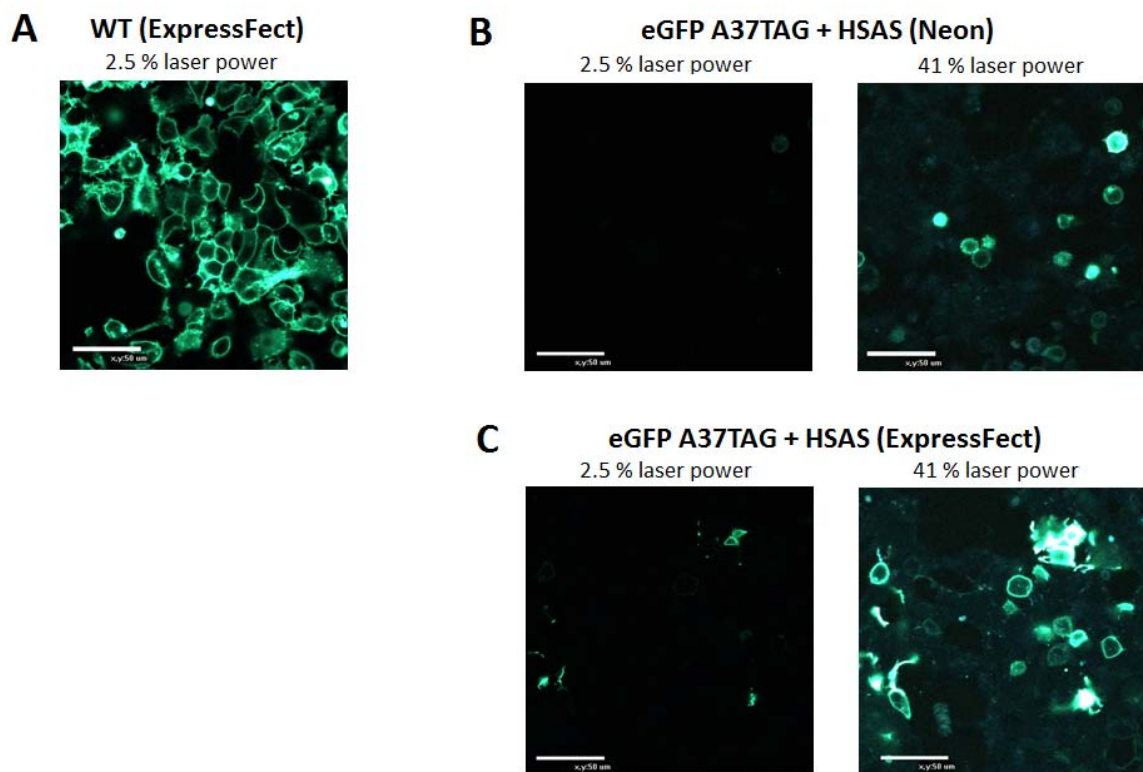


**Figure 5.7.** Confocal images of HEK293T cells expressing eGFP. A. Wild type eGFP expression (ExpressFect). B. Neon electroporation; suppression of eGFP A37TAG DNA by HSAS. C. ExpressFect; suppression of eGFP A37TAG DNA by HSAS. Images obtained using 2.5% laser power contain 90% saturation. Images obtained using 41% laser power contain 96% saturation.

#### *Using HSAS to Suppress an Amber Codon in the 5HT<sub>3A</sub> Receptor*

Returning to the 5HT<sub>3A</sub> receptor, we attempted to perturb receptor function by using HSAS to incorporate serine at position W183, the critical cation- $\pi$  interaction residue. Both electroporation and PEI were used to transfect a constant amount of 5HT<sub>3A</sub> W183TAG DNA with varying amounts of HSAS (**Table 5.12**). Electroporation of 2 and 4  $\mu$ g of HSAS produced functional receptors with an EC<sub>50</sub> of 370  $\mu$ M 5-HT (1200-fold shifted from wild type). It is likely that challenging the translational machinery to suppress a functionally important site with a non-native amino acid in all five subunits of the receptor can account for the observed low expression. However, this provided

additional evidence that tRNA was successfully delivered to the cells and protein translation occurred. No expression was detected from PEI transfection of HSAS.

**Table 5.12.** Comparison of Neon electroporation and PEI transfection using HSAS to incorporate serine at position W183 in the 5HT<sub>3A</sub> receptor. \*DNA and HSAS amounts are per 3 columns of a 96-well plate.

DNA ( $\mu\text{g}$ )*	HSAS ( $\mu\text{g}$ )*	Neon, Avg Max RFU	PEI, Avg Max RFU
2 (WT)	0	180.6	73.9
2 (W183TAG)	0.5	No Expression	No Expression
2 (W183TAG)	2	14.9	No Expression
2 (W183TAG)	4	33.5	No Expression

Suppression with HSAS was further optimized by attempting wild type recovery of residue S61 in the 5HT<sub>3A</sub> receptor. Electroporation, PEI, and ExpressFect were used to transfect a constant amount of 5HT<sub>3A</sub> S61TAG DNA and varying amounts of HSAS (**Table 5.13**). Transfection efficiency was compared by monitoring the average maximal RFU. HSAS suppression was most efficient with electroporation, since this method required the least amount of HSAS. In fact, protein expression decreased with increasing amounts of HSAS. Variable expression was detected from ExpressFect and required more HSAS than electroporation. Cells appeared viable after PEI transfection, but no expression was detected.

**Table 5.13.** Comparison of Neon electroporation, PEI, and ExpressFect: Wild type recovery using HSAS to incorporate serine at position S61 in the 5HT<sub>3A</sub> receptor. \*DNA and HSAS amounts are per 3 columns of a 96-well plate.

DNA ( $\mu\text{g}$ )*	HSAS ( $\mu\text{g}$ )*	Neon, Avg Max RFU	PEI, Avg Max RFU	ExpressFect, Avg Max RFU	ExpressFect, Avg Max RFU
		<b>11/15/10</b>	<b>11/15/10</b>	<b>11/15/10</b>	<b>12/1/10</b>
2 (WT)	0	297.1	195.7	320.5	309.5
2 (S61TAG)	2	93.8	No Expression	No Expression	No Expression
2 (S61TAG)	4	37.7	No Expression	80.9	No Expression
2 (S61TAG)	8	No Expression	No Expression	78.3	No Expression

Given that suppression yielded much lower expression compared to wild type, preparation of the membrane potential dye was optimized to a 1:2 dilution in flex buffer to increase signal detection. The average maximal RFU was measured from cells electroporated with 2  $\mu\text{g}$  5HT<sub>3A</sub> S61TAG DNA and varying amounts of HSAS and incubated with the newly prepared dye (**Table 5.14**). For each HSAS concentration transfected, increased signal was detected using the 1:2 dye dilution compared to the 1:10 dilution (**Table 5.13**). The 1:2 dye dilution was used in all further FlexStation assays.

**Table 5.14.** Monitoring RFU using the 1:2 dye dilution: Wild type recovery using HSAS to incorporate serine at site S61 in the 5HT<sub>3A</sub> receptor.

\*Note that  $\mu\text{g}$  of DNA and tRNA is per 3 columns of a 96-well plate.

DNA ( $\mu\text{g}$ )	HSAS ( $\mu\text{g}$ )	Neon, Avg Max RFU
2 (WT)	0	371.5
2 (S61TAG)	2	112.4
2 (S61TAG)	4	121.4
2 (S61TAG)	8	91.9

### *Neon Electroporation and ExpressFect: Double Transfections*

We next explored the possibility that transfecting a second dose of DNA and/or tRNA to the cells might enhance protein expression. Cells were electroporated with 2  $\mu\text{g}$  of 5HT<sub>3A</sub> S61TAG DNA and 4  $\mu\text{g}$  HSAS using condition 7 (1200 V, 30 ms, 1 pulse). Following 24 hr incubation, 24 preprogrammed electroporation conditions were sampled to electroporate the cells with a second dose of 4  $\mu\text{g}$  HSAS (**Table 5.15**). Condition 22 (1400 V, 10 ms, 3 pulses) resulted in the greatest maximal RFU (390). ExpressFect was also used to doubly transfect cells with DNA and/or HSAS, but these experiments gave significantly lower expression in comparison to electroporation.

**Table 5.15.** Optimization of Neon electroporation for double transfection of HSAS to incorporate serine at position S61 in the 5HT<sub>3A</sub> receptor. 2 µg of DNA and 4 µg of HSAS was transfected per 3 columns of a 96-well plate.

Condition	Max RFU	Condition	Max RFU
<b>1 (single)</b>	17.4	<b>13</b>	No Expression
<b>2</b>	161.1	<b>14</b>	118.8
<b>3</b>	158.1	<b>15</b>	209.8
<b>4</b>	170.5	<b>16</b>	278.4
<b>5</b>	193.4	<b>17</b>	54.0
<b>6</b>	172.6	<b>18</b>	135.9
<b>7</b>	219.2	<b>19</b>	223.5
<b>8</b>	264.5	<b>20</b>	279.7
<b>9</b>	315.7	<b>21</b>	260.1
<b>10</b>	216.8	<b>22</b>	<b>390.0</b>
<b>11</b>	253.7	<b>23</b>	273.1
<b>12</b>	277.1	<b>24</b>	183.1

Using the electroporation protocol for double transfection, cells were challenged to incorporate tryptophan at position W183 using *in vitro* aminoacylated THG73-W. Cells were electroporated first with 2 µg of 5HT<sub>3A</sub> W183TAG DNA and 8 µg of THG73-W, followed by a second electroporation of the same concentration of DNA and/or tRNA 24 hr later (**Table 5.16**). No readthrough was detected and despite the promising results with HSAS, no expression was observed for electroporation of THG73-W.

**Table 5.16.** Double Neon Transfection: Wild type recovery incorporating tryptophan at position W183 in the 5HT<sub>3A</sub> receptor. \*DNA and tRNA amounts are per 3 columns of a 96-well plate.

DNA (µg)*	tRNA (µg)*	Nucleic Acid Double Transfected	Avg Max RFU (12/21/10)
2 (WT)	0	DNA only	Instrument disrupted, data lost
2 (W183TAG)	8 (THG73-76mer)	tRNA only	No Expression
2 (W183TAG)	8 (THG73-W)	tRNA only	No Expression
2 (W183TAG)	8 (THG73-W)	tRNA + DNA	No Expression

### **RNA Transfections of the 5HT<sub>3A</sub> Receptor**

Considering that efficient delivery of aminoacylated tRNA into the cells is half the battle, we tested several reagents designed for efficient transfection of RNA material.

*TransIT*-mRNA, TransMessenger, and Lipofectamine RNAiMAX transfection reagents were used in these studies and are intended for transfection of mRNA or siRNA. Here we describe our efforts to adapt these protocols to cotransfect DNA and tRNA material into HEK293T cells.

According to the *TransIT*-mRNA transfection protocol, transfection of wild type 5HT<sub>3A</sub> DNA was performed using various ratios of Boost:*TransIT* reagent (**Table 5.17**). Significant receptor expression, as measured by average maximal RFU, was observed for 2 µg of DNA. Receptor expression was further increased under conditions using a minimum of 7.5 µL of *TransIT* and a 1:2 ratio of Boost:*TransIT*.

**Table 5.17.** Optimization of *TransIT* Transfection. \*DNA amount is per 3 columns of a 96-well plate.

WT DNA (µg)*	Boost Reagent (µL)	<i>TransIT</i> (µL)	Avg Max RFU
0.02	5	7.5	No Expression
0.1	5	7.5	107.0
0.5	5	7.5	308.9
2	5	7.5	467.6
2	1.25	2.5	408.1
2	3.75	7.5	497.8
2	7.5	15	541.8
2	15	30	563.5

After determining the optimal Boost:*TransIT* ratio, the *TransIT* protocol was used to suppress an amber stop codon using HSAS. Cells were transfected with various amounts of 5HT<sub>3A</sub> S61TAG DNA and HSAS (**Table 5.18**). Cells experienced decreased viability and reduced protein expression when transfected using large amounts of *TransIT* transfection reagent (*i.e.*, 15 and 30 µL *TransIT*). Lowering the amount of *TransIT* to 7.5 µL improved expression, while 2.5 µL of *TransIT* gave very low expression. We concluded that 2 µg of S61TAG DNA, a minimum of 4 µg of HSAS, and 7.5 µL of *TransIT* were necessary to achieve efficient expression.

**Table 5.18.** Optimization of *TransIT* Transfection: Wild type recovery using HSAS to incorporate serine at position S61 in the 5HT<sub>3A</sub> receptor. \*DNA and HSAS amounts are per 3 columns of a 96-well plate.

5HT <sub>3A</sub> DNA (μg)*	HSAS (μg)	Boost Reagent (μL)	<i>TransIT</i> (μL)	Avg Max RFU
<i>DNA constant, vary HSAS and Boost:TransIT</i>				
2 (WT)	0	7.5	15	471.1
2 (S61TAG)	4	7.5	15	113.1
2 (S61TAG)	8	7.5	15	94.6
2 (S61TAG)	8	15	30	Cells Died
<i>Vary DNA, constant HSAS, vary Boost:TransIT</i>				
0.5 (S61TAG)	4	3.75	7.5	95.2
1 (S61TAG)	4	3.75	7.5	91.1
0.5 (S61TAG)	4	7.5	15	44.8
1 (S61TAG)	4	7.5	15	73.2
<i>Constant DNA, vary HSAS, using 2.5 μL TransIT</i>				
2 (WT)	0	1.25	2.5	167.7
2 (S61TAG)	2	1.25	2.5	No Expression
2 (S61TAG)	4	1.25	2.5	37.4
2 (S61TAG)	8	1.25	2.5	33.5
<i>Constant DNA, vary HSAS, using 7.5 μL TransIT</i>				
2 (WT)	0	3.75	7.5	489.0
2 (S61TAG)	2	3.75	7.5	162.9
2 (S61TAG)	4	3.75	7.5	353.5
2 (S61TAG)	8	3.75	7.5	340.0

Using the optimized *TransIT* condition, cells were subjected to double transfections, in which the second transfection contained either DNA and HSAS or only HSAS (**Table 5.19**). Double transfection of both DNA and HSAS produced significantly more cell death and lower expression than observed for single transfection. However, when only HSAS was delivered during the second transfection, results were similar to those observed for single transfection, but did not provide any additional benefit over the single transfection. These same conditions were used to doubly transfect cells with 5HT<sub>3A</sub> W183TAG DNA and THG73-W tRNA. Unfortunately, no expression was detected for double transfection of either DNA and tRNA or tRNA only (**Table 5.20**), an observation common to all experiments challenging the cells to express protein using this *in vitro* aminoacylated and stoichiometric tRNA.

**Table 5.19.** Double *TransIT* Transfection: Wild type recovery using HSAS to incorporate serine at position S61 in the 5HT<sub>3A</sub> receptor. The first transfection contains both DNA and HSAS, but the second transfection contains *either* DNA and HSAS *or* HSAS only. \*DNA and HSAS amounts are per 3 columns of a 96-well plate.

DNA (μg)*	HSAS (μg)*	Boost Reagent (μL)	<i>TransIT</i> (μL)	2X (DNA+HSAS) Avg Max RFU	2X (HSAS only) Avg Max RFU
2 (WT)	0	3.75	7.5	621.6	626.0
2 (S61TAG)	2	3.75	7.5	46.2	177.7
2 (S61TAG)	4	3.75	7.5	51.9	321.4
2 (S61TAG)	8	3.75	7.5	85.0	390.1

**Table 5.20.** Double *TransIT* Transfection: Wild type recovery of tryptophan at position W183 in the 5HT<sub>3A</sub> receptor. The first transfection contains both DNA and tRNA, but the second transfection contains *either* DNA and tRNA *or* tRNA only. \*DNA and tRNA amounts are per 3 columns of a 96-well plate.

W183TAG DNA (μg)*	tRNA (μg)*	Boost Reagent (μL)	<i>TransIT</i> (μL)	2X (DNA+tRNA) Avg Max RFU	2X (tRNA only) Avg Max RFU
2	8 (THG73-76mer)	3.75	7.5	No Expression	No Expression
2	2 (THG73-W)	3.75	7.5	No Expression	No Expression
2	4 (THG73-W)	3.75	7.5	No Expression	No Expression
2	8 (THG73-W)	3.75	7.5	No Expression	No Expression

Additional RNA transfection methods were tested, but proved inferior to the *TransIT* method. Suppression experiments using TransMessenger consumed more transfection reagent and produced significantly decreased RFU signals compared to *TransIT* (*i.e.*, 70 vs. 350 RFU, respectively). Alternatively, the Lipofectamine RNAiMAX transfection protocol yielded mediocre expression for transfection of wild type DNA and no expression for suppression experiments. Experimental details for TransMessenger and RNAiMAX transfections are located in **Tables 5.21-5.24**.

**Table 5.21.** Optimization of TransMessenger transfection conditions. \*DNA amount is per 3 columns of a 96-well plate.

WT DNA ( $\mu\text{g}$ )*	TransMessenger ( $\mu\text{L}$ )	Avg Max RFU
0.1	8	207.6
0.5	8	366.0
2	8	346.8
2	4	No Expression
2	8	376.0
2	16	287.5
4	8	310.0
4	16	361.7

**Table 5.22.** Optimization of TransMessenger transfection conditions: Wild type recovery incorporating serine at position S61 in the 5HT<sub>3A</sub> receptor. \*DNA and HSAS amounts are per 3 columns of a 96-well plate.

DNA ( $\mu\text{g}$ )*	HSAS ( $\mu\text{g}$ )*	TransMessenger ( $\mu\text{L}$ )	Avg Max RFU
<i>Constant DNA, vary HSAS, constant TransMessenger</i>			
2 (WT)	0	8	274.7
2 (S61TAG)	2	8	No Expression
2 (S61TAG)	4	8	No Expression
2 (S61TAG)	8	8	No Expression
<i>Vary DNA, constant HSAS, vary TransMessenger</i>			
0.5 (S61TAG)	4	8	42.5
1 (S61TAG)	4	8	47.2
0.5 (S61TAG)	4	16	74.1
1 (S61TAG)	4	16	120.4
<i>Constant DNA, vary HSAS, using 16 <math>\mu\text{L}</math> TransMessenger</i>			
2 (WT)	0	16	208.4
2 (S61TAG)	2	16	63.8
2 (S61TAG)	4	16	No Expression
2 (S61TAG)	8	16	No Expression
<i>Constant DNA, vary HSAS, using 32 <math>\mu\text{L}</math> TransMessenger</i>			
2 (WT)	0	32	181.8
2 (S61TAG)	2	32	69.9
2 (S61TAG)	4	32	52.9
2 (S61TAG)	8	32	No Expression

**Table 5.23.** Optimization of Lipofectamine RNAiMAX transfection conditions. \*DNA amount is per 3 columns of a 96-well plate.

WT DNA ( $\mu\text{g}$ )*	RNAiMAX ( $\mu\text{L}$ )	Avg Max RFU
<i>Vary DNA, constant RNAiMAX</i>		
0.02	7.5	82.3
0.1	7.5	141.5
0.5	7.5	209.1
2	7.5	270.6
<i>Constant DNA, vary RNAiMAX</i>		
2	2.5	162.0
2	7.5	146.1
2	15	163.3
2	30	42.9

**Table 5.24.** Optimization of Lipofectamine RNAiMAX transfection conditions: Wild type recovery incorporating serine at position S61 in the 5HT<sub>3A</sub> receptor. \*DNA and HSAS amounts are per 3 columns of a 96-well plate.

DNA ( $\mu\text{g}$ )*	HSAS ( $\mu\text{g}$ )*	RNAiMAX ( $\mu\text{L}$ )	Avg Max RFU
2 (WT)	0	15	113.8
2 (S61TAG)	0	15	No Expression
2 (S61TAG)	4	15	No Expression
2 (S61TAG)	8	15	No Expression

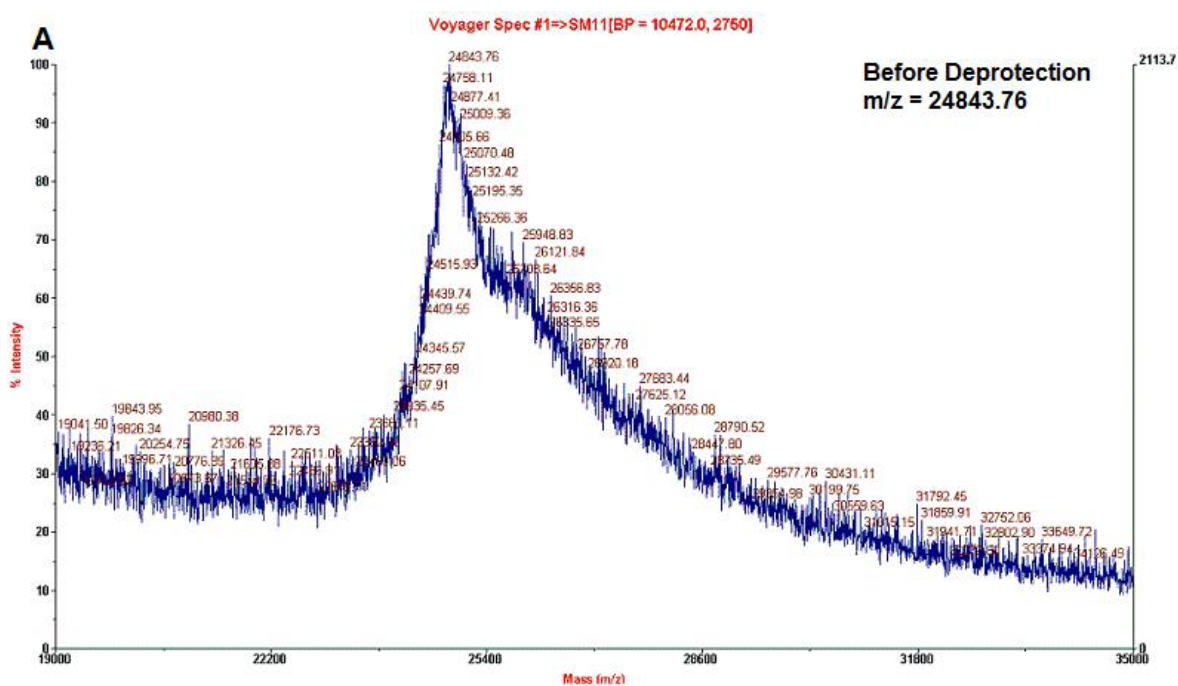
### 5.4.3 Possible Challenges for Nonsense Suppression in Mammalian Cells

A puzzling result that recurred throughout these studies is that HSAS tRNA easily suppressed the amber stop codon in 5HT<sub>3A</sub> receptors expressed in HEK293T cells, but *in vitro* aminoacylated tRNAs (*e.g.*, THG73 and YFaFS) did not. We then questioned the integrity of the tRNA in response to transfection conditions. Specifically, does the amino acid fall off of the tRNA before entering the cell *or* does aminoacylated tRNA enter the cell, but is translationally incompetent? We addressed the first question in two ways.

#### *Analyzing the Effect of Transfection Conditions on tRNA*

The integrity of *in vitro* aminoacylated tRNA was analyzed in response to the two most efficient transfection protocols previously identified: double Neon electroporation and single *TransIT* transfection. To test Neon electroporation, THG73-W was

deprotected for 10 min, electroporated using either condition 7 or 22, and analyzed using MALDI-TOF MS (**Figure 5.8**). To examine the effect of the *TransIT* protocol, THG73-W was deprotected for 10 min, incubated in the *TransIT* reagents for 24 hr, and analyzed using MALDI-TOF MS (**Figure 5.9**). As a control, MALDI-TOF MS analysis of THG73-W confirmed the removal of NVOC by deprotection through a mass change of 237.48 (NVOC=239.04) (**Figure 5.10**). Comparison of before and after deprotection for each transfection method did not differ significantly from the control suggesting that neither method should remove the amino acid from the tRNA.



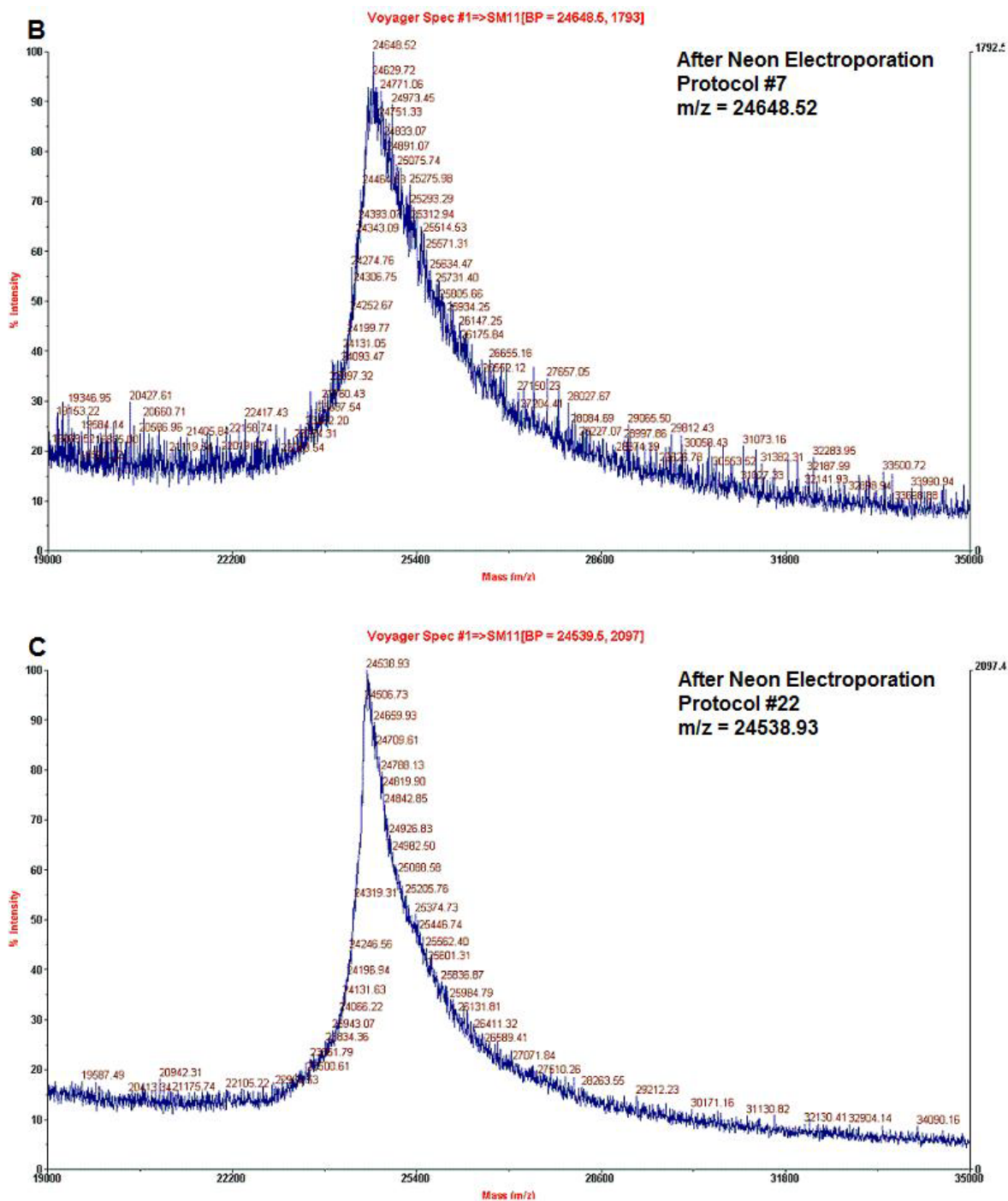


**Figure 5.8.** THG73-W in response to Neon transfection. A. MALDI of THG73-W-NVOC before deprotection by photolysis. B. MALDI of THG73-W after photolysis and Neon transfection using condition 7. C. MALDI of THG73-W after photolysis and Neon transfection using condition 22.

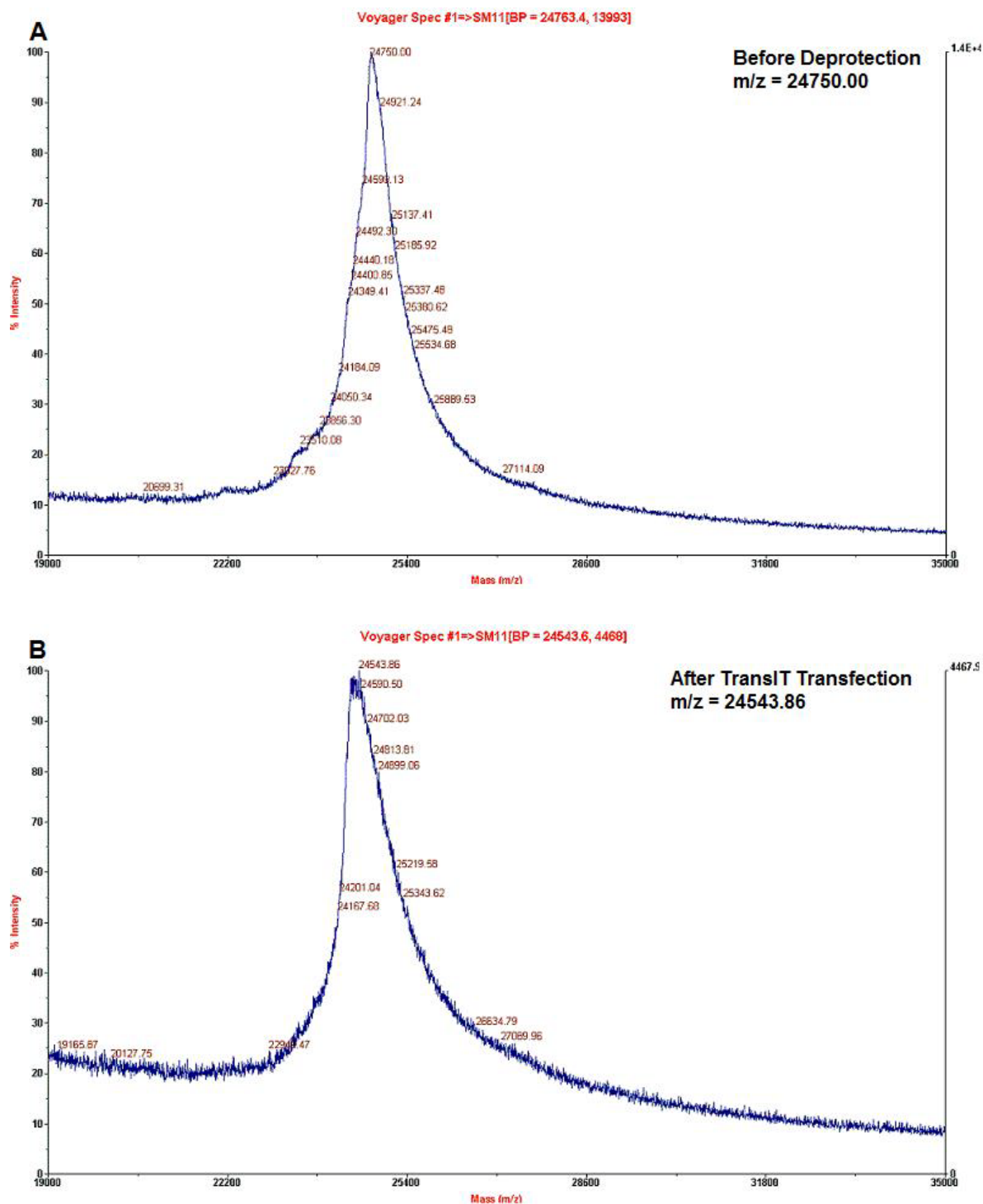


**Figure 5.9.** THG73-W after *TransIT* transfection. A. MALDI of THG73-W-NVOC before deprotection by photolysis. B. MALDI of THG73-W after photolysis and *TransIT* transfection.

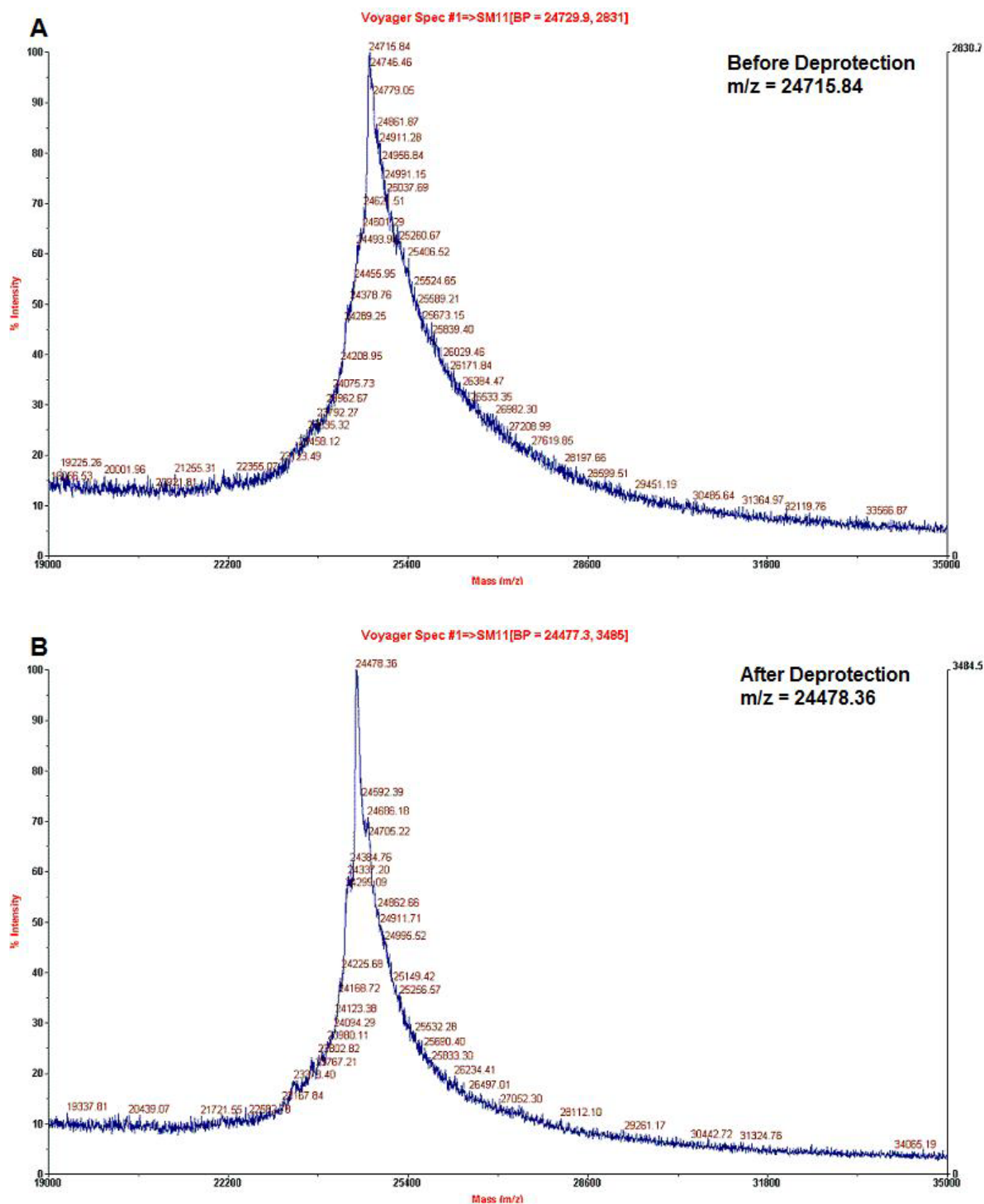


**Figure 5.10.** Deprotection of THG73-W-NVOC. A. MALDI of THG73-W-NVOC before photolysis. B. MALDI of THG73-W tRNA after photolysis for 5 min.

### ***Transfection of an $\alpha$ -hydroxy Acid***

An alternative approach to monitor the integrity of the tRNA is to transfect an  $\alpha$ -hydroxy acid, as these are relatively more stable than amino acids and therefore not protected. Cells were challenged to incorporate tryptophan- $\alpha$ -hydroxy (Wah) at position W183 in the 5HT<sub>3A</sub> receptor. Neon electroporation (condition 7) and *TransIT* transfection protocols were used to transfect 2  $\mu$ g of 5HT<sub>3A</sub> W183TAG DNA and various amounts of THG73-Wah tRNA (**Table 5.25**). No expression was observed for either transfection protocol.

**Table 5.25.** Comparison of Neon electroporation and *TransIT* transfection to incorporate tryptophan  $\alpha$ -hydroxy at position W183 in the 5HT<sub>3A</sub> receptor. \*DNA and HSAS amounts are per 3 columns of a 96-well plate.

DNA ( $\mu$ g)*	tRNA ( $\mu$ g)*	Neon, Avg Max RFU	<i>TransIT</i> , Avg Max RFU
2 (WT)	0	645.7	407.5
2 (W183TAG)	4	No Expression	No Expression
2 (W183TAG)	8	No Expression	No Expression
2 (W183TAG)	12	No Expression	No Expression

## **5.5 CONCLUSIONS AND FUTURE DIRECTIONS**

This chapter describes the development of methods to enhance nonsense suppression in mammalian cells with the ultimate goal of achieving robust protein expression via transfection of DNA and *in vitro* aminoacylated tRNA. We optimized two protocols to effectively deliver DNA and tRNA to HEK293T cells, such as double electroporation using the Neon transfection system and single transfection using *TransIT* transfection reagent. Both of these methods successfully suppressed a serine site in the 5HT<sub>3A</sub> receptor using HSAS tRNA, which is aminoacylated with serine *in vivo*. However, both transfection methods failed to produce functional protein when applied to

suppression of an amber stop codon utilizing *in vitro* aminoacylated tRNAs, such as THG73 and YFaFS.

Successful suppression experiments with HSAS tRNA indicated that tRNA is in fact delivered to the cells. Possible issues limiting the functionality of *in vitro* aminoacylated tRNAs could be their stability during the transfection processes and subsequent recognition by the mammalian translational machinery. MALDI-TOF MS analysis of deprotected THG73-W exposed to either transfection method suggested that only the NVOC protecting group was removed and the aminoacyl tRNA remained intact during transfection. These data support the idea that tRNA is delivered to the cell, but that either the amino acid falls off the tRNA inside the cell or the tRNA is translationally incompetent.

Translational incompetence may be attributed to the tRNA identity problem. This concept refers to the specific interactions between the tRNA molecule and its synthetase required for proper activity.<sup>24</sup> The success of nonsense suppression experiments rely on the principle that the mammalian synthetases will not recognize and aminoacylate the tRNA with an endogenous amino acid. One can imagine future experiments designed to bypass the tRNA identity problem entirely. This could be achieved by engineering a novel synthetase that retains tRNA recognition elements specific to the *in vitro* aminoacylated tRNA of interest, but does not recharge this tRNA with any endogenous amino acid. Essentially, this would create a “dummy” synthetase capable of binding the tRNA and “handing it off” to the ribosome. Complementary studies might include engineering the tRNA component to bind the synthetase. Mutagenesis would target the

identity element regions of tRNA, such as the distal ends of the tRNA and the anticodon loop.

Additionally, the possibility that the tRNA is not recognized by essential associated proteins (*e.g.*, EF-Tu) could contribute to hindered translational activity. As such, it may be useful to overexpress the mammalian elongation factor, EF-1 $\alpha$ , which is responsible for delivering aminoacyl tRNA to the ribosome. However, we note that several reports have confirmed the high conservation and abundant expression of EF-1 $\alpha$  in mammalian cells.<sup>25</sup>

## **5.6 ACKNOWLEDGMENTS**

Special thanks to Shawna Frazier for assistance with passaging techniques and cell counting as well as Crystal Dilworth for assistance with the confocal microscope.

## 5.7 REFERENCES

1. Noren, C. J.; Anthony-Cahill, S. J.; Griffith, M. C.; Schultz, P. G., A general method for site-specific incorporation of unnatural amino acids into proteins. *Science* 1989, 244, (4901), 182-8.
2. Nowak, M. W.; Gallivan, J. P.; Silverman, S. K.; Labarca, C. G.; Dougherty, D. A.; Lester, H. A., In vivo incorporation of unnatural amino acids into ion channels in *Xenopus* oocyte expression system. *Methods Enzymol* 1998, 293, 504-29.
3. Nowak, M. W.; Kearney, P. C.; Sampson, J. R.; Saks, M. E.; Labarca, C. G.; Silverman, S. K.; Zhong, W.; Thorson, J.; Abelson, J. N.; Davidson, N.; et al., Nicotinic receptor binding site probed with unnatural amino acid incorporation in intact cells. *Science* 1995, 268, (5209), 439-42.
4. Beene, D. L.; Brandt, G. S.; Zhong, W.; Zacharias, N. M.; Lester, H. A.; Dougherty, D. A., Cation- $\pi$  interactions in ligand recognition by serotonergic (5-HT<sub>3A</sub>) and nicotinic acetylcholine receptors: the anomalous binding properties of nicotine. *Biochemistry* 2002, 41, (32), 10262-9.
5. Lummis, S. C.; D, L. B.; Harrison, N. J.; Lester, H. A.; Dougherty, D. A., A cation- $\pi$  binding interaction with a tyrosine in the binding site of the GABAC receptor. *Chem Biol* 2005, 12, (9), 993-7.
6. Mu, T. W.; Lester, H. A.; Dougherty, D. A., Different binding orientations for the same agonist at homologous receptors: a lock and key or a simple wedge? *J Am Chem Soc* 2003, 125, (23), 6850-1.
7. Puskar, N. L.; Xiu, X.; Lester, H. A.; Dougherty, D. A., Two neuronal nicotinic acetylcholine receptors,  $\alpha 4\beta 4$  and  $\alpha 7$ , show differential agonist binding modes. *J Biol Chem* 286, (16), 14618-27.
8. Xiu, X.; Puskar, N. L.; Shanata, J. A.; Lester, H. A.; Dougherty, D. A., Nicotine binding to brain receptors requires a strong cation- $\pi$  interaction. *Nature* 2009, 458, (7237), 534-7.
9. Zhong, W.; Gallivan, J. P.; Zhang, Y.; Li, L.; Lester, H. A.; Dougherty, D. A., From ab initio quantum mechanics to molecular neurobiology: a cation- $\pi$  binding site in the nicotinic receptor. *Proc Natl Acad Sci U S A* 1998, 95, (21), 12088-93.
10. Werry, T. D.; Gregory, K. J.; Sexton, P. M.; Christopoulos, A., Characterization of serotonin 5-HT<sub>2C</sub> receptor signaling to extracellular signal-regulated kinases 1 and 2. *J Neurochem* 2005, 93, (6), 1603-15.
11. Kohrer, C.; Xie, L.; Kellerer, S.; Varshney, U.; RajBhandary, U. L., Import of amber and ochre suppressor tRNAs into mammalian cells: a general approach to site-specific insertion of amino acid analogues into proteins. *Proc Natl Acad Sci U S A* 2001, 98, (25), 14310-5.
12. Liu, C. C.; Schultz, P. G., Adding new chemistries to the genetic code. *Annu Rev Biochem* 79, 413-44.
13. Liu, W.; Brock, A.; Chen, S.; Schultz, P. G., Genetic incorporation of unnatural amino acids into proteins in mammalian cells. *Nat Methods* 2007, 4, (3), 239-44.
14. Zhang, Z.; Alfonta, L.; Tian, F.; Bursulaya, B.; Uryu, S.; King, D. S.; Schultz, P. G., Selective incorporation of 5-hydroxytryptophan into proteins in mammalian cells. *Proc Natl Acad Sci U S A* 2004, 101, (24), 8882-7.

15. Monahan, S. L.; Lester, H. A.; Dougherty, D. A., Site-specific incorporation of unnatural amino acids into receptors expressed in mammalian cells. *Chem Biol* 2003, 10, (6), 573-80.
16. Saks, M. E.; Sampson, J. R.; Nowak, M. W.; Kearney, P. C.; Du, F.; Abelson, J. N.; Lester, H. A.; Dougherty, D. A., An engineered Tetrahymena tRNA<sup>Gln</sup> for in vivo incorporation of unnatural amino acids into proteins by nonsense suppression. *J Biol Chem* 1996, 271, (38), 23169-75.
17. Capone, J. P.; Sharp, P. A.; RajBhandary, U. L., Amber, ochre and opal suppressor tRNA genes derived from a human serine tRNA gene. *EMBO J* 1985, 4, (1), 213-21.
18. Rodriguez, E. A.; Lester, H. A.; Dougherty, D. A., In vivo incorporation of multiple unnatural amino acids through nonsense and frameshift suppression. *Proc Natl Acad Sci U S A* 2006, 103, (23), 8650-5.
19. DuBridg, R. B.; Tang, P.; Hsia, H. C.; Leong, P. M.; Miller, J. H.; Calos, M. P., Analysis of mutation in human cells by using an Epstein-Barr virus shuttle system. *Mol Cell Biol* 1987, 7, (1), 379-87.
20. Pear, W. S.; Nolan, G. P.; Scott, M. L.; Baltimore, D., Production of high-titer helper-free retroviruses by transient transfection. *Proc Natl Acad Sci U S A* 1993, 90, (18), 8392-6.
21. Price, K. L.; Lummis, S. C., FlexStation examination of 5-HT<sub>3</sub> receptor function using Ca<sup>2+</sup> and membrane potential-sensitive dyes: advantages and potential problems. *J Neurosci Methods* 2005, 149, (2), 172-7.
22. Srinivasan, R.; Pantoja, R.; Moss, F. J.; Mackey, E. D.; Son, C. D.; Miwa, J.; Lester, H. A., Nicotine up-regulates alpha4beta2 nicotinic receptors and ER exit sites via stoichiometry-dependent chaperoning. *J Gen Physiol* 137, (1), 59-79.
23. Thompson, A. J.; Lochner, M.; Lummis, S. C., Loop B is a major structural component of the 5-HT<sub>3</sub> receptor. *Biophys J* 2008, 95, (12), 5728-36.
24. Giege, R.; Sissler, M.; Florentz, C., Universal rules and idiosyncratic features in tRNA identity. *Nucleic Acids Res* 1998, 26, (22), 5017-35.
25. Lee, S.; LeBlanc, A.; Duttaroy, A.; Wang, E., Terminal differentiation-dependent alteration in the expression of translation elongation factor-1 alpha and its sister gene, S1, in neurons. *Exp Cell Res* 1995, 219, (2), 589-97.